Master Thesis

DEVELOPMENT OF CONTROL STRATEGIES IN A ROBOTIC LOWER-LIMB EXOSKELETON FOR PATIENTS WITH MOBILITY IMPAIRMENTS

Miguel David Sánchez Manchola

Supervisor:

Prof. Dr. Carlos A. Cifuentes

Co-supervisor:

Prof. Dr. Marcela Múnera

A thesis submitted in fulfilment of the requirements for the Masters degree in Electronic Engineering

December 2019

"I said, "I'm empty enough. Fame and fortune are nothing to me."
The abbot shook his head and said, "No, emptiness is not nothingness.
Emptiness is a type of existence. You must use this existential
emptiness to fill yourself.""

Liu Cixin

"Anyone who has to call himself a genius... isn't."

Stephen King

"Regard readers not as being ignorant but, more likely,
innocent of your topic and its jargon. Write for them, not at them."

Alton Blakeslee

"Der Erfolg wird sich steigern, der Ehrgeiz wird wachsen,
die Absturzgefahr nimmt zu, je höher man steigt."

Erick Kästner

Acknowledgements

Esta tesis fue posible gracias al apoyo del proyecto Colciencias "Desarrollo de una plataforma robótica adaptable para rehabilitación y asistencia de la marcha" (contrato 801-2017), la red de investigación del CYTED REASISTE (subvención 216RT0505) y fondos de la Escuela Ing. Un agradecimiento especial a la EPF École d'ingénieur, y en particular a los Dr. Maxime Bourgain y Thomas Provot, por abrirnos las puertas de su laboratorio para realizar las pruebas de desempeño del exoesqueleto y siempre encontrarse a nuestra disposición para realizar el tratamiento de los datos.

Sin lugar a duda, un gran número de personas influyó a su manera en que este trabajo pudiera llegar a su término. En primer lugar, quisiera agradecer a mi madre Mireya, sin cuyo apoyo yo hoy no sería ni la mitad de lo que soy. A mi hermana Ángela y mi cuñado Ronall, quienes, junto con mi madre, siempre han creído en mí, incluso en circunstancias en las que ni siquiera yo sabía de lo que era capaz. También quisiera agradecer a mis directores de tesis por su constante aliento y guianza. A Carlos, cuya ambición me enseñó que hay que soñar en grande para lograr al menos una parte de lo que se quiere. A Marcela, cuya determinación me ensenó que es necesario hacer imponer tu voz si sabes que tienes algo qué aportar, y quien es un ejemplo de superación para toda mujer que quiera destacarse en el campo científico. De igual forma, quiero manifestar el inmenso aprecio y agradecimiento que le debo a mis compañeros de laboratorio, quienes me acompañaron tanto durante las largas jornadas de trabajo, como fuera del horario laboral. Con ellos viví dos años llenos de experiencias memorables que me enseñaron que nada se logra sin sacrificio, y que un poco de diversión de vez en cuando ayuda a sobrellevar la "exacerbación" en la que vivimos día a día. Gracias por soportar constantemente mi estrés y desaliento, por lidiar con mis imprudencias y por siempre estar ahí. Gracias a Alejandro, Andrés, Carlos, Daniel, Diego, Felipe, Jonathan, Luis, María José, Margarita, Nathalia, Orión, Pips, Sergio y Tim.

This thesis has been possible thanks to the support of the Colombian administrative department of science and technology *Colciencias* (grant ID No. 801-2017), CYTED research network REASISTE (grant 216RT0505), and funding from the Colombian School of Engineering Julio Garavito. Special thanks to the EPF EPF École d'ingénieur, in particular to Dr. Maxime Bourgain and Thoma Provot, for opening the doors of their laboratory to conduct the performance evaluation of the AGoRA exoskeleton and for being always avaible for the data handling.

Without a doubt, a great number of people has influenced to some extent to make this work come to its end. Firstly, I would like to thank my mother Mireya, without whose support I would not even be half of what I am now. To my sister Ángela and brother-in-law Ronall, who, together with my mother, have always believed in me, even in situations where I was not aware of what I was capable of. I would also like to thank my thesis supervisors for their constant encouragement and guidance. To Carlos, whose ambition taught me that you have to dream big if you want to accomplish at least part of what you wish. To Marcela, whose commitment taught me that you are obliged to speak up if you know your ideas are worth it, and who is a true example of perseverance and effort for young female scientists. Also, I wish to express my great gratitude and appreciation for my laboratory colleagues, who accompanied me during long working hours, as well as out of them. With them, I lived two years full of memorable experiences that taught me that nothing comes without sacrifice and that a bit of fun can help to cope with day-to-day problems. Thanks for standing my stress and dismay, for dealing with my indiscretions, and for always being there. Thanks to Alejandro, Andrés, Carlos, Daniel, Diego, Felipe, Jonathan, Luis, María José, Margarita, Nathalia, Orión, Pips, Sergio, and Tim.

Abstract

In the past years, robotic lower-limb exoskeletons have become a powerful tool to help clinicians improve the rehabilitation process of patients who have suffered from neurological disorders such as stroke and spinal cord injury. These robotic devices have emerged as a promising alternative to restore gait and improve motor function by applying intensive and repetitive training. However, active subject participation is considered to be an important feature to promote neuroplasticity during gait training. To this end, the present study presents the development of two high-level control strategies in the AGoRA exoskeleton, a wearable device designed to assist overground walking by actuating five degrees of freedom at the knee and hip joints. The proposed control approaches rely on an admittance controller to render velocity profiles according to the human-robot interaction forces, thus complying with the assistance-as-needed rationale, i.e. an assistive device should only intervene when the patient needs it. As a proof of concept of these control strategies, a pilot study was carried out to evaluate their short-term effect on the gait pattern of healthy subjects. No significant difference with respect to the unassisted condition in terms of spatiotemporal gait parameters and lower-limb kinematics proves the device to be compliant enough not to vary the typical walking behavior of able-bodied subjects. Future work should focus on the improvement of the fastening system and the robust tuning of the controller constants in pursuit of kinematic compatibility and enhanced compliance.

Keywords: Robot-Assisted Gait Training, Lower-Limb Exoskeleton, Stroke, Gait Phase Detection, High-Level Control Strategy, Assisted-As-Needed.

Glossary

AAN Assisted as Needed.

ADC Analog-Digital Converter.

ADL Activities of Daily Living.

AFO Ankle-Foot Orthosis.

AGoRA Development of an Adaptable Platform for Gait Rehabilitation and Assistance.

AM Assistance Mode.

BWS Body-Weight Support.

BWSTT Body-Weight Supported Treadmill Training.

CAN Controller Area Network.

CNS Central Nervous System.

Colciencias Colombian Administrative Department of Science, Technology and Innovation.

CP Cerebral Palsy.

CVA Cerebrovascular Accident.

DANE Colombian National Administrative Department of Statistics.

DoF Degree(s) of Freedom.

EMG Electromyography.

Escuela Ing. Colombian School of Engineering Julio Garavito.

FDA U.S. Food and Drugs Administration.

FEA Finite-Element Analysis.

FF Flat Foot.

FFw Feedforward.

FO Forward-Only Viterbi.

FSR Force Sensitive Resistors.

G Goodness Index.

GMM Gaussian Mixture Model.

GPDS Gait Phase Detection System.

GRF Ground Reaction Force.

HMM Hidden Markov Model.

HO Heel Off.

HREI Human-Robot-Environment Interaction.

HRI Human-Robot Interaction.

HS Heel Strike.

IC Initial Foot Contact.

IMU Inertial Measurement Unit.

LM Learning Mode.

OD Object Dictionary.

PPR Pulses per Revolution.

QUEST Quebec User Evaluation of Satisfaction with Assistive Technology.

RLCPD Registro para la localización y caracterización de personas con discapacidad.

RM Replay Mode.

RoM Range of Motion.

ROS Robot Operative System.

SCI Spinal Cord Injury.

SDO Service Data Object.

SEA Series Elastic Actuator.

SP Swing Phase.

SPT Standardized-Parameters Training.

SSH Secure Socket Shell.

SST Subject-Specific Training.

TB Threshold-Based Detection Algorithm.

TM Transparency Mode.

TNR True Negative Rate.

TO Toe Off.

TPR True Positive Rate.

URDF Universal Robot Description Format.

WHO World Health Organization.

List of Tables

List of Figures

Contents

Chapter 1

Introduction

The work presented here focuses on the development and preliminary validation of a human-robot interaction (HRI) strategy aimed to be implemented in the AGoRA lower-limb exoskeleton. Some crucial HRI concepts are addressed in the design of this exoskeleton to ensure natural communication channels between the user and the assisting device. A preliminary study, in which the developed control strategies are evaluated in healthy subjects, is also presented in this thesis document. This chapter comprises the motivation of this study and the research objectives. Additionally, the main contributions of this work and the document structure are included at the end of the present chapter.

1.1 Motivation

Different neurological pathologies, such as stroke, spinal cord injury (SCI) and cerebral palsy (CP), may affect human mobility to a total or partial extent. Particularly, the cerebrovascular accident (CVA) or stroke is considered to be a leading cause of severe disability in the US and Europe [1] with an estimation of at least 70 million victims suffering from this pathology around the world by 2030 [2]. Stroke survivors may

suffer from neurological deficiencies, such as hemiparesis, communication disorders or cognitive deficits [3]. Furthermore, according to recent studies, the incidence rate of SCI has been found to range between 250.000 and 500.000 people worldwide [4]. SCI victims might experience physical complications such as skin breakdown, muscle atrophy, and pain [5], in addition to being unable to walk, which leads to an increased risk of depression and the reduction of their life quality [6]. With the emergence of such neurological injuries, parts of the sensory-motor control loop responsible for locomotion may be disrupted, and the necessity for interactive solutions for these people with motor disabilities in need of daily assistance arises.

By addressing the problematic of lower-extremity impairments from a worldwide perspective, a survey from the United Nations has revealed that people older than 60 years represented $\sim$13% of the global population in 2017, and the growth rate of such a population is estimated at about 3% per year [7]. On this basis, one may infer that this aging behavior might progressively result in stronger pressure on health care budgets since nearly three-quarters of all strokes occur in people older than 65 y.o. [8] and the estimated cost of stroke in 2010 for the US was $73.7 billion (mean lifetime cost for an ischemic stroke of $140.048) [1]. Concerning mobility recovery, the proportion of patients reaching independence by 1 year after stroke ranges between 10% and 15% in a residential clinical institution [9], which underlines the lack of new strategies to promote, maintain and rehabilitate functional capacities of individuals with disabilities. By implementing such strategies, the attendance requirements and costs that these conditions pose to the patient, rehabilitation centers and society might be reduced [10].

This problem is even more evident in low and middle-income Latin American countries, where the disability rate has proven to be even greater compared to developed countries, according to a study conducted in 54 countries around the world [11]. By means of a survey containing 4 questions on functional limitations and a comparison with the world report on disability conducted by the World Health Organization

(WHO) in 2007, it is possible to envision the current panorama of disability in Latin America. Brazil, the Dominican Republic, and Ecuador take the first places on disability rate, with 16.8%, 11.8%, and 10.5%, respectively; whereas, in Colombia, the general population census carried out by the National Administrative Department of Statistics (DANE) revealed in 2005 that there are as many as 2.6 million people with permanent disabilities (6,3% of the total population). Out of this minority, 29.3% experience mobility-related difficulties with Vichada, Boyacá, and Nariño being the Colombian departments with the greatest mobility-related disability rate (each with over 1.5%) [12]. Despite the fact that these statistics on disability are more encouraging for the Colombian scenario, only 1 million people with disabilities are registered with the "Registro para la localización y caracterización de personas con discapacidad" (RLCPD, abbreviated in Spanish) [13], which makes an increase in the efficiency of national rehabilitation programs mandatory for ethical and financial reasons.

New technologies, early discharge after intensive training, and home rehabilitation are among the innovations proposed to achieve this aim [14]. Current literature suggests that rehabilitation interventions are more effective if they ensure early, intensive, task-specific and multisensory stimulation, thus favoring brain plasticity, i.e., the functional restoration of affected limbs through the reorganization of neuronal circuits [15, 16]. In fact, there is growing evidence proving that, particularly in the first 3 months of recovery after stroke, the motor system is plastic and motor training can be of great aid [17]. For the sake of physical therapy, assistive robotic devices have lately appeared as a potential rehabilitation solution since they are able to increase stability while empowering the user [18] and relieving the therapist's workload at a reasonable cost [19].

In recent years, a new category of lower-extremity orthotics, known as robotic lower-limb exoskeletons, has come along to integrate technology, electronics, and mechanics for purposes of physical rehabilitation [20]. The main goal of such powered assistive devices is to interface with the residual neuromusculoskeletal structures, so that the

human support, control, and actuation loops are reconnected. A robust control system for such orthoses is therefore recommended, in order to take into account the HRI and consistently accommodate gait patterns that are potentially far-removed from the nominal condition [21]. This provides the immediate benefit of reenabling locomotive activities of daily living (ADL), and potentially the long-term benefit of rehabilitating and retraining abnormal gait patterns over time [22].

In spite of the mentioned promising potential of the robotic rehabilitation technologies, which would undoubtedly improve the patient's quality of life, their benefits are still to be explored through research. Within this context, the Colombian Ten-Year Plan for Public Health (2012-2021) [23] also aims to develop a model of comprehensive health care for people with disabilities which guarantees rehabilitation focused on their own characteristics and needs. The AGoRA lower-limb exoskeleton, which is framed within the AGoRA project, intends to contribute to these ends by promoting feasible rehabilitation alternatives based on compliant HRI strategies.

1.2 Framework

This thesis is developed in the context of the project "Development of an Adaptable Platform for Gait Rehabilitation and Assistance" (AGoRA), supported by the Colombian Administrative Department of Science, Technology and Innovation *Colciencias* (grant 801-2017), CYTED research network REASISTE (grant 216RT0505), and funding from the Colombian School of Engineering Julio Garavito (Escuela Ing.). This project is mainly led by Dr. Carlos A. Cifuentes (professor of the Dpt. of Biomedical Engineering, research group *GiBiome* and head director of the *Center for Biomechatronics* at Escuela Ing.) and receives collaboration from the main clinical partner in this project "Clínica Universidad de la Sabana", and international research groups around the world: the Group of Neural and Cognitive Engineering from the Spanish National Research Council (led by Dr. Eduardo Rocon), the Automation Institute of

San Juan, Argentina (led by Dr. Ricardo Carelli), and the Group of Robotics and Industrial Automation from the Federal University of Espírito Santo in Vitória, Brazil (led by Dr. Anselmo Frizera).

The main purpose of this project is the development of a gait rehabilitation platform comprised by: (i) a smart walker, and (ii) an active lower-limb exoskeleton, controlled by a multimodal interface which serves as a communication channel among the patient, the health professionals, and the rehabilitation therapy. Additionally, a second interface is expected to sense information from the environment and ensure safe navigation within the rehabilitation setting by taking into account the human-robot-environment interaction (HREI). Fig. 1.1 shows a sketch with the main components of this platform such as a common microcontroller, actuation mechanisms (e.g., construction motor-encoder-gearbox), and sensors in charge of assessing human's performance (e.g., electromyography (EMG) sensors), measuring the HRI (e.g., strain gauges and triaxial force sensors) and HREI (e.g., laser range finder (LRF) and video camera).

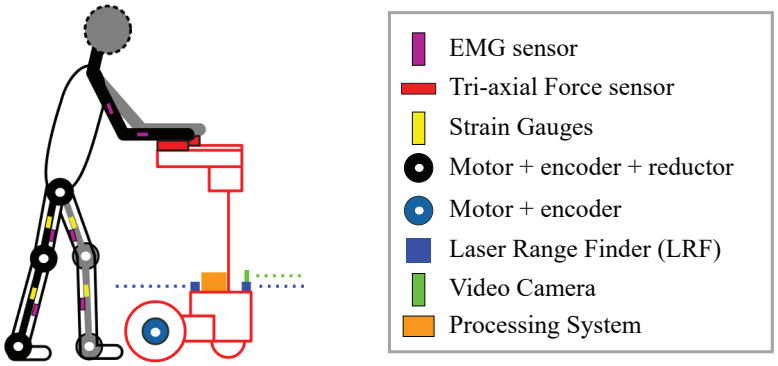

Figure 1.1: *AGoRA project.* Development of an adaptable platform for gait rehabilitation and assistance, which comprises a processing system, actuation mechanisms, and sensors for HRI and HREI.

Within this context, the present project intends to make a breakthrough in rehabilitation therapies and robotic gait assistance, improving the conditions of bioinspiration and interaction with the environment of the devices found in the literature. This project also proposes a framework for the training of teachers and young Colombian

researchers in the field of rehabilitation robotics and seeks to answer the following research question: Is it possible to perform a more efficient gait rehabilitation, with better results than traditional therapies, implementing an adaptable robotic platform?

1.3 Objectives

The main goal of this thesis is to implement high-level control strategies on a modular lower-limb exoskeleton and validate its functionality in healthy subjects to answer the following research question: what are the most significant effects of the AGoRA exoskeleton on the gait pattern of male healthy subjects? Along with the primary objective, some specific objectives are presented below.

- Conduct a systematic literature review to understand the human control of postural balance, and the different mechanisms that help towards overcoming mobility impairments.
- Control the actuation mechanism based on electric motors by means of a low-level approach and achieve the integration of different sensing devices oriented at the HRI, e.g. strain gauges, inertial measurement units (IMU), and encoders.
- Develop a state-of-the-art high-level control strategy for ensuring an appropriate HRI between the exoskeleton and its user, and implement it with the ready available hardware.
- Evaluate the short-term effects of the final system on healthy users without any mobility impairments.

1.4 Contributions

This thesis mainly contributes to the AGoRA project, which primarily focuses on the development of an adaptable platform for gait rehabilitation and assistance. By

conducting this master thesis, a series of technical and scientific contributions are obtained:

1. The design and implementation of a low-level software architecture mounted on the Robot Operating System (ROS) which integrates the AGoRA exoskeleton's sensory interface and actuation mechanism. Such architecture was constructed in such a way that it initializes each connected module (e.g., the actuation mechanism and sensors at each exoskeleton joint), and set their corresponding configuration parameters. This allows the device to be modular, by only assisting the human joints that have been affected.

2. The design and validation of a machine-learning-based gait phase detection algorithm which only makes use of a single IMU placed on the dorsal side of the foot to accurately segment the gait cycle. This partitioning method is used as the middle layer of the overall control architecture whose output is used to actuate the exoskeleton in accordance with each user's gait pattern.

3. The design and implementation of several high-level control strategies, known as Assisted-As-Needed (AAN), which take into account the user's motion intention to move the actuation mechanisms only when the user needs it. By estimating the interaction force between the mechanical structure and the subject via strain gauges, admittance-based controllers make a non-backdrivable device more compliant to the user's movements.

4. The overall electronic construction and the preliminary evaluation of the robotic lower-limb exoskeleton "AGoRA" meant for gait rehabilitation, which will be of great help for other master students who will be completing their thesis within the AGoRA project.

5. The implementation of this device also presents a promising potential as a rehabilitation alternative that will be further validated once long-term trials with pathological subjects are conducted within a clinical setting.

1.5 Document Organization

This master thesis document specifically comprises the mechanical, electronic and control design of the AGoRA exoskeleton. Additionally, it presents the experimental trials conducted with six healthy subjects as a preliminary evaluation of the different types of control implemented on the device. The document is organized in 7 chapters. Chapter 1 presents the motivation of the present work and its main objectives and contributions. Chapter 2 summarizes the main causes of mobility impairments and the state of the art of currently-available rehabilitation alternatives, ranging from conven-

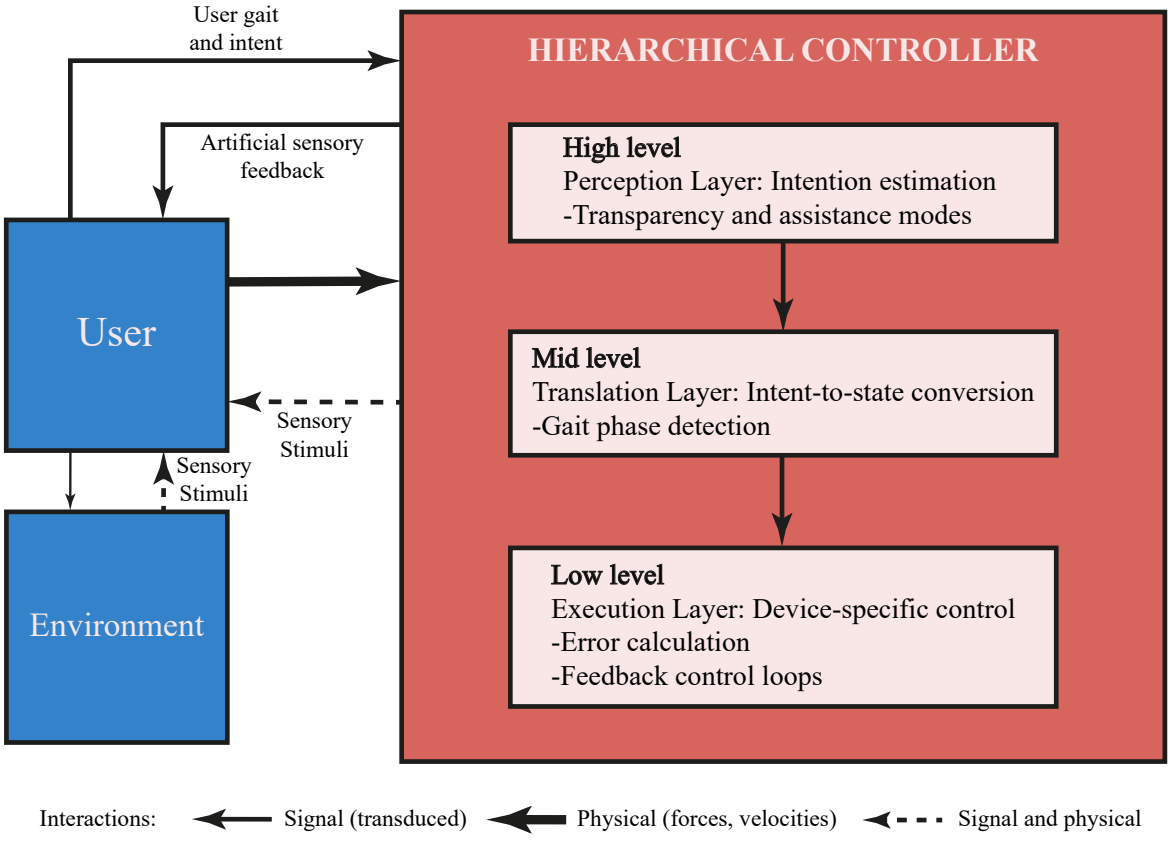

Figure 1.2: *Generalized control framework of the lower-limb exoskeleton AGoRA*. The proposed framework illustrates the physical and signal-level interactions among the powered orthotic device, its user and their environment. A hierarchical control structure is implemented with the estimation of the user's locomotive intent taking place at the high level and a device-specific controller responsible for accomplishing the desired device state at the low level. Adapted from [22].

tional therapy to robot-assisted gait training. Chapter 3 describes the hardware and low-level control architectures implemented in the AGoRA exoskeleton (see *Low level* in Fig. 1.2), which integrates the actuation mechanism and different sensors in such a manner that the device joints may be arranged depending on each user's requirements. A middle layer of the control system, consisting of an online machine-learning-based gait phase detection algorithm, is included in Chapter 4 (see *Middle layer* in Fig. 1.2). Chapter 5 further addresses the proposed high-level control strategies that take into consideration the human-robot force interaction to intervene just when it is mandatory (see *High level* in Fig. 1.2). The preliminary validation of the implemented control strategies in healthy subjects and the analysis of the outcomes of such trials are presented in Chapter 6. Finally, Chapter 7 gathers the main conclusions of this work and some future work planned for the use of the AGoRA exoskeleton in the clinical setting.

Chapter 2

Assistive Devices: Human Mobility and Gait Rehabilitation

2.1 Introduction

Mobility is one of the most important human faculties and can be defined as the ability of an individual to freely move through multiple environments and perform activities of daily living (ADL) with ease [18, 24]. Following a neurological dysfunction, such as stroke, mobility may be affected and only a short-time period might remain to take advantage of the inherent adaptability and plasticity of the central nervous system (CNS) [17]. Reestablishing effective mobility for individuals with lower-limb impairments is often a complex challenge and frequently involves the interdisciplinary efforts of many medical, surgical, and rehabilitative specialists [25]. Thus, robotic-based training is considered to be a potential aid, not only for patients but for health-care professionals as well.

This chapter provides a brief overview of some of the most common lower-limb neurological dysfunctions which may lead to some level of disability, and the loss of quality of life and independence. This summary mainly focuses on those conditions which

impair mobility and the different treatment strategies and assistive devices currently used to overcome the subsequent limitations.

2.2 Causes of Mobility Impairment

Several conditions affect mobility and understanding their implications at different cultural and socio-economical levels is crucial to propose novel therapeutic alternatives. Therefore, a brief description of the most common walking diseases is included hereunder. These conditions include, but are not limited to, stroke, Spinal Cord Injury (SCI), Cerebral Palsy (CP) and aging. Their physiological, functional, social and economic impacts highlight the importance of rehabilitation for promoting gait restoration.

2.2.1 Cerebrovascular accident (CVA) or Stroke

Brain damage occurs when the blood supply stops flowing to the brain, resulting in the rapid death of brain cells. If oxygen and glucose are not restored soon, the brain starts experiencing irreversible damages. This loss of brain functions due to insufficient blood flow is known as stroke [26]. Risk factors include age, hypertension, diabetes, high cholesterol, smoking, sedentary lifestyle, overweight and atrial fibrillation [27]. Stroke can be either ischemic and hemorrhagic, with the ischemic type being the most prevalent category ($\sim 85\%$ of all cases) [28].

Stroke is considered to be one of the most significant causes of disability in adults worldwide, affecting mobility during ADL, as well as communication and cognition [29]. As a result of this condition, compensatory mechanisms may come along to counteract the loss of structure and function post-disease. Chronic stroke often results in contralateral hemiparesis or hemiplegia, i.e., the weakness or paralysis on one side of the body, respectively [25]. Furthermore, several spatiotemporal and kinematic parameters are affected by the appearance of the stroke, which include speed decrease,

timing asymmetry, shorter stride and step length, impaired swing initiation, and weakness in the hip flexor, quadriceps and plantarflexor muscles. In addition, CVA might provoke different gait disorders, such as foot drop, alterations in postural stability, spasticity (i.e., velocity-dependent resistance to sudden passive movement), increased risk of falls, reduced dexterity, fatigability, ankle dorsiflexion and knee flexion limited or absent in swing phase, and reduced hip flexion [30–32].

Regarding the post-stroke recovery rate, a 2008 study carried out in Italy (involving up to 500 study subjects) showed that about 45% of patients with stroke leave the rehabilitation unit on a wheelchair, less than 15% are able to walk indoor without aids, less than 10% are able to walk outdoors, and less than 5% are able to climb stairs [33]. Thus, the widely-recognized problem of stroke is not death, but motor impairment, which makes the CVA a serious global health-care problem that costs more than 4% of the total health-care expenses in developed countries [34].

2.2.2 Spinal Cord Injury (SCI)

SCI is the consequence of damage in the spinal cord nerves, either temporary or permanent, and can affect the motor, sensory and autonomic function. Depending on where the spinal cord and nerve roots were damaged, the severity level may be classified into complete (total loss of function) or incomplete (which can vary from having no effect on the patient to severe mobility impairment) [30, 35, 36]. This condition significantly compromises spatiotemporal and kinematic parameters, so that SCI victims may suffer from reduced cadence, short stride length, reduced knee excursion, weakness in quadriceps, and hip and knee flexor muscles, excessive co-activation of antagonist muscles, and hyperactive stretch reflexes. Additionally, gait disorders, e.g., impaired balance, increased risk of falls, foot drop and abnormal muscular tone, may appear post-SCI [30, 31, 35].

Since there exist no interventions able to promote regeneration of spinal cord nerve

pathways nowadays [37], the aim of rehabilitation interventions for such patients is mostly focused on helping them to achieve greater autonomy in daily life. In most cases, this is made through the use of a wheelchair, which is currently the main tool capable of helping SCI patients to regain a degree of mobility, even though the pursuit of greater independence can be often hindered by obstacles, both physical and psychological [37].

2.2.3 Other Conditions

Cerebral palsy (CP) is related to a non-progressive movement and posture development disorder, attributed to a defect or lesion in the brain that appears in infancy or early childhood [38]. CP is often associated with different physical and associative dysfunctions such as sensory deficits, cognitive impairment, communication and motor disabilities, behavior issues, seizure disorder, pain, and secondary musculoskeletal problems [38, 39]. The Centers for Disease Control and Prevention in the United States have estimated that the lifetime cost to care for an individual with CP is nearly $1 million (2003), and the combined lifetime costs for all people with CP who were born in 2000 will total $11.5 billion in direct and indirect costs [40].

On top of the above-mentioned CNS dysfunctions, the continuous aging tendency has become a global issue due to the socio-economical implications produced by the impact of physical deterioration in elderly people on health-care systems around the world. By the year 2050, the aging problem is expected to be even worse since the proportion of the world's population over 60 years will nearly double from 12% in 2015 to 22% [41]. The frailty of elderly people is reflected by reduced daily physical activities such as walking less because of significantly reduced muscle mass and strength. In the worst-case scenario, their muscles could further deteriorate and an accelerated decline of the neuromusculoskeletal systems may occur [8, 42]. Particularly, one-fourth of all SCIs [25] and nearly three-quarters of all strokes [8] occur in people older than 65 y.o. This relevant issue highlights the need for new affordable and practical rehabilitation

strategies that can be deployed in the context of developing countries.

2.3 State of the Art of Gait Rehabilitation

The present review on gait rehabilitation is mainly focused on therapy approaches for stroke patients since the requirements for promoting neural plasticity should be taken into account in the design and implementation of control strategies in the AGoRA exoskeleton.

2.3.1 Traditional Therapy

At present, gait rehabilitation is mostly based on physical therapy interventions with robotic-based training still only seldom employed. Regardless of the specific technique, each approach requires customized preparatory exercises, physical therapist's observation and direct manipulation of lower limbs during gait over a regular surface [16]. According to the theoretical principles included in a Cochrane review in 2007, neurological gait rehabilitation can be classified into two main categories: neurophysiological and motor learning [43].

In the neurophysiological technique, the therapist acts as a problem solver and decision-maker by supporting the correct movement patterns, so that the patient is a relatively passive recipient [16]. Among the neurophysiological approaches, Bobath stands as the most widely accepted treatment in Europe. This method consists of trying to inhibit increased spasticity by passive mobilization associated with tactile and proprioceptive stimuli [44].

The motor learning approaches, on the other hand, encourage active patient involvement [16], thus making patient cooperation a prerequisite and the neurophysiological assessment a mandatory feature. Since therapy should target each patient's specific needs, task-specific and context-specific training are widely-acknowledged principles

in the motor-learning framework. Although several neurorehabilitation techniques have been developed to restore neuromotor function by involving therapist guidance for support and demonstration (instead of providing sensory input), tailored methods for specific pathologies and subjects are still considered to be the gold standard [16]. Within this context, the combination of rehabilitation devices and conventional approaches appears to be more effective than over-ground gait training alone in the recovery of independent walking in the sub-acute phase of stroke (especially within the first 3 months after CVA) [45, 46].

2.3.2 Rehabilitation Machines

A rehabilitation machine is a mechatronic system able to support the therapist during the administration of customized rehabilitation programs. There are different types of gait rehabilitation devices which can be basically classified into two categories: alternate and augmentative devices [47]. The alternate devices are mainly used by individuals with total disability or very limited mobility. They do not generally exercise the affected lower limbs, e.g., wheelchairs or autonomous special cars [48]. On the contrary, the augmentative devices are primarily aimed at individuals with reduced mobility, but who can generate some movements that are useful for their rehabilitation process [47]. The latter will be the main focus of this section.

Robot-assisted gait therapy relies on a robotic orthosis to help the patient retrain motor coordination by undertaking carefully directed, repetitive, task-specific motor activities [49]. The history of robot-assisted training started with the adaptation of industrial robotic actuation mechanisms to the field of rehabilitation and evolved to more advanced robotic devices that can be divided into exoskeletons (or active orthoses) and end-effector-based systems [50]. Exoskeletons and active orthoses can be considered wearable robots, and present a slight difference between them. The term exoskeleton generally refers to a mechanical device that is able to enhance its user's strength and endurance. Conversely, an active orthosis is a device with powered

actuation, usually used to modify or recover lost motor functionalities. However, this distinction is not clear-cut [51], and for the case of this document, both terms are used interchangeably.

Lower-limb exoskeletons are primarily developed for three main applications nowadays. The first application of exoskeletons is aimed at enhancing the physical abilities of able-bodied subjects (i.e., human strength augmentation) [51]. The second application is human locomotion assistance, which is frequently targeted at paralyzed individuals who have lost lower-limb motor and sensor function [52]. And finally, the third application focuses on gait rehabilitation, i.e., helping people with mobility impairments in the restoration of musculoskeletal strength, motor control, and gait [51].

Since the repetitive movements performed by therapists during gait training represent a tiring job because they have to manually move the patients' paretic legs continuously, rehabilitation robotics appears as an opportunity to increase the sustaining time of each training session [37, 53] while easing the workload of health specialists and closely monitoring the patient's progress throughout treatment [37]. Preliminary findings suggest that exoskeletal gait training is equivalent to traditional therapy in chronic stroke patients, whereas sub-acute survivors may experience further benefits from robotic-based gait training [5]. Although the robotic gait method has shown improved patient outcomes, there is not yet enough statistical evidence to assure a definitive advantage of robotic training [37].

Within this context, a thorough literature review on the most cited lower-limb active exoskeletons was carried out in Scopus, Web of Science and Pubmed till May 2019. Different pathologies were included in this literature search even though the present work mainly focuses on stroke rehabilitation since the assistive strategies applied in other frameworks might contribute to the control paradigm addressed in this work. Further sections comprise the devices mentioned most frequently in the literature while

classified into two main categories, namely stationary and ambulatory rehabilitation machines. The following search terms were used in this study to conduct the mentioned literature review:

$$\{\text{leg} \vee \text{hip} \vee \text{knee} \vee \text{ankle} \vee \text{foot} \vee [\text{lower} \wedge (\text{limb}^* \vee \text{extremity} \vee \text{body})]\} \wedge (\text{robot}^* \vee \text{exoskeleton} \vee \text{“powered orthosis"}) \wedge (\text{stroke} \vee \text{CVA} \vee \text{“cerebrovascular accident"} \vee \text{“cerebral infarct"} \vee \text{hemiplegia} \vee \text{hemiparesis} \vee \text{paraplegia} \vee \text{paralysis} \vee \text{SCI} \vee \text{“spinal cord injury"} \vee \text{“cerebral palsy"}) \wedge (\text{gait} \vee \text{walk}^* \vee \text{ambulation})$$

2.3.2.1 Stationary Rehabilitation Alternatives

The stationary systems mainly consist of a fixed structure and a mobile ground platform (e.g., treadmill or footplates). The treadmill approach uses a robotic device connected to the patient's lower limbs together with a body-weight support (BWS) system, fundamental to off-load a part of the patient's weight, whilst programmable footplates simulate the gait phases [54]. There is conflicting evidence proving that treadmill-based robotics might not be as effective as conventional therapy or body-weight supported treadmill training (BWSTT), since pre-set belt speed creates an environment where patients do not self-initiate gait and there is a lack of variability in visuospatial flow (highly present in overground gait) [5, 55].

2.3.2.1.1 Lokomat

Lokomat [57] (Hocoma, Switzerland) is the best-selling commercial gait rehabilitator and trainer for clinical patients nowadays. It is a robotic device consisting of a powered orthosis with integrated computer-controlled linear actuators at each hip and knee

Figure 2.1: Lokomat. Extracted from [56]

joints, BWS and a treadmill (Fig. 2.1). Gait pattern and guidance force are adjusted depending on the patient's needs to optimize the functional training in the sagittal, frontal and transverse planes [54]. The orthosis has 4 Degrees of Freedom (DoF) in total, and the hip and knee joints are actuated by linear drives to assist along the sagittal plane. Force sensors mounted between the actuator and the orthosis measure force interaction [8]. Lokomat also possesses an augmented feedback module which offers the possibility to provide stimulating, interactive and direct feedback to the patient by displaying the results of the exercises on a screen to enhance patient motivation. By adjusting the level of difficulty, training sessions can be tailored to each subject's specific requirements [54]. The effectiveness of Lokomat in gait rehabilitation for neurological patients has been verified through worldwide clinical studies [57].

2.3.2.1.2 LOPES

The Lower Extremity Powered ExoSkeleton (LOPES) [59] (University of Twente, Netherlands) is a robotic device that assesses motor skills and assists stroke patients in stroke rehabilitation (Fig. 2.2). LOPES uses the concept of series elastic actua-

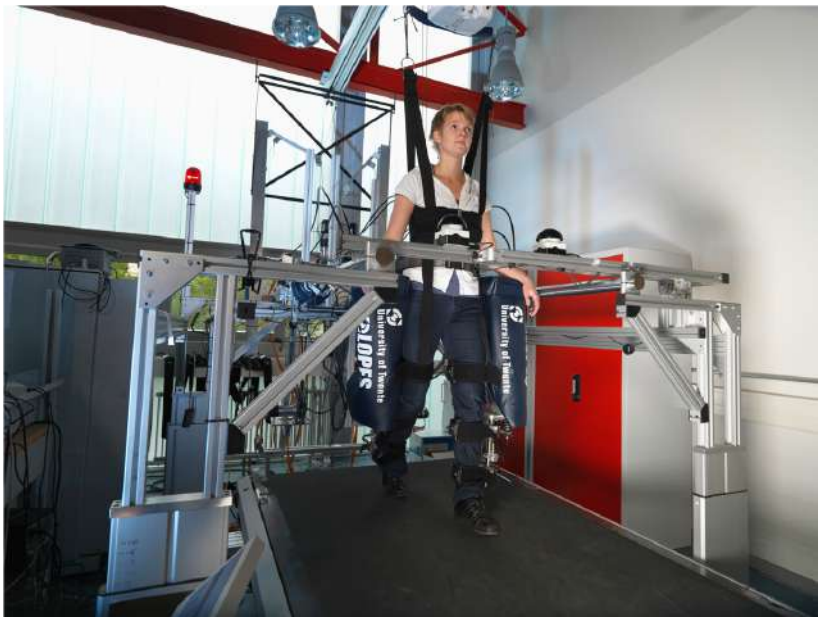

Figure 2.2: LOPES. Extracted from [58].

tors (SEA) based on a Bowden-cable-based actuation mechanism [19]. Three actuated rotational joints and a great number of DoF on the exoskeleton offer a wide range of possibilities to adjust the support to each individual and to regain motor function [54]. Different from other orthoses, LOPES is connected to the fixed world at pelvis height, so that its weight can be compensated and corrective joint torque can be applied to the patient's pelvis [50]. Two gait training modes have been used by LOPES, namely patient-in-charge (unhindered walking) and robot-in-charge modes (fully-passive walking) [19]. The impedance-based control implemented in this device has proven to be beneficial in chronic incomplete SCI patients, improving speed, walking distance, spatio-temporal parameters and hip range of motion (RoM) [58].

2.3.2.2 Ambulatory Rehabilitation Alternatives

Overground walking systems follow the patient's walking movements and allow them to move under their own control through an autonomous wearable robot, rather than moving only according to predetermined movement patterns [54]. Overground gait training, in comparison with BWSTT, has the potential of higher therapeutic outcomes

due to its associated biomechanics being close to that of natural gait [60]. Moreover, these devices present additional advantages in the rehabilitation field on account of the task-specific training associated with this robot-based approach and how it encourages the patient's involvement during therapy [37].

2.3.2.2.1 Rewalk

Figure 2.3: ReWalk. Extracted from [60].

The ReWalk (Argo Medical Technologies, Israel) was the first exoskeleton suit cleared by the U.S. Food and Drug Administration (FDA) in 2014 to be used as a personal device at home (Fig. 2.3). Currently, ReWalk also has the capacity for stair climbing/descent but this feature has not been yet approved by the FDA and is not available outside the research environment [52]. The exoskeleton is controlled by on-board computers carried in a backpack on one's shoulders, encourages self-initiated gait by sensing the forward tilt of the upper body through a motion sensor, and mimics the typical gait pattern [8, 54]. ReWalk is intended to be used with two Canadian sticks

to ensure the stability of standing and walking [54]. Moreover, clinical trials with this device have shown that paralyzed subjects are able to stand upright and walk with increased independence after undergoing therapy with it [61].

2.3.2.2.2 Ekso

Figure 2.4: Ekso. Extracted from [20].

Ekso (Ekso Bionics, USA) is a self-powered exoskeleton, able to increase the strength and endurance of the human being. In earlier stages, it was called the BLEEX and then eLegs. In April 2016, Ekso Bionics received approval from the FDA to market the device for SCI, and also for people with post-stroke hemiplegia (first FDA approval for use with stroke survivors) [62]. Ekso weighs 20 kg, has a maximum speed of 0.8 m/s and a battery life of 6 h and is suitable for users weighing up to 100 kg, who can transfer themselves from a wheelchair to a chair [54]. Similar to the HAL and ReWalk, Ekso bilaterally actuates the knee and hip joints [20] whilst the exoskeleton ankle joints allow passive spring movement limited to the sagittal plane. Ekso requires provided crutches whose bottoms are instrumented with force sensors so that a step will not be triggered unless both crutches are firmly held against the ground [63]. The feasibility for using it has been proven for SCI [64] and larger-scale clinical trials are

being undertaken around the world [8].

2.3.2.2.3 Vanderbilt Exoskeleton

Figure 2.5: Vanderbilt lower-limb orthosis. Extracted from [65]

The Vanderbilt lower-limb orthosis [66] (Vanderbilt University, USA) is designed to assist the hip and knee joints of SCI patients by means of two brushless DC motors on each thigh segment. Its total weight is 12 kg, which is relatively light compared to other similar exoskeletons [8]. The orthosis controller consists of four motion states: standing, right forward, left forward, sitting. For each state, the joint angles are pre-programmed based on recorded trajectories drawn from healthy subjects and transitions between states are triggered by user's vocal commands [65]. This orthosis has been implemented in patients with a T10 motor and sensory injury, enabling them to walk faster after 1 year of therapy with amplitudes of intervened joints similar to those of healthy subjects [67].

The main features of the above-mentioned lower-limb exoskeletons are summarized in Table 2.1 for both the stationary and ambulatory approaches.

Table 2.1: *Summary of stationary and ambulatory lower-limb active exoskeleton reviewed in the state of the art.* TBI: Traumatic Brain Injury, CoP: Center of Pressure, BMI: Brain-Machine Interface.

Exoskeleton	Application	Target Pathology	Actuated DoF	Actuator	Sensors	Control Strategy
Lokomat [8, 47, 54]	Gait rehabilitation	Stroke, SCI, TBI	Hip and knee flexo-extension (two legs)	Electric motors	Force sensors between actuators and orthosis	Impedance control and conventional PD controller
LOPES [47, 54, 59]	Gait rehabilitation	Stroke & SCI	Vertical and horizontal pelvis translation, hip and knee flexo-extension & hip abd/adduction	Servomotors and Linear Motors	EMG and torque sensors	Impedance control
ReWalk [8, 47, 54]	Human locomotion assistance	SCI	Hip and knee flexo-extension (double legs)	Electric motors	Series of sensors that measure upper-body tilt angle, joint angles and ground reaction	Closed-loop PID controller

Ekso [8, 47]	Gait rehabilitation & human locomotion assistance	Stroke, SCI, multiple sclerosis & CP	Hip and knee flexo-extension (double legs)	Electric motors	Force sensors at the bottom of crutches	Augmentative and progressive training
Vandelbilt [8, 65]	Human locomotion assistance	SCI	Hip and knee flexo-extension (double legs)	Electric motors	Accelerometers and joint angle sensors to estimate CoP in the sagittal plane	Predefined gait trajectory control

2.4 Conclusions

All currently existing lower-limb wearable robots have been developed aiming at assistance, i.e., they are configured in such a way that patients are able to rehearse a typical gait pattern (usually drawn from healthy subjects) while wearing such a device. The repetition of these predefined gait kinematics is expected to result in the improvement of motor function [37]. Robot-based training has an additional advantage with respect to conventional therapy, namely the online/offline quantitative, objective assessment of several parameters associated with the patient's performance during therapy [14]. Additionally, significant advances have been made in terms of the safety and portability of the lower-limb exoskeletons, the skills they train and the reduction of the effort needed to command them [64, 68].

In spite of the great number of advantages of the robotic-based gait training, the use of robots should not replace the neurorehabilitation therapy performed by a physiotherapist. Rehabilitation machines, as all technological devices, must be considered as tools available for the health professional and never rehabilitative per se [69]. The robot should alleviate the labor-intensive phases of physical therapy, thus allowing the physical therapist to concentrate on functional rehabilitation during individual training and to supervise multiple patients at the same time. With this approach, the expertise and time of qualified personnel are optimized, increasing the rehabilitation program's efficacy and efficiency [14, 70].

Even though these assistive and rehabilitation devices continue to improve, likely providing psychological and physical benefits, their inter-subject anticipated benefits are only starting to gather (mostly focusing on SCI) and need further research [5, 64, 68].

Chapter 3

Hardware and Control Architectures of the AGoRA Exoskeleton[1]

3.1 Introduction

Physical Human-Robot Interaction (HRI) involves the use of sensors, actuators, algorithms and control strategies that are capable of recognizing the complex human expressions and its physiological phenomena [71]. In considering the design of wearable robots, the physical interaction represents the most critical aspect, as any movement or force applied to the patient's body must be consistent with their capabilities [72]. Therefore, during the design process of an exoskeleton, one has to ensure that the data acquisition scheme is well-defined and that such a module is able to detect the device's current state, its interaction with the environment, and the HRI forces [72]. Apart from that, in order to interact with humans, wearable robots are expected to be flexible, adaptable, and, most importantly, safe. One of the benchmarks for achieving this goal is compliance. Compliance plays an important role in human adaptations

[1]Part of this chapter is based on the following conference proceedings:
Sanchez-Manchola, M., Gomez-Vargas, D., Casas, D., Munera, M., & Cifuentes, C. A. (2018). Development of a Robotic Lower-Limb Exoskeleton for Gait Rehabilitation: AGoRA Exoskeleton. In 2018 IEEE ANDESCON, ANDESCON 2018 - Conference Proceedings.

to environmental changes and securing stable gait [73]. However, compliance has not yet found its way into commercial wearable robots, which usually use direct-drive actuation due to its high bandwidth and controllability [74].

Based on these requirements, a thorough explanation of the hardware architecture and control system of any wearable system is important to understand its capabilities and justify the fulfillment of the target population's needs. This chapter aims at this end by presenting the mechatronic design and the low-level control architecture of the AGoRA exoskeleton.

3.2 Hardware Architecture

3.2.1 Mechanical Design

Bioinspiration has been extensively adopted in the development of wearable robots in recent years [20]. In particular, the bio-inspired exoskeleton proposed here is built in such a way that it possesses an anthropometric topology. The exoskeletons with anthropomorphic topology intend to resemble the human topology as much as possible. This is possible by taking into account the lower and upper-limb power trains, the DoF of each human joint of interest and the exoskeleton's dimensions, which must avoid bulkiness and high weight. These design criteria are meant to allow the assistive technologies to apply the right amount of assistance at the right time while maintaining normal human biomechanics.

The AGoRA exoskeleton is an active assistive device which is mainly intended as a rehabilitation tool for stroke patients, but that could be also used for gait compensation in patients who have suffered a spinal cord injury and present lower-limb paralysis as a consequence. It is primarily conceived for overground gait training in a clinical environment as a bilateral (unilateral, as the case might be), wearable device. The exoskeleton has 4 actuated DoF which correspond to the hip and knee flexo-extension

(i.e., movement along the sagittal plane), as shown in Fig. 3.1. The hip joint has an additional passive abd/adduction DoF which plays an important role in the lateral balance control [75]. This abd/adduction DoF is part of the originality of the present device since most robot-based assistive technologies frequently hinder this particular movement [20].

Although the Range of Motion (RoM) in the frontal plane is relatively small at the human hip joint ($\sim 10°$) [76], the hip abd/adduction DoF presents a high correlation between strength and gait velocity at a comfortable pace [77]. Thus, the abd/adduction axis on the exoskeleton consists of a self-aligning hinge that, in parallel with a composite material, conditions the user's hip RoM. This system tenses two composite

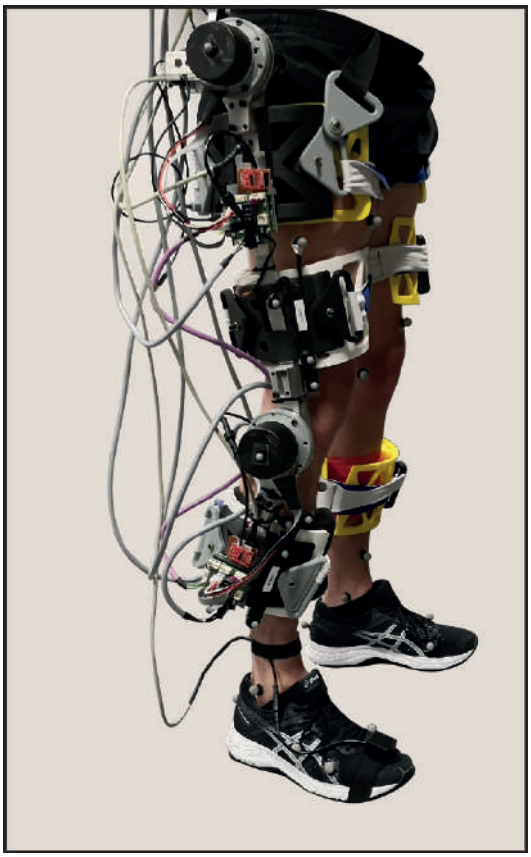

Figure 3.1: *Hip and knee joints of the AGoRA exoskeleton.* The human hip and knee joints are assisted in the sagittal plane, whilst a passive DoF in the frontal plane does not hinder the hip abd/adduction.

tendons (fishing rod around a 2.85 mm Filaflex thread) which are connected to a steel link for load transmission to the lateral structures, so that hip abd/adduction RoM is restricted within a nominal human range (as may be seen in Fig. 3.2).

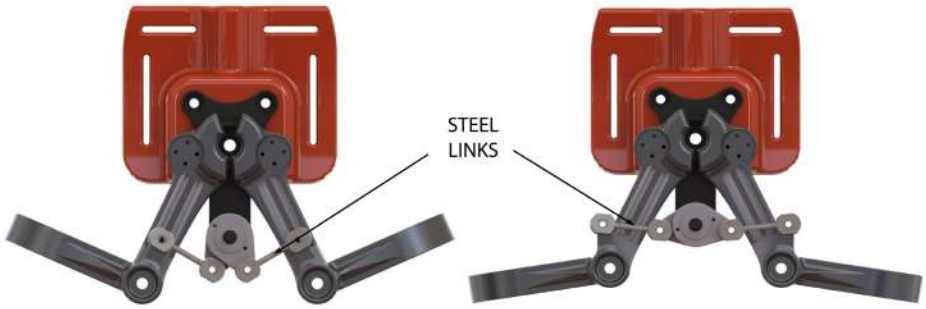

Figure 3.2: *Hip abd/adduction DoF of the AGoRA exoskeleton.* A passive variable-stiffness system, which utilizes composite tendons, enable such hip DoF with a certain level of stiffness.

As weight is a crucial aspect in the design and fabrication of wearable robots [21], choosing a light but high-resistant material is critical. For the case of this exoskeleton, most of its mechanical structure is made of duralumin, a material with both the mentioned properties and low corrosion (an important attribute for clinical settings). Even though this structure can be considered rigid, its design possesses a soft geometry, i.e., sharp points, sharp edges, and protrusions are avoided, so that stress risers disappear and aesthetics improve. These design criteria allow the device to have a total weight of 15 kg with the actuation mechanisms mounted on all hip and knee joints.

An assistive device is also intended to follow the wearer's kinematics by guaranteeing kinematic compatibility, i.e., the correct alignment of the exoskeleton hinges with the biological axes of rotation. Hence, another significant design factor is the adjustability of each link length [78]. To this end, the length of each exoskeleton segment can be adjusted to different anthropometric measures without losing functionality. Via a mechanism of two telescopic bars that can be pushed one inside the other, the thigh and shank segments can be adjusted to encompass a wide range of body dimensions. The setting spectrum covers heights ranging from 1.70 to 1.83 m, which satisfies most of the Colombian male population [79], and a maximum bodyweight of up to 90 kg

(loading capacity validated by means of a 3D finite-element analysis (FEA)).

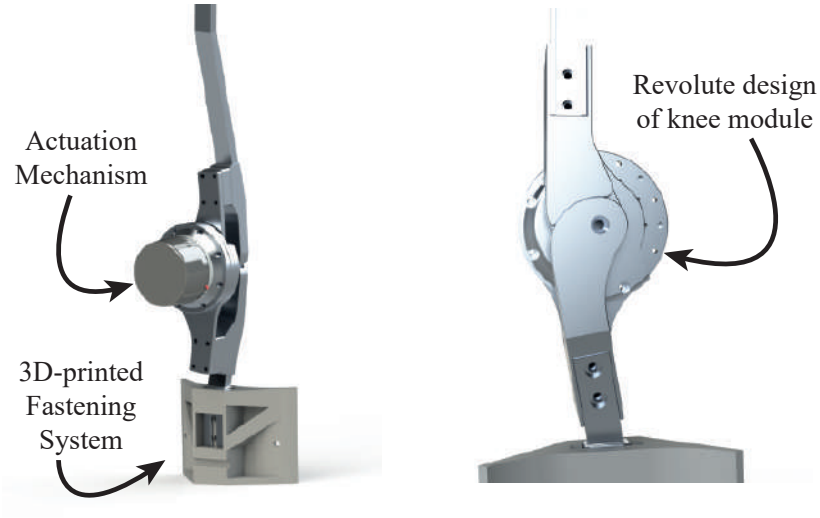

Figure 3.3: *Knee module of the AGoRA exoskeleton.* A 3D-printed fastening system ensures proper torque transmission of a motor-gearbox construction which serves as actuation mechanism on the exoskeleton knee module.

Moreover, another feature that contributes to reaching a proper transfer of torque is the fastening system, and its design must be undertaken on the basis of compliance, comfort, adjustability, and wear resistance [80]. In particular, adjustable rounded leg braces carriers with Velcro straps (see Fig. 3.3) were 3D-printed using a composition of PLA and carbon fiber (the latter being a highly stress-resistant material). The interface in contact with the user is also 3D-printed using TPU, which is a comfortable material that minimizes pressure against the user's skin and prevents injury [79]. The mechanical design described in this subsection has been conceived and become real thanks to the effort of an interdisciplinary team which includes mechanical engineers.

3.2.2 Actuation Mechanism

The main selection criteria used for the actuators of the AGoRA exoskeleton were the specific power (ratio of actuator power to actuator weight) and portability. In wearable robotics, different actuator technologies, e.g., electric, pneumatic, hydraulic and Series Elastic Actuators (SEA), are commonly used. Hydraulic and pneumatic actuators are

known for their high force density and high force or torque characteristics and have been used in many applications [81]. However, hydraulic and pneumatic actuators have the disadvantage of being bulky and requiring complex control systems. Conversely, SEA-based actuation involves an elastic element, usually a spring, placed in series with the actuator's output [82]. Nonetheless, the smooth coordination of force and position between patient and device still represents a challenge among different users for this type of actuators [83].

Based on the fact that electric motors provide a reduction in power consumption during gait [84], and, particularly, DC motors meet the criteria of necessary power with a compact and portable structure, a brushless flat DC motor (EC-60 flat 408057, Maxon Motor AG, Switzerland) (see Fig. 3.4a) coupled with a harmonic drive gear (CSD-20-160-2AGR, Harmonic Drive LLC, USA) (see Fig. 3.4b) were selected to be the actuation mechanism for the hip and knee joints of the AGoRA exoskeleton. This coupling of a harmonic drive to the motor shaft output was chosen because this construction provides more torque at lower speeds (gear ratio of 160:1) while preserving lightweight and reduced volume. The proposed assembly (shown in Fig. 3.5) provides a continuous net torque of 35 Nm and peak torques of 180 Nm, which is in accordance with the design requirements for most patients [85, 86]. As control strategies meant to assist the human gait cycle do not require continuous torque, but higher torque

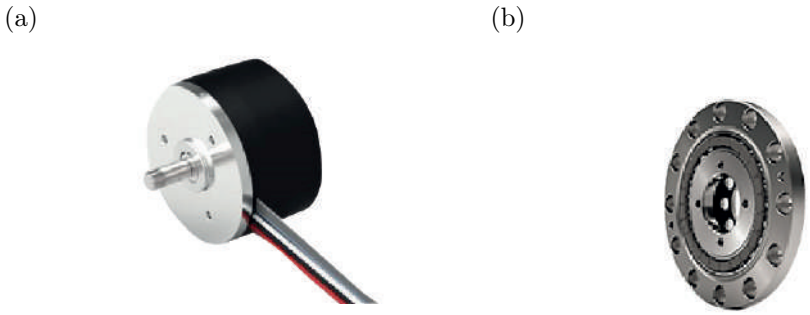

Figure 3.4: (**a**) *Brushless DC motor* and (**b**) *Harmonic Drive gear* of the AGoRA exoskeleton. Their combination can provide a peak torque of up to 180 Nm.

profiles at specific times, the peak torque profile of the selected actuators is more than sufficient for the application presented in this work.

3.2.3 Sensors

HRI is an important factor to ensure user's comfort, safety and a reduced energy consumption [87]. Accordingly, the AGoRA exoskeleton is designed in such a way that there are no sensors physically attached to the user's skin. The exoskeleton is equipped with two types of sensors: kinematic and kinetic. Kinematic sensors are used for measuring hip and knee angular position, and foot angular velocity, whilst kinetic sensors measure the force of interaction between the user's limbs and the mechanical structure of the exoskeleton.

Besides the internal relative incremental encoder of each DC motor (used for the implementation of position and impedance controllers), the exoskeleton has an absolute

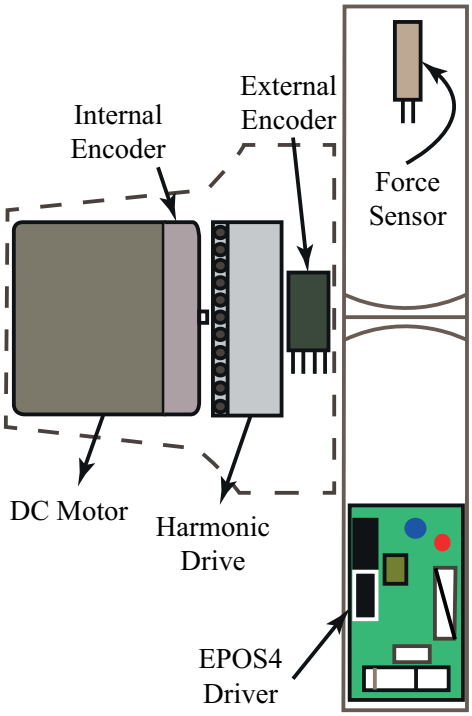

Figure 3.5: Schematic drawing of each joint assembly of the AGoRA exoskeleton.

magnetic encoder placed concentrically to each joint assembly (see Fig. 3.5). This absolute rotary encoder produces a unique digital code for each position of the motor shaft, whereas voltage outputs of the motor encoders proportionally vary to the joint angular displacement. Additionally, the motor drivers are able to measure motor velocity and position by means of embedded incremental encoders and hall effect sensors.

Further, strain gauges (632-180, RS Pro, UK) mounted on each exoskeleton link are used as force sensors (see Fig. 3.5). The resistance gauge consists of a thin semiconductor grid that is bonded to the metal rods of the exoskeleton. Under certain torsional stress, the wired grid undergoes a change in length and cross-section which produces a proportional variation of resistance [81]. Their placement on the exoskeleton was determined through FEA, ensuring that the chosen points presented high deflection upon slight interaction forces. These force sensors are connected in a half Wheatstone bridge configuration to enhance their measurement accuracy and to correct changes resulting from temperature variations. A commercial 24-bit Analog-Digital Converter (ADC) for weigh scales (HX711, Avia Semiconductors, Czech Republic) is used to

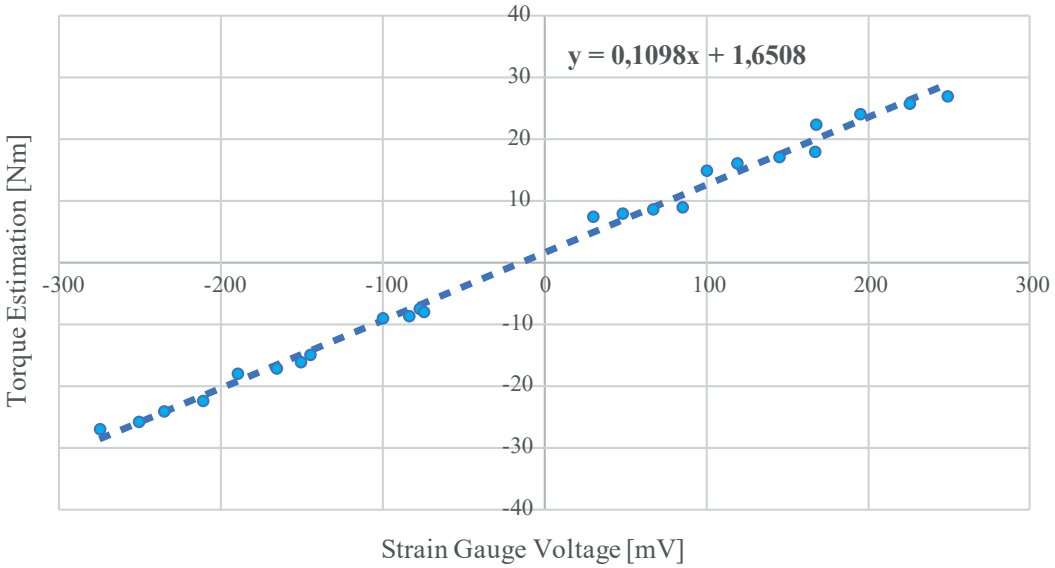

Figure 3.6: Strain gauge characterization curve.

balance the bridge and to amplify the output 50 times. Its output signal covers torque measurements ranging from -40 to 40 Nm, thus complying with the maximum continuous torque of the actuators. This construction provides the estimation of the HRI torque by using a linear equation (as depicted in Fig. 3.6), which was obtained through a calibration process done with several known weights (as shown in Fig. 3.7) and the least-square algorithm. Once the strain gauges were attached to the exoskeleton links, they were covered and protected with a hard resin. This material avoids humidity and external contamination that could damage the strain gauges or interfere with the measurements.

Figure 3.7: *Strain gauge calibration setup.* A set of calibrated weights was used to model an estimation of the interaction torque.

In addition to the above-mentioned sensors, a custom insole instrumented with Force Sensitive Resistors (FSR) (Ref. 402, Interlink Electronics, USA), and an Inertial Measurement Unit (IMU) (BNO055, BOSCH, Germany) placed on the dorsal side of the foot are used to accurately detect four gait phases (see Fig. 3.8). The used FSR consists of a conductive polymer film with a circular sensing area of 18.22 mm in diameter and a negligible thickness of 0.5 mm, while the used IMU integrates a triaxial 14-bit accelerometer, a triaxial 16-bit gyroscope, with a measurement range of $\pm 2000\,^{\circ}/s$, a triaxial geomagnetic sensor and a 32-bit cortex M0+ microcontroller in a single package. The gait phase partitioning module, which serves as a control middle-layer, is discussed in depth in Section 4.

3.3 Low-Level Control Architecture

The low-level control architecture of the AGoRA exoskeleton is represented in Fig. 3.8. The electronic hardware is divided into three main parts:

- The main board, responsible for setting all configuration parameters and target setpoints of the low-level controllers, as well as synchronizing all joint movements.
- The motors drivers, dedicated to sensor data acquisition and the implementation of low-level controllers on each joint's actuator independently.
- The data bus, a real-time network connecting the main board and the motors drivers through a gateway communication protocol.

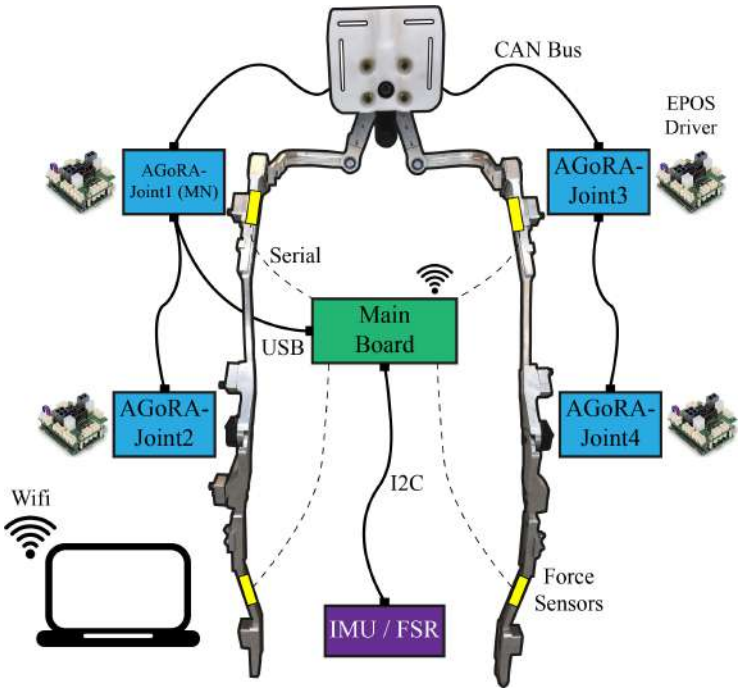

Figure 3.8: *Low-level control architecture of the AGoRA exoskeleton.* Main board communicates with motor drivers through a data bus to actuate each joint module independently.

Modularity is an important consideration when designing an exoskeleton control architecture for patients whose needs may vary in terms of the affected joints, the tasks

meant to be performed in therapy and the assisted DoF. Therefore, a centralized architecture would hinder easy donning/doffing and processing processes [88]. With this in mind, we rather opted for a distributed architecture with motor drivers commanding each joint module independently for the design of the AGoRA exoskeleton. By this means, unilateral hip-knee construction or individual joint versions of the device can be prepared according to each patient's requirements.

The main board of the AGoRA exoskeleton is mainly based on a Raspberry Pi 3 Model B (Raspberry Pi Foundation, UK), whose small size ($85.6 \times 56.5 \times 17$ mm) allows it to be placed on the exoskeleton back frame. The board also has several communication ports: Serial, I2C, USB, and Wifi. A non-standardized serial protocol is used by the strain-gauge acquisition board to transmit the voltage measured on each joint module. Further, the I2C bus is meant for the acquisition of IMU data, whilst the USB module allows the device to communicate with the master motor driver (configured at the hip exoskeleton joint by default). Likewise, the Wifi-based protocol, known as Secure Socket Shell (SSH), is used to send data wirelessly to a laptop, where sensor data coming from the exoskeleton can be displayed in real-time and stored for offline analysis. While the laptop is connected to the Wifi hotspot created by the main board, this external computer can also be used to carry out costly processing algorithms that may be disrupting the normal operation of the main board.

3.3.1 Motor Drivers

The AGoRA exoskeleton is a multi-DoF device with a considerable number of sensor inputs and control outputs. By creating a network structure with a single node on each joint module, only three wires are required: the one distributing power supply, and the others corresponding to the USB communication between main board and master motor driver, and the CAN (Controller Area Network) bus for the communication among motor drivers (as shown in Fig. 3.8).

Taking this distributed approach into consideration, the four exoskeleton joints are equipped with an EPOS4 (Maxon Motors AG, Switzerland) developed by the manufacturer specifically for the brushless DC motors described in Section 3.2.2. The motor drivers are in charge of the sensor data acquisition of each joint module: angular position, motor torque, motor velocity, and motor position. The sensor analog inputs are converted to a digital value of 12 bits by an ADC embedded in the EPOS4 with a resolution of 5.64 mV [89]. Fig. 3.9 illustrates the motor driver and its functional scheme.

The EPOS4 motor driver is commanded through an object dictionary (OD) which is the heart of the device. It represents the link between the data bus and the application. The application uses the data from the OD as input to perform its task and also writes its results and outputs to the same dictionary. This configuration also allows communication among different motor drivers to be carried out by sharing their ODs with each other. By using this setup, communication with each exoskeleton joint comes down to writing and reading parameters from the corresponding OD [90].

The EPOS4 controller architecture contains three built-in low-level control loops: current regulation is used in all operation modes, whilst position or velocity regulation are

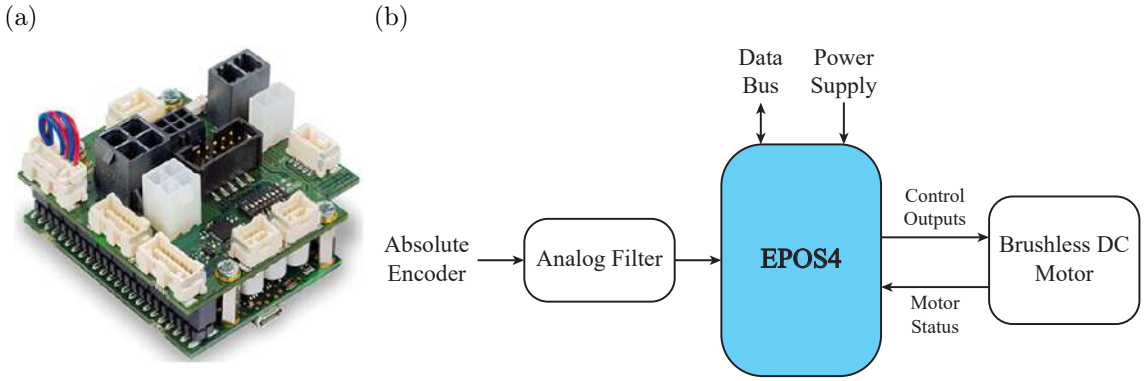

Figure 3.9: (**a**) *EPOS4 motor driver.* (**b**) *Functional scheme of the motor driver* responsible for sensor data acquisition and control of brushless DC motor in each joint module.

only used in position-based or velocity-based modes, respectively [91]. Fig. 3.10 shows an overview of the low-level control architecture of each exoskeleton joint module.

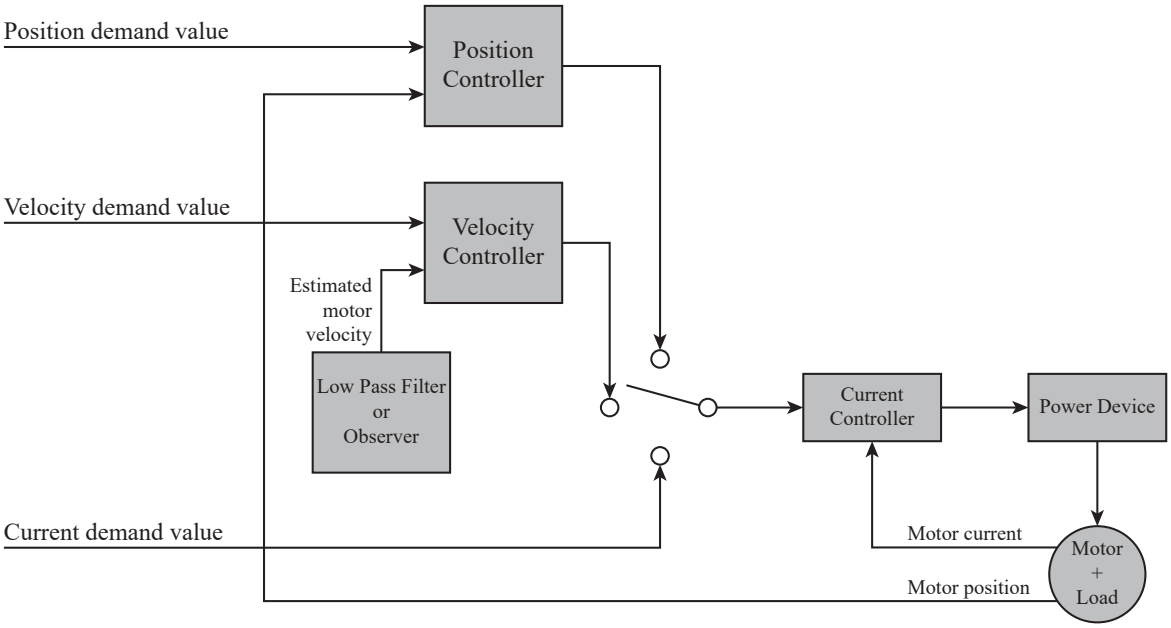

Figure 3.10: Overview of the low-level control architecture of each exoskeleton joint module

3.3.1.1 Current Controller

During a movement within the drive system, forces or torques must be controlled. Therefore, as a principal regulation structure, the EPOS4 offers current-based control. Fig. 3.11 displays the scheme of the current regulator. Current controller parameters can be used in analytical or numerical simulations via the transfer function shown in Equation 3.1.

$$c_{current}(s) = K_p + \frac{K_i}{s} \tag{3.1}$$

where K_p and K_i are the current controller proportional and integral gains, respectively. Total transport delay of the current regulation is always smaller than 0.06 ms. In order to prevent degradation of the control performance when the control input

stays at the limit value for long time, an anti-windup algorithm is implemented preventing the integral part of the PI controller to take values larger than the ones bound on the control input [91].

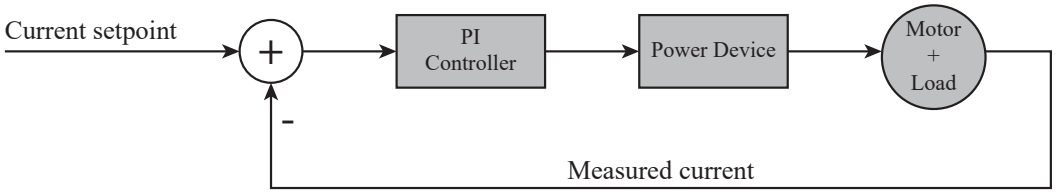

Figure 3.11: Low-level current controller of the EPOS4.

3.3.1.2 Position Controller (with feedforward)

The EPOS4 is able to close a positioning control loop based on the subordinated current control. Fig. 3.12 shows the scheme of this low-level position controller. The position controller is implemented as PID controller. To improve the motion system's setpoint following, positioning regulation is implemented by feedforward (FFw) control. Thereby, velocity FFw serves for compensation of speed-proportional friction, whereas acceleration FFw considers known inertia. In addition, the differential part of the PID controller signal is low-pass filtered before it is added to the proportional and

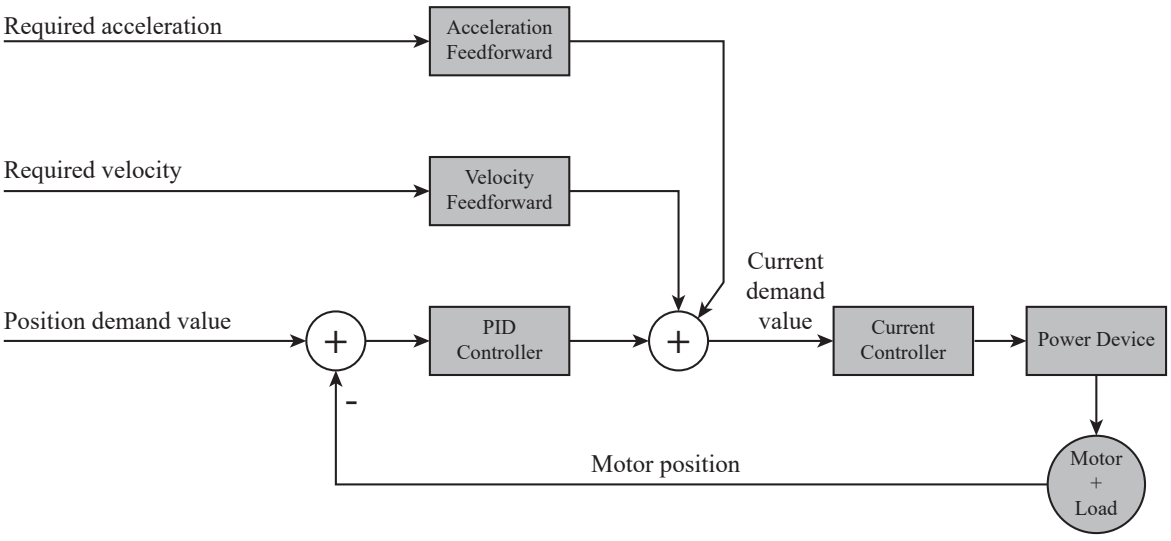

Figure 3.12: Low-level position controller of the EPOS4 with feedforward.

integral parts. Low-pass filtering is done to prevent negative influence on the control performance by the differentiation of noisy-measured motor position. Position controller parameters can be used in analytical or numerical simulations via the transfer function shown in Equation 3.2.

$$c_{position}(s) = K_p + \frac{K_i}{s} + \frac{K_d \cdot s}{1 + \frac{K_d}{10 \cdot K_p} \cdot s} \tag{3.2}$$

where K_p, K_i and K_d are the position controller proportional, integral and derivative gains, respectively. The anti-windup method is also used to prevent integration wind-up in the PID controller when the actuators are saturated [91].

3.3.1.3 Velocity Controller (with feedforward)

The EPOS4 also offers velocity regulation on the subordinated current control. Fig. 3.13 displays the scheme of this low-level velocity controller. Velocity controller parameters can be used in analytical or numerical simulations via the transfer function shown in Equation 3.3.

$$c_{velocity}(s) = K_p + \frac{K_i}{s} \tag{3.3}$$

where K_p and K_i are the velocity controller proportional and integral gains, respectively. The anti-windup algorithm is also implemented here to prevent integration wind-up in the PI controller when the actuators are saturated. The estimation of the motor velocity is done by using the measured time between consecutive sensor edges, which is then low-pass filtered to eliminate the effects of measurement noise.

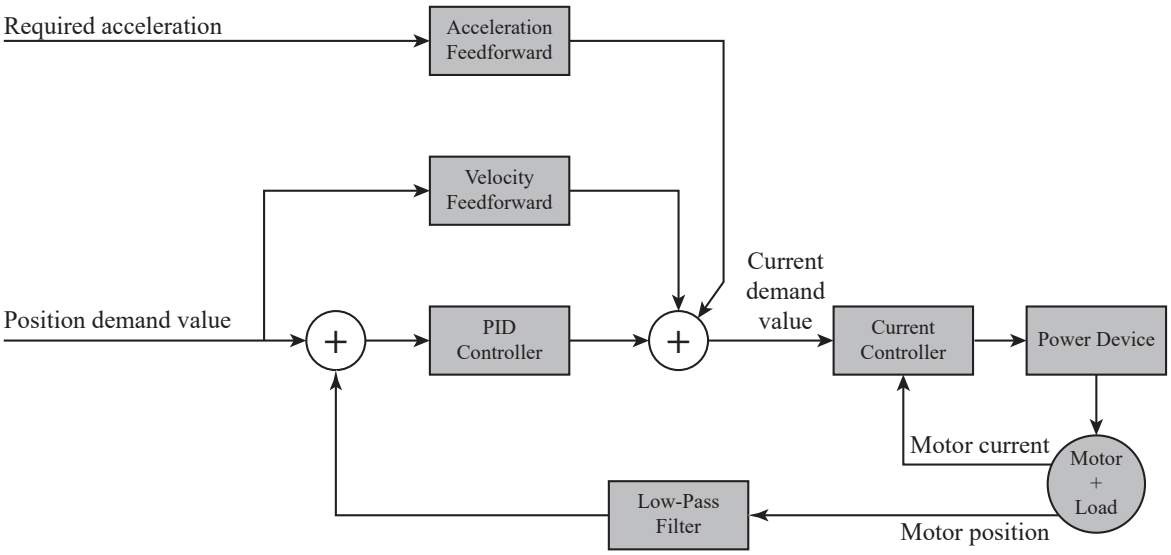

Figure 3.13: Low-level velocity controller of the EPOS4 with feedforward.

3.3.2 Bus Data

The data bus used in the AGoRA exoskeleton consists of a network structure with a deterministic real-time communication based on CAN technology running at 1 Mbps. CAN is a bus topology for the transmission of messages designed to reduce the volume, complexity, and difficulty of wiring. To read a message coming from a CAN node, each motor driver has an identifier associated to it, which allows it to be distinguished from other data frames by the master motor driver [26, 86]. By using the gateway functionality of the EPOS4, the main board can access all EPOS4 devices connected to the CAN bus via the gateway device's USB port (see Fig. 3.14). Each communication cycle in the gateway protocol involves the following process:

- The USB master (i.e., main board) sends a command including the node ID to the device working as a gateway by using a maxon-specific USB protocol (Label 1 in Fig. 3.14).

- The gateway decides whether to execute the command or to translate and forward it to the CAN bus depending on the device ID included in the data frame.

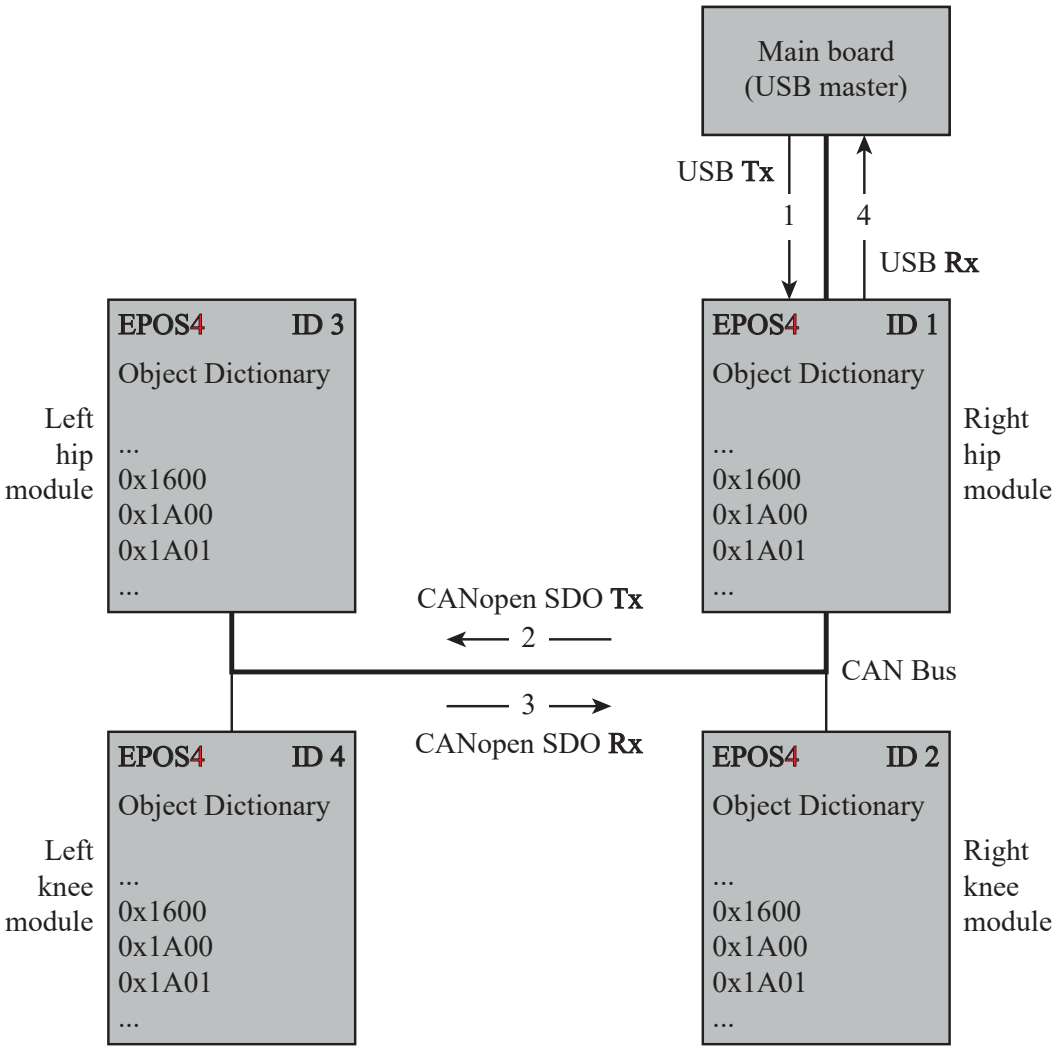

Figure 3.14: Gateway communication of the AGoRA exoskeleton.

Data between the gateway and the addressed device is exchanged using CANopen SDO (Service Data Object) protocol according to CiA 301 (Label 2 in Fig. 3.14).

- Once the command has been executed in the addressed device, it sends the corresponding CAN frame (containing the locally collected sensor data) back to the gateway. The gateway receives the CAN frame corresponding to a SDO service (Label 3 in Fig. 3.14).

- Finally, this CAN frame is translated back to the USB frame and sent back to the main board [92] (Label 4 in Fig. 3.14).

3.4 Power System

Since the AGoRA exoskeleton is meant for overground walking tasks, there has to be an energy storage module powering its electronics in order to make the device autonomous. Thus, a lithium-ion battery pack of 36 V_{DC} and 4.4 Ah is used to power the exoskeleton. Step-down regulators are used to generate 24 V_{DC} and 5 V_{DC} from the main power source (References SIG214-45 and LM2596, respectively). These voltages are used to power the motors and their drives, and the main boards and the force sensor amplifiers, respectively. The battery pack weighs 960 g and measures 57 × 85 × 135 mm, which allows it to be placed in a small backpack that the user wears, containing also the main board and voltage regulators. Fig. 3.15 displays a scheme of the power transmission described above, which is expected to allow the exoskeleton run for at least one hour of continuous operation.

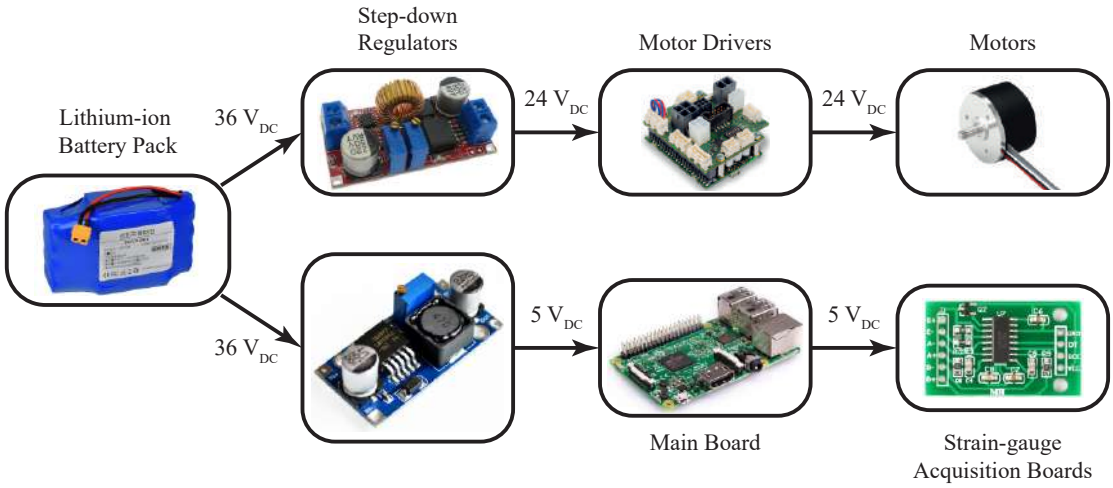

Figure 3.15: Power transmission of the AGoRA exoskeleton.

3.5 Software Design

The control architecture of the AGoRA exoskeleton is mounted on the Robot Operative System (ROS), a Linux-based meta-operative system widely used in the field of robotics. It is a trending robot application development platform that provides various

features such as message passing, distributed computing, code reusing, and so on [93]. Among the most important advantages that ROS presents, we find abundant ready-to-use capabilities, multiple tools for debugging, visualization, and simulation (e.g., `rqt_gui`, `RViz`, and `Gazebo`), a lot of sensors and actuators already supported, inter-platform operability (i.e., ROS runtime processes, also known as nodes, can be written in C, C++, Python or Java), modularity and robustness against unexpected disconnections or data loss, concurrent resource handling, and an active developer community willing to support queries from other users.

Within this software framework, a C-library provided by the manufacturer [94] to command the EPOS4 motor driver was wrapped in a ROS package (i.e., the most basic unit of ROS software). This wrapper comprises customized functions to handle all EPOS4 functionalities such as functions for initialization, communication, configuration, operation, data recording, and error overview. As the manufacturer library supports different computer architectures, the developed ROS package detects the instruction set architecture (ISA) of the computer in which it is running and installs the corresponding library. Thus, this feature allows cross-computer installation on any Linux-running device, including the Advanced RISC Machine (ARM) processors such as the one included in the Raspberry Pi. By using this wrapper, a C++ motor class, which immediately sets several configuration parameters depending on the node ID and keeps available the mentioned functions, was created.

As motor parameters, position sensors parameters, and controller gains must be set prior to motor activation, the motor class follows the flowchart shown in Fig. 3.16 to initialize each actuation mechanism upon class declaration. Table 3.1 shows the parameters that must be either retrieved or modified during the initialization procedure, arranged based on each subprocess (A-G). The motor/gearbox parameters were determined based on the motor datasheet [95] and the gearbox specifications [96], while the controller gains were tuned using the EPOS Studio software available on Windows [91].

Figure 3.16: Initialization of EPOS4 motor driver.

Subprocess	Access Right	OD entry	Object name	Value
A	R	0x2000-00	Node-ID	Configured by DIP switches
	W	0x2001-00	CAN bit rate	1 Mbps on master motor driver
B	W	0x6420-00	Motor type	EC motor block commutated
	W	0x3001-01	Nominal current	4430 mA
	W	0x3001-02	Output current limit	3000 mA (limited to power supply output)
	W	0x3001-03	Number of pole pairs	7
	W	0x3001-04	Thermal time constant winding	36.8 s
	W	0x3001-05	Torque constant	53.4 mNm/A
	W	0x6080-00	Max. motor speed	6000 rpm
	W	0x3003-03	Max. gear input speed	6500 rpm
C	W	0x3010-01	Encoder resolution	4096 PPR
	W	0x3010-02	Encoder type	Inc. encoder 1 without index (2-channel)
D	W	0x607D-xx	Software position limit	Custom for each joint module
E	W	0x30A0-01	Current controller P gain	937.294 mV/A
	W	0x30A0-02	Current controller I gain	430.053 mV/A· s
F	W	0x30A2-01	Velocity controller P gain	427.769 mA· s/rad
	W	0x30A2-02	Velocity controller I gain	4442.130 mA/rad
	W	0x30A2-03	Velocity FFw gain	0 mA· s/rad
	W	0x30A2-04	Aceleration FFw gain	2.575 mA· s^2/rad
G	W	0x30A1-01	Position controller P gain	13723.863 mA/rad
	W	0x30A1-02	Position controller I gain	47995.592 mA/rad· s
	W	0x30A1-03	Position controller D gain	327.017 mA· s/rad
	W	0x30A1-04	Velocity FFw gain	0 mA· s/rad
	W	0x30A1-05	Acceleration FFw gain	2.597 mA· s^2/rad

Table 3.1: *Configuration parameters set during the initialization process of the EPOS4.* W: Write-access. R: Read-access. PPR: Pulses per Revolution.

By looking up through a configuration file where the connected joint modules are declared, the corresponding motor classes can be easily instantiated and configured depending on their designated parameters (depicted in Table 3.1). This design is thus versatile and provides the device with modularity at the software level, which is an important factor in wearable robots as was described earlier. Future iterations of the present device, which should include a graphical user interface, would only have to modify the mentioned configuration file before running the initialization processes.

3.6 Safety

Safety is one of the most important features in rehabilitation robotics. Since the device is secured to the subject's limbs, its movement should be as compliant as

possible to human movements. Especially in clinical environments, where patients frequently exhibit muscular weakness and mobility deficits, several safety measures should be incorporated in the mechanical structure, as well as at different levels of the exoskeleton control system [26].

In regards to the kinematic configuration, the maximum RoM possible across all joints is shown in Table 3.2. These values were established based on normal gait on healthy subjects [24] so that users are also able to perform sit-to-stand and stand-to-sit movements [97]. Based on these anatomical restrictions, the angular joint limitation of the AGoRA exoskeleton is kept by both software (by default) and hardware (end-stop at the exoskeleton knee joint). Since some patients present certain flexo-extension limitations (other than those included in Table 3.2) due to their pathological gait, an initial calibration stage runs at the beginning of each trial to eventually shorten the default joint RoM (see subprocess D in Fig. 3.1).

Table 3.2: Degrees of Freedom (DoF) and Range of Motion (RoM) across all exoskeleton joints.

Joint	DoF	Actuation	RoM
Hip	Flexion/Extension	Active	100° / 20°
Hip	Add/Abduction	Passive	10° / 10°
Knee	Flexion/Extension	Active	100° / 3°

Furthermore, an emergency button is included within the hardware architecture which is wired in such a way that a single push disconnects most of the exoskeleton (except for the main board) from the power supply. Therefore, the patient should hold the button during the therapy at all times, and he/she should be instructed to press it under any situation that may compromise their safety or comfort. The engineer responsible for the mainboard can additionally disable the whole system with a simple keyboard shortcut.

3.7 Conclusions

This chapter described the mechanical design and development of the AGoRA exoskeleton, as well as the used electronic hardware and the low-level control architecture proposed in pursuit of modularity. The device is an active lower-limb exoskeleton meant for rehabilitation of stroke patients who usually need early, repetitive, and task-specific training to overcome their mobility impairment. The AGoRA exoskeleton integrates a non-backdrivable actuation mechanism along with multiple sensors oriented at the proper HRI, which represents one of the proposed specific objectives of this dissertation.

The AGoRA exoskeleton can be easily adjusted to different anthropometric measures so that people from 1.70 to 1.83 m in height, and up to 90 kg in weight may fit into this assistive device. The overall hardware and control architectures also allow the preparation of different knee-hip versions which may be configured depending on the patient's characteristics or needs. Further, for the sake of comfort and reliability, the exoskeleton is designed with no sensors physically attached to the user's skin. Most sensors are integrated into the exoskeleton frame, thus easing the donning/doffing process with pathological patients.

Finally, several features were implemented in the exoskeleton hardware and software for increased patient's safety. In the mechanical design, a physical stop limits the knee RoM and guarantees that the device will never exceed human RoM. Apart from default limitations in terms of joint RoM kept by software, each RoM can be customized at the beginning of each trial if necessary. Also, the electronic hardware uses a CAN bus that ensures correct communication among motor drivers and, in case of a failure that cannot be fixed via software, powers off the device.

Chapter 4

Gait Phase Detection of the AGoRA Exoskeleton[1]

4.1 Introduction

Gait analysis is used for different applications in the field of medical rehabilitation. For instance, it is of great help to therapists who wish to monitor the recovery of patients going through rehabilitation processes [59]. Gait classification can be also implemented within clinical settings as part of the commanding parameters of functional electrical stimulation [98], the estimation of fall risk in elderly population [99], the detection of an abnormal gait pattern in patients with paretic limbs and their classification based on known pathologies [100]. Additionally, in the field of robotics, researchers have managed to program humanoid robots to use human-based gait trajectories generated via gait classification [101], as well as consistently control wearable assistive devices such as robotic prostheses [102] and orthoses [103] for the recovery of lower-limb mobility.

[1]This chapter is mostly based on the following journal article:
Sánchez Manchola, M. D., Pinto Bernal, M. J., Munera, M., & Cifuentes, C. A. (2019). Gait Phase Detection for Lower-Limb Exoskeletons using Foot Motion Data from a Single Inertial Measurement Unit in Hemiparetic Individuals. Sensors, 19(13), 2988. https://doi.org/10.3390/s19132988

Due to the recent rise in the use of lower-limb exoskeletons as an alternative for gait rehabilitation, gait phase detection has become an increasingly important feature in the control of these devices. Also, in pursuit of highly functional, low-cost recovery devices, a reduced number of sensors for the partitioning of gait cycle is desirable, especially in developing countries whereby limited budgets are allocated specifically for biomedical advances. Taking this into account, two gait phase partitioning algorithms that use motion data from a single Inertial Measurement Unit (IMU) placed on the dorsal side of the foot were implemented in order to unveil which detection methodology best suits the AGoRA exoskeleton. The present chapter comprises the validation and comparison of a threshold-based (TB) algorithm and a machine-learning-based detection method via offline processing. Based on the better performance of the latter, its real-time implementation and the associated preliminary results are also addressed hereby. For further information on the offline validation, the reader is recommended to refer the associated journal article [104].

4.2 Gait Phase Detection Systems (GPDS)

In regards to gait partitioning, one may consider different granularities, i.e., number of involved gait phases. The main nomenclature divides the gait cycle into two events, namely, stance and swing phases. A two-phase model has proven to be sufficient to control the knee module of an active orthosis whose actuation is only performed at the beginning of these gait subsections [105]. Nonetheless, the most widespread approach relies on a four-phase model, which comprises: (i) the initial foot contact (IC) with the ground or Heel Strike (HS); (ii) the loading response phase or Flat Foot (FF); (iii) the heel lifting or Heel-Off (HO); and (iv) the initial Swing Phase (SP) or Toe-Off (TO) [106]. Such a gait granularity has been used for the actuation of multiple robotic Ankle-Foot orthoses (AFO) [107, 108]. Taking into account the above, a granularity of four gait phases was chosen to be employed in the AGoRA exoskeleton which is expected to integrate an active AFO in the medium term .

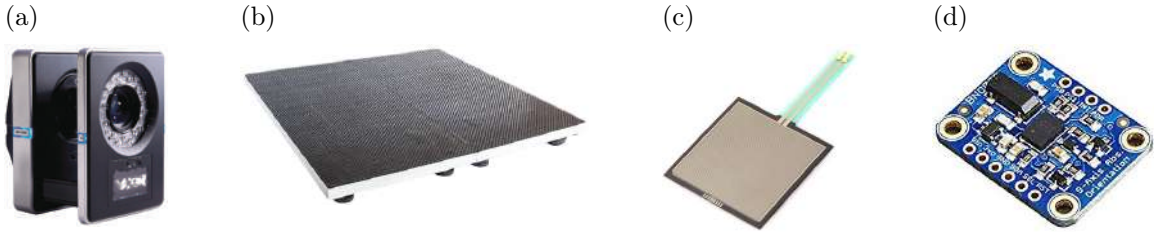

Figure 4.1: *Equipment for gait phase detection.* (a) Motion capture system, (b) force platform, (c) Force Sensitive Resistor (FSR), and (d) Inertial Measurement Unit (IMU).

Regardless of the detection method, various technologies are used to capture gait phases. On the one hand, non-wearable sensors, such as motion-capture-based systems (see Fig. 4.1a) and force platforms (see Fig. 4.1b), set the benchmark in accuracy for walking kinematics [109]. However, such sensors are expensive and limited to indoor use [110]. For this reason, wearable sensors have become popular due to their affordability, shorter donning/doffing times, and less complex post-processing [106, 111]. Among wearable sensors meant for gait segmentation, foot pressure insoles or footswitches (see Fig. 4.1c) are considered the best detection option, since each gait phase can be related to a specific pressure pattern [112]. Nevertheless, pressure insoles must be tailored for each subject's foot, which incurs higher research costs, and are continuously exposed to tear and friction, which results in a shorter lifetime [113]. Therefore, the use of either whole IMU (consisting of gyroscopes, accelerometers, and magnetometers), or the combination of such inertial sensing components, has risen lately. In this work, such sensors (see Fig. 4.1d) are used as means of gait phase detection thanks to their cost-effectiveness [111], and the fact that inertial quantities present typical waveform features during a gait cycle [106].

Studies have been conducted positioning IMUs on the waist [114], thigh [115], shank [116], and foot instep [98, 117]. We considered the shank location due to low inter-subject variability [118] and the fact that there is less soft tissue movement compared to the thigh [116]. However, we opted for fastening the IMU to the foot instep because

of the better performance that scalar classifiers have shown with the sensor placed on this location, even compared to other vectorial classifiers that involve further inertial sensors placed at different lower-limb locations [119].

Several computational methods have been previously proposed for the automatic segmentation of the gait cycle, which fall into two main categories. The first category is comprised of algorithms, which divide the gait phases based on the threshold selection of either raw or processed data [120, 121]. Secondly, some machine-learning approaches have emerged in recent years to substitute the aforementioned techniques that rely on hand-crafted feature extraction. Among artificial intelligence schemes, Hidden Markov Models (HMM) have demonstrated superior performance [106] since the single supervised training of a continuous HMM, followed by a classification based on foot gyroscope signals, has proven to be sufficient to achieve an accurate detection rate [119].

4.3 Theoretical Approach

Two classification strategies have been implemented in the AGoRA exoskeleton for the automatic identification of four gait phases, drawn from inertial data coming from a single IMU located at the foot instep. The first and most easily implemented strategy is a TB algorithm that determines the gait phases of interest by establishing certain decision rules and thresholds (to be described shortly), which must be met to jump from one gait phase to another. The other partitioning method may be viewed as a machine-learning algorithm since it requires a training stage and a posterior testing stage [105]. Specifically, the implemented algorithm is based on a continuous HMM.

Several approaches have previously been proposed for the automatic segmentation of the gait cycle. Most of these differ from the present work in that it presents the comparison among a variety of well-known segmentation approaches with respect to FSR-based reference values from a considerable number of study subjects with both

typical and pathological gait patterns. By doing so, the performance of such detection algorithms is assessed in a target population which, to the best knowledge of the author, has not yet been addressed with this particular experimental setup, namely hemiparetic adults.

4.3.1 Threshold-Based Detection Algorithm (TB)

The implemented threshold-based (TB) detection algorithm is similar to those developed by Rueterbories et al. [98], and Catalfamo et al. [116], whose studies use inertial sensors positioned on the volunteer's shank to gather linear acceleration and angular velocity signals. Conversely, for the case of the present study, the mediolateral axis rotation component of the foot accelerometer (A_y) and gyroscope (G_y) signals are fed to the TB algorithm as inputs, as the movement of lower-limb joints during walking occurs mostly along the sagittal plane. Time stamps are also used as algorithm inputs since this detection algorithm makes use of spatial thresholds as well as temporal limits. By this means, each gait phase can be associated with a sequence of wave-related features without any complex processing that would result in a high computational load [122]. For more information on the TB's feature extraction process, the author recommends to read the publication associated with this chapter [104].

4.3.2 Classification Using a Hidden Markov Model (HMM)

An HMM is a doubly stochastic process with N underlying discrete states that are not observable, i.e., its state sequence is hidden to the observer who only has access to the emissions of each state [123]. The second embedded stochastic process describes the emissions from Y observations, i.e., either the sensor readout or feature vectors extracted from them, in terms of discrete probabilities or Probability Density Functions (PDF) [124]. HMM is a statistical model widely used to estimate a sequence of hidden states in a time series [105], which for the case of gait phase detection corresponds to the gait events ($N = 4$).

HMM can be expressed as a function of a set λ of statistical measures:

$$\lambda = (A, B, \pi) \tag{4.1}$$

which includes the probability distribution matrix of state transition A, the probability distribution matrix of observation symbols B, and the initial state distribution vector π.

The normal gait pattern repeats itself indefinitely with a known sequence of gait events, which, probabilistically speaking, means that it may either remain in the current state or eventually transition to the consecutive state. This behavior has been recently modeled using a left-right model [119, 124], whose main feature is to limit transitions to consecutive states of the Markov chain. Since transitions represent a narrow fraction of the gait cycle, their associated probabilities assume lower values than those related to permanence in the same state. Thus, the transition matrix A may be implemented as shown in Equation 4.2 [119].

$$A = \{a_{ij}\} = \begin{bmatrix} 0.9 & 0.1 & 0 & 0 \\ 0 & 0.9 & 0.1 & 0 \\ 0 & 0 & 0.9 & 0.1 \\ 0.1 & 0 & 0 & 0.9 \end{bmatrix} \tag{4.2}$$

where a_{ij} denotes the transition probability from state S_i to state S_j.

Because the initial state of the model is unknown, an initial state distribution vector π that allocates the same probability to all states, i.e., each state has the same probability of being the first in a state sequence, was chosen. Finally, a bivariate GMM with three components was utilized to describe the emissions from each state. These emissions allude to feature vectors that include the angular velocity measured at any sampling time, and its time derivative computed by means of a first-order finite dif-

ference approximation, i.e., the angular acceleration [125]. This particular stochastic model yields the best trade-off between complexity and accuracy for gyroscope signals [115, 124].

The development of a continuous HMM entails two main procedures: a training stage and a test stage. The first phase refers to the adjustment of model parameters λ to optimally adapt them to an observed training dataset [123]. The Baum-Welch algorithm, the most common solution to this issue, is implemented in the present

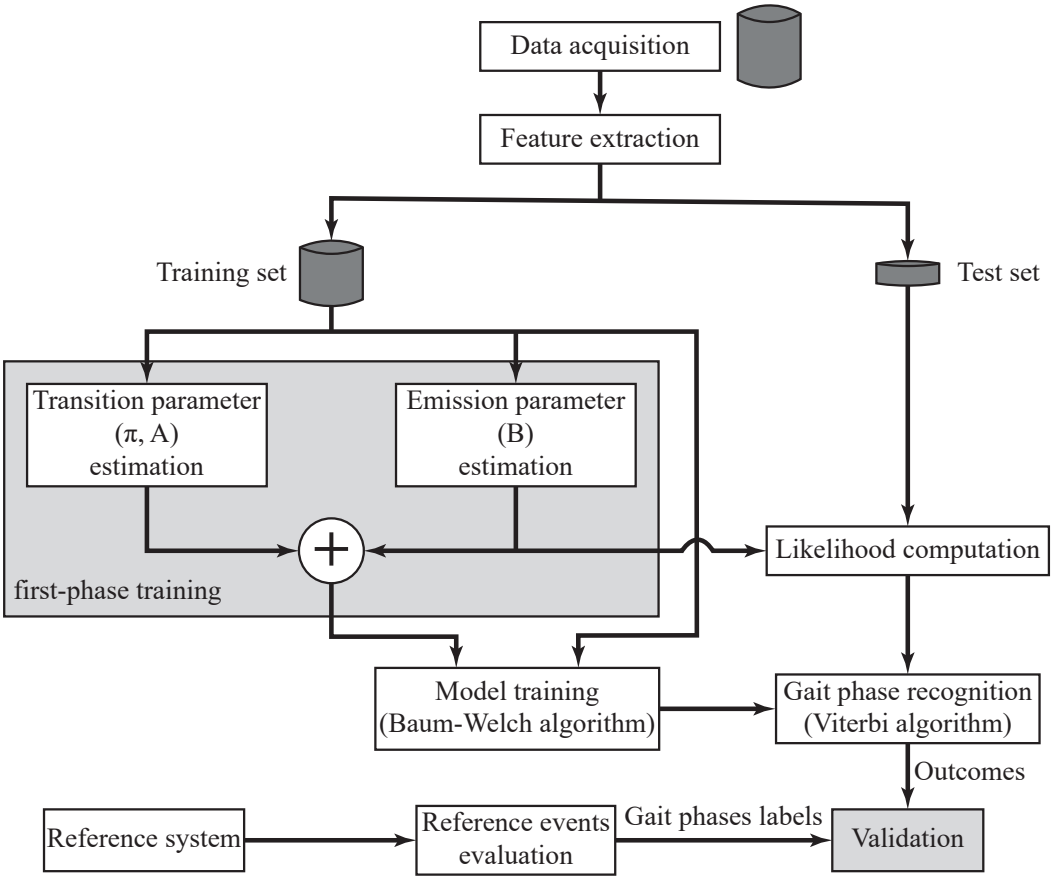

Figure 4.2: *Flowchart that illustrates the validation methodology of HMM*. A model is trained by means of the Baum-Welch algorithm, after applying feature extraction to the acquired dataset. The optimal state sequence is then computed through the Viterbi algorithm by using feature vectors from the test dataset, and the performance evaluation is conducted with respect to gait phases labels drawn from the reference system.

work. This training procedure basically starts with an initial parameter set (*first-phase training* in Figure 4.2), on the basis of which it extracts probabilistically weighted state sequences. The initial model is repeatedly updated with these new transition and emission probabilities until a desired level of convergence is reached [115].

Subsequently, the test stage allows feature classification based on the trained model achieved in the training phase, i.e., the search for the optimal state sequence is undertaken. The most widely used optimality criterion is carried out by the Viterbi algorithm, which finds the most likely state sequence [123]. Despite its computational efficiency, this algorithm is not suitable for real-time implementation since the indicators it uses are computed based on a whole observation dataset. The validation of the classifier outputs is therefore offline compared with respect to an FSR-based reference system that provides the actual gait phases labels.

4.4 Offline Validation

4.4.1 Experimental Procedure

The experimental protocol was performed with the aim of quantifying the detection success ratio of the described algorithms within a varied spectrum of walking styles. To this end, eighteen participants were enrolled in this study, forming two groups: a control group with nine healthy subjects (H, 4 females, 5 males, 23.22 $\pm$ 1.99 y.o., 1.70 $\pm$ 0.046 m, 66.87 $\pm$ 4.29 kg), who had no known orthopedic, metabolic, or neurological impairment that could modify their natural walking pattern; and an experimental group with nine patients (P, 4 females, 5 males, 41.33 $\pm$ 15.83 y.o., 1.71 $\pm$ 0.098 m, 72.28 $\pm$ 7.73 kg), who had suffered from post-stroke hemiparesis for at least one year. All subjects were informed about the scope and purpose of the experiment, and written consent was obtained from each of them prior to the study. The protocol was approved by the Ethics Committee of the Colombian School of Engineering Julio Garavito, Bogota, Colombia.

Volunteers were first instructed to perform three 10-m tests at a self-selected speed in order to determine their normal overground speed, which was successively set on a rehabilitation treadmill (NIZA RX K153D-A-3, SportFitness, Colombia). Participants were equipped with a custom insole instrumented with FSR (described in Section 3.2.3) on their dominant side (for the case of H group) or their affected side (for the case of P group), which matched each subject's shoe size and represented the reference system, and an IMU (Described in Section 3.2.3) placed on their foot instep. Special care was taken when aligning the IMU y-axis with the sagittal plane since the accelerometer signal was taken into account within the TB classification [98]. The FSR sampling rate was 200 Hz, twice as much as the one at which the IMU acquired data (100 Hz), since there must be a greater amount of reference values in order to accomplish a proper assessment of the gait phase detection algorithms. Synchronized data capture was ensured by integrating a data acquisition node in the Robot Operative System (ROS). The experimental setup described here is illustrated in Fig. 4.3.

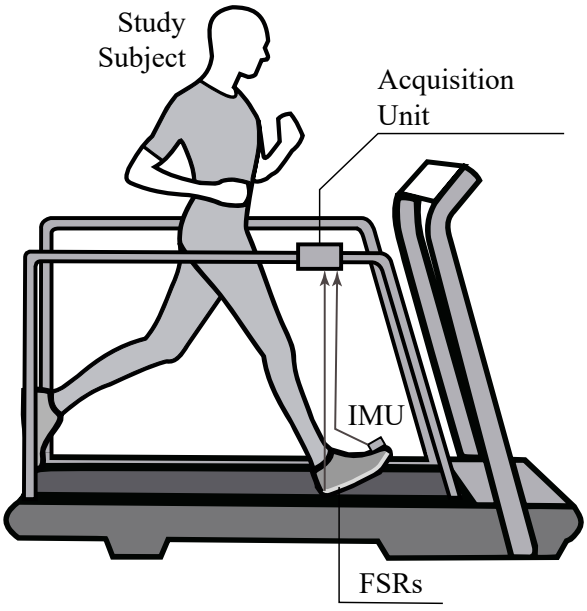

Figure 4.3: *Experimental setup for validation of gait phase detection methods.* Each subject was instrumented on their dominant/affected side with a custom FSR-equipped insole and an IMU placed on the dorsal side of their foot. Foot motion data were captured by using a Raspberry Pi running ROS to ensure synchronized data acquisition.

Participants were then asked to walk for at least 180 s on the already configured treadmill at a zero-degree inclination while wearing a security harness (if they considered it necessary). H group walked within a speed range of 0.639-0.944 m/s, whereas P group walked within a speed range of 0.278–0.667 m/s. All tasks were repeated three times so that enough data to train the HMM-based method were collected. A resting period of at least 2 min was carried out between tasks to prevent fatigue. Data acquisition only started once the self-selected speed was reached, and the treadmill speed was only reduced after all data were acquired to prevent data capture during the transient state. The entire experiment, including donning/doffing times related to instrumentation procedures and walking tasks, was completed within 30 min for all volunteers.

4.4.2 Data Processing

To assess the performance of each detection algorithm with respect to a reference system, four FSR placed on an insole custom for each user were implemented. The exact location of these FSR was the hallux, the first and fifth metatarsophalangeal, and the heel. The reason this distribution of pressure centers was chosen is based on how the vertical Ground Reaction Force (GRF) shows unique pattern characteristics in these specific regions [112]. By means of this type of sensors, the gait phases of interest can be detected through a simple binary algorithm, as can be seen in Fig. 4.4. Only the heel FSR should be activated at HS since this gait phase consists of the first heel contact and the start of the gait cycle. In the case of FF, some studies suggest that all FSR should be activated in order to detect this gait phase [119, 126]. However, even though this presumption might be true for non-pathological subjects, for the treated patient sample of this work, the activation of the toe and heel FSR had to be discarded in this condition to improve the accuracy of the FSR-based gait phase detection (gray dots in Fig. 4.4). This change was decided during offline data pre-processing from footage taken during experimental trials. Likewise, the HO occurrence depends not

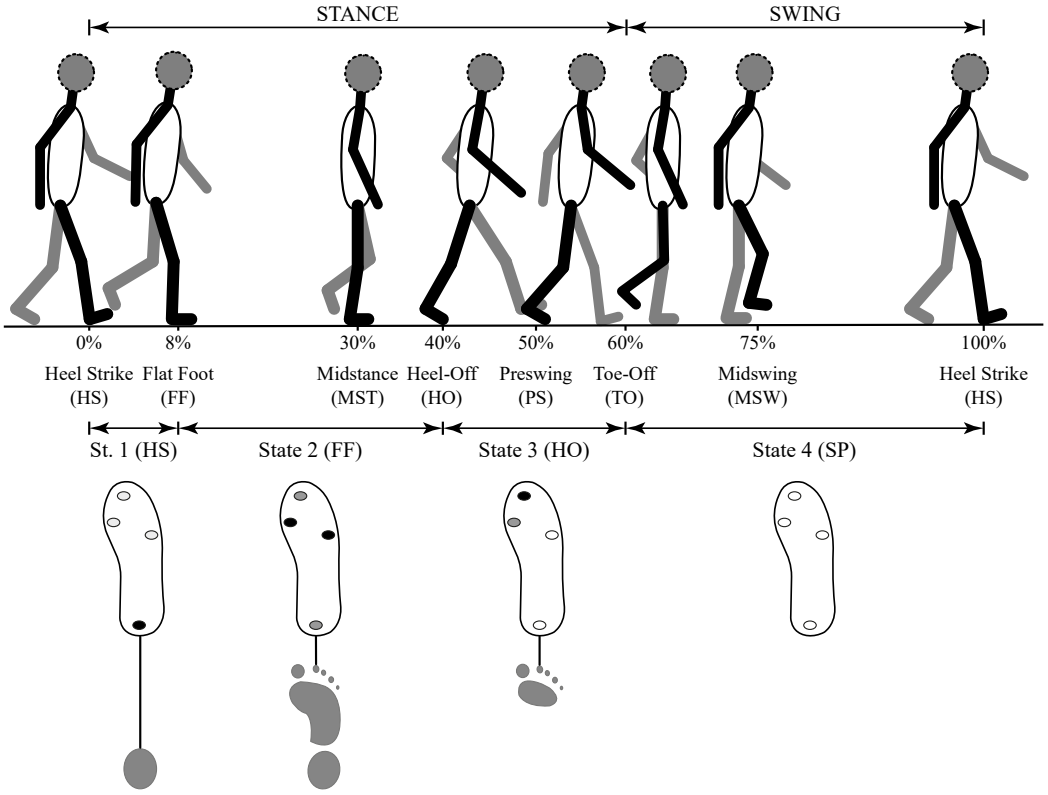

Figure 4.4: *Gait phase detection based on FSR activation patterns.* The gait cycle may be divided into seven phases, but four detected phases are sufficient for control purposes of an AFO. With this particular granularity, gait phases can be sequentially referenced from FSR data as follows: (i) HS State: Heel FSR is activated; (ii) FF State: first and fifth metatarsal FSR must be activated (black dots), and the activation of heel and toe FSR is considered depending on specific study subject (grey dots); (iii) HO State: toe FSR must be activated, and the activation of first metatarsal FSR is considered depending on specific study subject; and (iv) SP State: all FSR must be deactivated. Adapted from [126].

only on the toe FSR activation, but the first metatarsus FSR might also be taken into account depending upon offline video analysis. Finally, SP detection was given under the release of all FSR.

Data processing was performed offline using MATLAB software (MathWorks, 2018a, Naticks, USA) and an Asus VivoBook S15 S510UA (IntelCore i5-8250U, CPU@1.80 GHz, China) running Ubuntu 18.04. The gyroscope and accelerometer outputs were first treated with a median filter to eliminate atypical data values and a second-order

low-pass filter Butterworth (cut-off frequency: 17 Hz for accelerometer signals, and 15 Hz for gyroscope signals) [117, 119]. Then, inertial signals were interpolated to match the FSR frequency and partitioned into the gait phases of interest according to the previously described FSR-based segmentation logic. Finally, the partitioned angular velocity data of each gait event were time-normalized, and means and standard deviations of the obtained dataset were used to train parameters of the continuous HMM by means of the Baum-Welch algorithm.

The training stage of the HMM-based method was conducted by means of two different approaches: the well-known intra-subject procedure, hereafter referred to as subject-specific training (SST); and the inter-subject procedure, hereafter addressed as standardized parameters training (SPT). The SST model parameters were trained by means of a leave-one-out cross-validation applied to the three walking trials, whereby two trials were used for training and the remaining one for validation [119]. The cross-validation analysis was repeated in a recursive manner for each subject of both study groups so that it was repeated for all trials in turn. On the other hand, since pathological gait pattern greatly varies from one subject to another, we decided to validate an additional SPT procedure. By means of this technique, a standardized parameters set was computed on the basis of data gathered from healthy subjects, on account of the low inter-subject variability exhibited by their angular velocity waveforms [127]. A different validation approach was undertaken for each study group during SPT, in such a way that for H group, for instance, the training dataset for each examined subject was collected from the first two trials of the remaining individuals, while the last trial related to the subject under consideration was used for validation later. Conversely, for P group, the average of angular velocities acquired from healthy subjects during the first two trials was used to construct the training dataset. The final trial of each patient was subsequently involved in the validation stage [105]. Finally, for the case of the TB algorithm, all walking trials were utilized, one after the other, as the validation dataset of such a classification method.

4.4.3 Data Analysis

The performance of the proposed gait detection methods was evaluated through two indices: the timing error, i.e. the time difference of each detected gait event with respect to the FSR-based reference system, and the goodness index (G). G represents a Euclidean distance in the Receiver Operating Characteristic (ROC) space, which poses as a global index of the classifier capability and is based on its sensibility and sensitivity values [105]. The sensitivity, also known as True Positive Rate (TPR), is computed as follows:

$$TPR = \frac{\text{True Positive}}{\text{True Positive} + \text{False Negative}} \tag{4.3}$$

where a true positive is considered if the classifier prediction and the reference value match within a tolerance window of 60 ms centered at each time step [128], in such a way that a gait phase was counted as detected even though it was missed by around six samples. Otherwise, such classification is considered a false positive. Likewise, the specificity, also known as True Negative Rate (TNR), is computed as follows

$$TNR = \frac{\text{True Negative}}{\text{False Positive} + \text{True Negative}} \tag{4.4}$$

where the non-transitions similarly detected by classifier and reference signal correspond to true negative; otherwise, they have been accounted for by false negatives. G is then expressed as:

$$G = \sqrt{(1 - TPR)^2 + (1 - TNR)^2} \tag{4.5}$$

G can assume values between 0 and $\sqrt{2}$, and a classifier can be considered: (i) optimum when $G \leq 0.25$; (ii) good when $0.25 < G < 0.7$; (iii) random if $G = 0.7$; and (iv) bad

if $G > 0.70$ [129].

The software package SPSS (IBM-SPSS Inc., USA) was used for the statistical analysis. The normal distribution of all performance indices was first verified by means of the Shapiro-Wilks test. Since most data did not exhibit a normal distribution, Friedman tests were carried out to find statistically significant differences among classifiers and, where applicable, differences with respect to the reference values. Bonferroni's tests were undertaken as a post-hoc test in case significant differences were found.

4.4.4 Results

Timing differences between the reference gait labels and the corresponding gait phases detected by either the TB or the HMM-based method are presented in Table 4.1. Almost all timing errors are negative, which indicates anticipation in the gait detection regardless of the segmentation method used. A performance improvement by the HMM-based algorithm was statistically significant for at least one training modality, i.e., either SST or SPT, for all gait phases in the case of healthy subjects ($p < 0.05$). Gait detection for patients, on the other hand, only exhibited a significant difference between algorithms in terms of timing errors in the detection of FF.

Table 4.1: *Timing errors of the detected gait phases* (mean ± std) [ms]. These data were generated by comparing the estimates provided by each classifier with the reference data. Asterisks and obelisks indicate significant differences between marked algorithms (Bonferroni, $p < 0.05$).

	H Group			**P Group**		
	TB Method	**SST Method**	**SPT Method**	**TB Method**	**SST Method**	**SPT Method**
HS	-37 ± 101 *	-55 ± 98 *	-17 ± 10	-17 ± 20	-22 ± 16	-20 ± 17
FF	-57 ± 102 *†	-57 ± 97 *	-23 ± 3 †	-28 ± 12 *†	-29 ± 12 *	-29 ± 12 †
HO	13 ± 30 *	-36 ± 62	-18 ± 6 *	9 ± 29	-19 ± 18	-19 ± 19
SP	-49 ± 96 *	-58 ± 108 *	-18 ± 13	-24 ± 15	-27 ± 14	-23 ± 19

In Figure 4.5 the mean values and standard deviations of the Goodness index (G) for both H and P groups are reported. In addition to that, statistically significant differences among classifiers are included. The TB algorithm presented not only mean

values of G that were found to be in the bad range ($G > 0.7$) for both H and P group, but also significant differences compared to both training modalities of the HMM-based detection method. As for this latter detection algorithm, their G values were found to be in the good range ($0.25 \leq G \leq 0.7$) for both study groups, with the best classification performance presented by SST. Comparing the SST and SPT procedures, significant differences between the two training approaches were only observed for the H group.

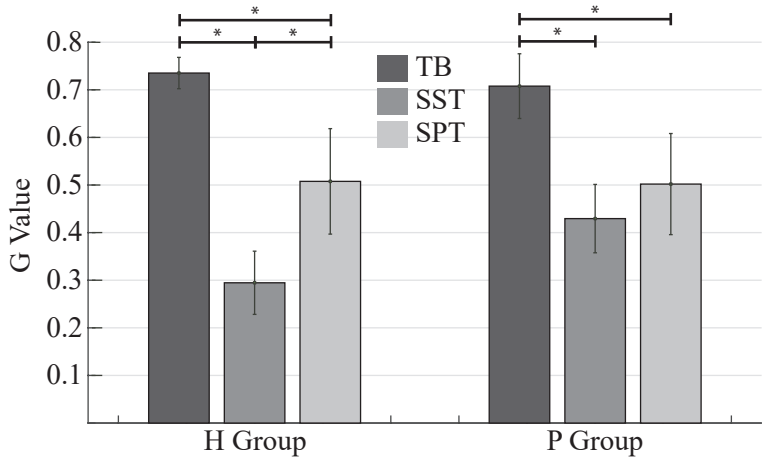

Figure 4.5: *Goodness index* (G) *for healthy subjects* (H) *and subjects with mobility impairments* (P) *for each detection algorithm.* Asterisks indicate statistically significant differences among classifiers (Bonferroni, $p < 0.05$).

4.4.5 Discussion

The TB detection method exhibited similar time differences, compared to reference values established through the FSR insole-mounted system, to those found by Rueterbories et al., whose study involved both healthy and hemiparetic participants wearing biaxial accelerometers on their foot [98]. Furthermore, compared with the findings of Mannini et al., our TB algorithm presents fewer time differences in the detection of stance subphases, i.e. FF and HO, for healthy subjects [124]. However, other studies, which utilized only one inertial sensor, e.g. an uniaxial gyroscope on either the user's shank or foot instep [116, 118] or an uniaxial accelerometer on the lower trunk

[130], showed smaller time delays in a two-phase model (Table 4.1), thereby implying a better performance than the one achieved by the TB algorithm described here. It is important to keep in mind that these results were yielded even though this method was developed based on feature extraction procedures used in previous studies [98, 116], but applied to foot angular velocity and linear acceleration signals. In addition, it should be noted that the gait phase detection by footswitches such as FSR depends significantly on the choice of threshold level that is applied to their output signals, thus producing small differences when applying different threshold settings [117]. Compared to the machine-learning method, HMM outperformed the TB method by showing significant differences with smaller timing errors for all gait phases in healthy subjects either using SST or SPT, as found by Mannini et al. [124, 127]. For the case of hemiparetic subjects, only the detection of FF showed a significant difference among classifiers, which is an important gait event used to avoid the occurrence of false positives in the control system of a robotic orthosis while its user remains in an idle state [119].

Finally, in regards to the goodness index (G), which involves both specificity and sensibility values in order to precisely evaluate the classifier performance, it is worth noting that the TB algorithm showed results within the bad range for both healthy subjects and participants with impairments, which, taking into account the already analyzed results, makes it the worst classifier for gait phase detection. For the case of HMM-based methods, on the other hand, G values within the good and excellent range were observed for both study groups, in spite of some high values of standard deviation exhibited in the SST timing error results (see Table 4.1). Even though a significant difference was found between training techniques for H group, which validates the presumption formulated on the basis of the accuracy values, the inter-subject approach based on standardized data drawn from healthy subjects still has an acceptable segmentation performance (see Fig. 4.5). On the contrary, the training procedures did not exhibit any noteworthy difference when applied to data drawn from patients,

which implies that similar and even better results may be achieved by an inter-subject trained model, as was reported in [105, 129]. Therefore, the use of standardized parameters extracted from healthy subjects seems to lead to a sufficiently robust trained model that may even match the performance achieved by models constructed with SST, without the necessity of continuously carrying out a training stage.

4.5 Online Implementation

Knowing that the gait phase classification using an HMM and foot gyroscope signals is sufficient to make an accurate GPDS, its real-time implementation becomes fundamental for it to be used in lower-limb rehabilitation robots. As the reader may remember from Section 4.3.2, the construction of an HMM entails two main phases: the training stage and the test stage. For the case of the HMM training procedure (see Fig. 4.2), the Baum-Welch algorithm applied via the subject-specific approach remains an appropriate option to fit a model. However, the test stage, which is mostly tackled by the Viterbi algorithm (see Fig. 4.2), should be addressed by other alternatives for real-time applications. Therefore, in order to better understand the transition to an online algorithm, it is worth explaining the differences between the standard approach to decode the most-likely state sequence and online techniques that rely on fixed observation windows, along with the implications of the latter in terms of processing power requirements.

4.5.1 Standard Viterbi Algorithm

The standard Viterbi is a dynamic programming technique that consists in retrieving a state sequence that maximizes the maximum a-posteriori probability, i.e. the optimal path s* [131]. This alignment between observations and states is usually performed in two main iterative steps [132]:

1. A forward step computes the partial likelihood $\delta_t(i)$ and stores the best predecessor for each state i at time t in a matrix of back-pointers $\psi_t(i)$.

2. A bactracking step on $\psi_t(i)$ builds the optimal path starting from the end of the observation sequence.

The Viterbi algorithm, despite its computational efficiency, is not suitable for online applications since the back-pointers it uses are computed based on a whole observation dataset. On this basis, new online decoding approaches such as the Forward-Only Viterbi (FO) have been developed to overcome this limitation, taking advantage of the partial backtracking of fixed observation windows.

4.5.2 Forward-only Viterbi (FO)

The FO modification of the Viterbi algorithm is applied to each signal in order to find the l-th state of likely sequence l_{t_n} and the probability associated at each i-th state $\delta_{t_n}(i)$ [119]. Particularly, this decoding approach can be deployed by implementing the pseudo-code presented in Algorithm 1.

Algorithm 1 FO algorithm

Require:
procedure INITIALIZATION
    $\delta_{t_0}(i) \leftarrow \pi_i b_i(Y(t_0)),\ 1 \leq i \leq N$;
    $l_{t_0} \leftarrow \text{argmax}_{1 \leq i \leq N}\, \delta_{t_0}(i)$;
end procedure
Ensure: l_{t_n}
for each new frame b **do**
    $\delta_{t_n}(i) \leftarrow max(\delta_{t_{n-1}}(i)A_{ij}) \times B_i(Y(t_n))$;
    $l_{t_n} \leftarrow \text{argmax}_{1 \leq i \leq N}\, \delta_{t_n}(i)$;
end for

A study performed by Mannini et al., however, found that this Viterbi decoding procedure is plagued by erroneous events that consist of missed and additionally detected

gait strides [133]. Contrary to the mentioned study, in which a heuristic strategy discarded detected gait strides if their time duration was less than 250 ms, we do not take into account gait phases that last less than 150 ms (i.e., the shortest period for HS in healthy subjects during comfortable walking [134]).

4.5.3 Preliminary Results

After deploying the above-described algorithm in ROS, an experimental protocol was performed aiming at quantifying its latency values , i.e., the time difference between the detected gait segmentation produced by the proposed algorithm and the reference labels generated by means of the custom insole-based system. To this end, one healthy male subject (27 y.o., 68.4 kg, 1.70 m) without any known lower-limb impairment or mobility deficit was recruited. Once the subject was equipped, he was instructed to walk for at least 180 s on a rehabilitation treadmill configured at a zero-degree inclination level and a comfortable speed (0.833 m/s, computed as the mean value of three 10-m tests). This walking trial was repeated three times so that enough data was available to train the model.

Data acquisition and processing were undertaken online using the main board (Raspberry Pi). Both the FSR and IMU sampling rates were set to 100 Hz, and data acquisition was synchronized by means of timestamps generated by ROS. The training stage of the HMM-based method was conducted by implementing the well-know intra-subject approach, i.e., the foot-motion data captured in the two first walking trials was used to feed the Baum-Welch algorithm, whilst the last trial served as the dataset for the validation stage.

Fig. 4.6 features the gyroscope signal along the sagittal plane (y-axis for the reference framework of the used IMU), reference labels drawn from the FSR-based reference system and gait phases detected via FO . This data is displayed across two gait cycles from the entire last trial, and better represents the latency values mentioned previously.

In particular, the latency is comprised within the time window delimited by the online detected gait phase transition and the reference transition (vertical ascents of red and green lines, respectively).

By computing such latency of detection for each gait phase of interest, together with

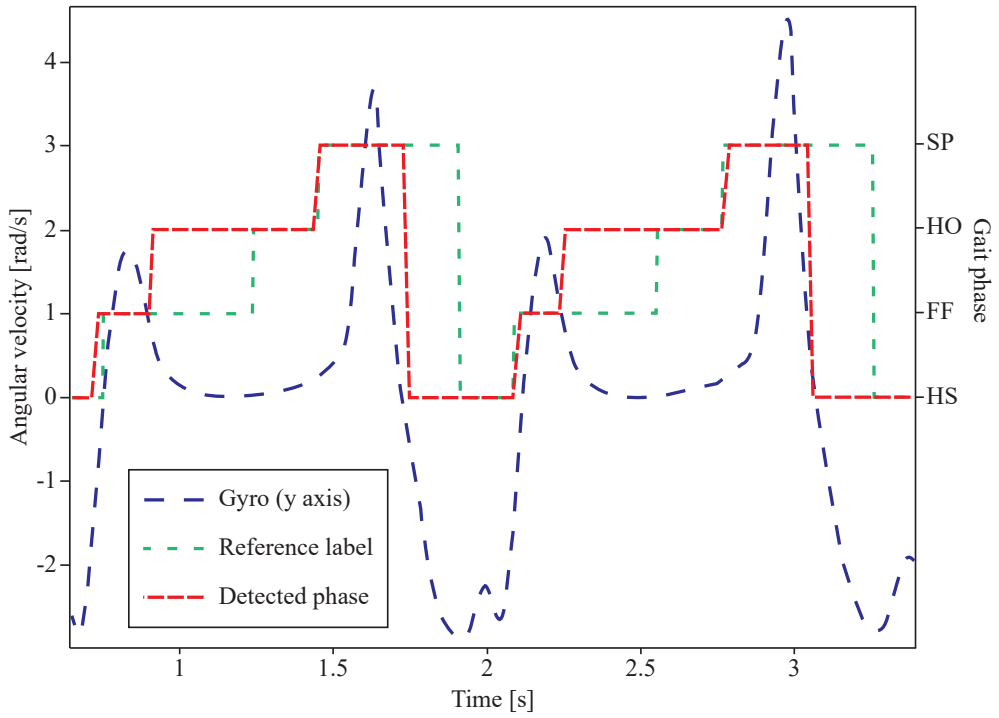

Figure 4.6: Gyroscope signal along the sagittal plane (y-axis), reference labels and the detected gait phases across two gait cycles by means of FO.

Table 4.2: *Latency values between detected gait subphase and reference label* [ms] (mean ± std. deviation), together with typical phase duration for healthy subjects walking at a comfortable speed and the percentage within the gait cycle (value in parentheses) are presented as a means of reference.

	FO	**Typical**
HS	-174 ± 25	80.1 (8%)
FF	-20 ± 50	320.4 (32%)
HO	-322 ± 13	200.3 (20%)
SP	-3.1 ± 18	400.5 (40%)
Insertions (%)	0	
Deletions (%)	0	

the percentage of deletions and insertions, online timing errors can be reported as in Table 4.2. Compared to previous studies that also used similar decoding approaches, our results seem to be higher since, in such works, the detection latency was found to be less than 100 ms for almost all gait phases [127]. However, HO was also the gait phase whose estimate was affected by the higher variability (~ -322 ms), whereas SP was the one with better detection rate, which might be helpful in applications in which the prevention of toe drag is crucial. The reason for the higher latencies and the fact that almost all gait phases yielded negative values might be underpinned again by the variability associated with the gait phase detection through footswitches, which results from small differences that appear among different threshold settings [117]. Furthermore, the absence of insertions and deletions suggests that this approach is efficient enough not to take into consideration detected phases beyond the established transitions. On this basis, it is reasonable to state that the accuracy rate found in the offline validation (Section 4.4) has not been diminished to a significant extent.

4.6 Conclusions

In this chapter, the validation of two algorithms: a TB and a HMM-based method, in the gait event detection of healthy subjects and patients with gait abnormalities is addressed, with the objective of figuring out which detection method outperforms for a GPDS that only makes use of an IMU placed on the subject's foot instep. The TB algorithm takes the foot angular velocity and linear acceleration along the sagittal plane as inputs, since the data fusion of these parameters allows the compensation of the drift error [106] and the use of a single-axis angular velocity signal may cause problems in situations where the subject spontaneously changes direction or turns [98]. When implementing only the HMM-based technique, it is not mandatory to take any special care to align the IMU sensitive axis perpendicular to the sagittal plane or the use of a Kalman filter for the effects induced by magnetic distortions [124] since only gyroscope signals are fed to this machine-learning scheme. The training stage used in

this study is undertaken by implementing two different approaches: an intra-subject or SST and an inter-subject approach that trains the gait detection model based on standardized parameters from the dataset of the healthy group.

Its offline validation yielded results in terms of timing errors and goodness index which indicate that the best classifier is the HMM-based method, whose standardized parameter training showed similar performance rates to those exhibited by the intra-subject technique in pathological subjects. Such findings suggest that the use of a single gyroscope on the dorsal side of the foot is sufficient to accurately detect gait phases within the control system of a lower-limb orthotic device.

Furthermore, the real-time implementation of the HMM-based detection scheme was possible by deploying an online hidden-state decoding method, namely the FO Viterbi algorithm. Preliminary results in terms of latency values, obtained involving a healthy subject, suggest that this decoding approach might be suitable for its application in a robotic assistive device meant for gait rehabilitation since no gait subphase yielded latencies higher than their average duration in healthy subjects walking at a comfortable speed. Further research should focus on the recruitment of further healthy and pathological subjects to validate the efficiency of such decoding algorithms in a wider patient sample.

Chapter 5

High-Level Architecture of the AGoRA Exoskeleton[1]

5.1 Introduction

In order to induce motor learning based on the principle of neuroplasticity, studies have shown that therapy is only effective if task-oriented activities are performed whereby patient effort is promoted [135]. In pursuit of that, robot-assisted therapy based on Assisted-as-needed (AAN) control strategies mainly aims to avoid any intervention as long as the patient moves along a pre-defined behavior established in the low-level control modules. On this basis, lower-limb active orthoses should exert a restoring force that proportionally increases with the path deviation, thus complying with the rationale of assisting only when it is strictly necessary [136]. The present chapter seeks to describe in-depth the high-level architecture of the AGoRA exoskeleton which relies on AAN control strategies to better assist patients with hemiparesis.

[1]Part of this chapter is based on the following conference proceedings:
Sanchez Manchola, M. D., Arciniegas Mayag, L. J., Munera, M., & Cifuentes Garcia, C. A. (2019). Impedance-based Backdrivability Recovery of a Lower-limb Exoskeleton for Knee Rehabilitation. In 2019 IEEE 4th Colombian Conference on Automatic Control (CCAC) (pp. 1–6). IEEE. https://doi.org/10.1109/CCAC.2019.8921278

By the term "high-level", to be further mentioned in this chapter, the author means the aspects of the control system that are explicitly designed to promote motor plasticity [136]. “High level" control algorithms are those which infer the human intention and determine the assistance strategies on its basis, rather than control the actuators to achieve a desired position, force, etc (i.e. the “low level" approach) [51]. For the case of the AGoRA exoskeleton, such a "high-level" control approach is supported by position, velocity, and force low-level controllers, previously described in Section 3.3.

The control architecture proposed in this chapter is intended to be used in a unilateral version of the AGoRA exoskeleton, i.e. the orthosis is meant to assist the hip and knee joints of one side of its user. By implementing this configuration, the author expects to create a device that may contribute to the problem area exposed in Section 1.1, where stroke survivors play an important role. Since these patients tend to suffer from hemiparesis or weakness on only one side of their body, unilateral assistance poses a promising rehabilitation alternative for this population in particular. By modeling the kinematics of such a structure, its dynamics can be anticipated and compensated to some extent through a feedforward (FFw) control loop.

5.2 Feedforward Control

One side of the AGoRA exoskeleton may be described as a 2-DoF mathematical model comprised of two main parts: a kinetic model and a friction model. The kinetic model relates to the ideal torque behavior of the exoskeleton joints, whereas the friction model depicts the torque value the actuation mechanism needs to exert to compensate for the influence of friction. Both models serve as feedforward (FFw) control loops of the overall high-level architecture to generate compensation torque profiles.

5.2.1 Kinetic Model

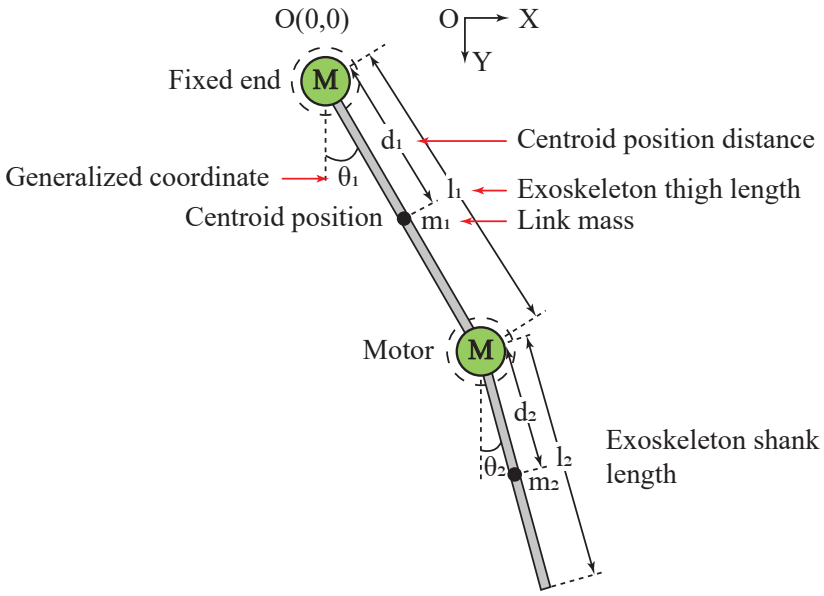

Figure 5.1: Kinetic model of 2-linkage robot. Adapted from [137].

As the actuated motion of the AGoRA exoskeleton takes place along the sagittal plane, the kinetic model is analyzed in a single plane. Thus, the lower-limb wearable robot may be simplified as shown in Fig. 5.1. In this study, the method of Lagrange is used to establish the kinetic model of the exoskeleton. The corresponding Lagrange equation is given in Eq. 5.1 and 5.2.

$$L = E_k - E_p \tag{5.1}$$

$$T_s = \frac{1}{dt}\left(\frac{\partial L}{\partial \dot{\theta}_i}\right) - \left(\frac{\partial L}{\partial \theta_i}\right) \tag{5.2}$$

where E_k is the total kinetic energy of the system; E_p is the total potential energy of the system; L is the Lagrange function; T_s is the joint torque; and θ_i and $\dot{\theta}_i$ $(i = 1,\ 2)$ are the generalized coordinate and velocity, respectively [137]. E_p and E_k can be

rewritten as in Eq. 5.3 and 5.4.

$$E_p = \sum_{i=1}^{2} m_i g y_i \tag{5.3}$$

$$E_k = \sum_{i=1}^{2} \left[\frac{1}{2} m_i \left(\dot{x_i}^2 + \dot{y_i}^2 \right) + \frac{1}{2} I_i \dot{\theta_1}^2 \right] \tag{5.4}$$

where m_i is the link mass; l_i is the rotational inertia; g is the acceleration of gravity; and $(x_i,\ y_i)$ is the centroid position of link. For simplicity, the fixed end $O(0,\ 0)$ in Fig. 5.1 is chosen as coordinate origin [137]. According to the geometric relation, the centroid position $(x_i,\ y_i)$ can be written as in Eq. 5.5.

$$\begin{cases} x_i = \sum_{j=1}^{i-1} \left(l_j \sin \theta_j \right) + d_i \sin \theta_i \\ y_i = \sum_{i=1}^{i-1} (l_j \cos \theta_j) + d_i \cos \theta_i \end{cases} \tag{5.5}$$

where d_i is the distance of centroid position from joint; l_i is the link length; and θ_i is the angular displacement between link and vertical shaft (generalized coordinate) [137]. Moreover, the centroid velocity can be also expressed as in Eq. 5.6.

$$\begin{cases} \dot{x_i} = \sum_{j=1}^{i-1} \left(l_j \dot{\theta_j} \cos \theta_j \right) + d_i \dot{\theta_i} \cos \theta_i \\ \dot{y_i} = -\sum_{i=1}^{i-1} (l_j \dot{\theta_j} \sin \theta_j) - d_i \dot{\theta_i} \sin \theta_i \end{cases} \tag{5.6}$$

where $\dot{\theta_i}$ is the angular velocity (generalized velocity) [137]. Integrating equations from 5.1 to 5.6, the dynamics of a 2-link exoskeleton robotic system without considering the human limb dynamics are modelled as presented in Eq. 5.7.

$$M(\theta)\ddot{\theta} + C(\theta, \dot{\theta})\dot{\theta} + G(\theta) = T_s \tag{5.7}$$

where $q,\ \dot{q},\ \ddot{q} \in \mathbb{R}^2$ represent position, velocity and acceleration vector in the joint space, respectively. $M(\theta) \in \mathbb{R}^{n\times n}$ is the symmetric positive definite inertia matrix. $C(\theta,\ \dot{\theta}) \in \mathbb{R}^{2\times 2}$ denotes the Centripetal and Coriolis forces, and $G \in \mathbb{R}^2$ is the gravitational force vector [137, 138].

The inertia matrix $M \in \mathbb{R}^{2\times 2}$ and the Coriolis matrix $C \in \mathbb{R}^{2\times 2}$ in Equation 5.7 are determined as shown in Equations 5.8 and 5.9, respectively [138, 139].

$$
\begin{aligned}
M &= \begin{bmatrix} M_{11} & M_{12} \\ M_{21} & M_{22} \end{bmatrix}, \\
M_{11} &= I_1 + I_2 + m_1 d_1^2 + m_2 l_1^2 + m_2 d_2^2 + 2 m_2 l_1 d_2 \cos\theta_2, \\
M_{12} &= I_2 + m_2 d_2^2 + m_2 l_1 d_2 \cos\dot{\theta}_2, \\
M_{21} &= I_2 + m_2 d_2^2 + m_2 l_1 d_2 \cos\theta_2, \\
M_{22} &= I_2 + m_2 d_2^2.
\end{aligned}
\tag{5.8}
$$

$$
\begin{aligned}
C &= \begin{bmatrix} C_{11} & C_{12} \\ C_{21} & C_{22} \end{bmatrix}, \\
C_{11} &= 2 m_2 l_1 d_2 \dot{\theta}_2 \sin\theta_2, \quad C_{12} = m_2 l_1 d_2 \dot{\theta}_2 \sin\theta_2, \\
C_{21} &= -m_2 l_1 d_2 \dot{\theta}_1 \sin\theta_2, \quad C_{22} = 0.
\end{aligned}
\tag{5.9}
$$

Finally, the gravitational torque vector $G \in \mathbb{R}^2$ is stated in Equation 5.10 [138, 139]. By exporting the exoskeleton's kinematics from the CAD software *Solidworks* (where it has been initially modeled) and having its position and velocity behaviors monitored through the motor encoders, the torque related to the device kinematics may be easily compensated via software.

$$
\begin{aligned}
G &= \begin{bmatrix} g_1 \\ g_2 \end{bmatrix}, \\
g_1 &= m_2 g \left(d_2 \sin\left(\theta_1 - \theta_2\right) + l_1 \sin\theta_1 \right) + m_1 g d_1 \sin\theta_1, \\
g_2 &= m_2 g d_2 \sin\left(\theta_1 - \theta_2\right).
\end{aligned} \tag{5.10}
$$

5.2.2 Friction Model

Kinematic equation 5.7 depicts the rigid kinematic model of the AGoRA exoskeleton, i.e., the effect of non-rigid forces such as friction is not taken into consideration. Since friction torque plays an important role in exoskeleton control [140], a better description of the actual system should include the well-known friction torque model, which encompasses both dynamic friction and steady friction. Such a friction model is given by Eq. 5.11.

$$
T_f = \begin{cases} F_c \mathrm{sgn}(\dot{\theta}) + \sigma\dot{\theta}, \ \dot{\theta} \neq 0 \\ T_m, \left(|T_m| < F_s\right) \ \& \ \left(\dot{\theta} = 0\right) \\ F_s, \left(|T_m| \geq F_s\right) \ \& \ \left(\dot{\theta} = 0\right) \end{cases} \tag{5.11}
$$

where $F_c \in \mathbb{R}^2$ is the Coulomb friction torque; $\sigma\dot{\theta} \in \mathbb{R}^2$ is the viscous friction torque; $F_s \in \mathbb{R}^2$ is the static friction torque and $T_m \in \mathbb{R}^2$ is the starting torque of the motor-gearbox construction [137]. According to the mechanical structure, one can imply that:

$$
T_s = K_g T_m - T_f \tag{5.12}
$$

where K_g is the gear ratio. By implementing a FFw control loop both kinematic and friction behaviors, which are intrinsic to the AGoRA exoskeleton, can be suppressed

to a certain extent via software by using the parameters presented in Table 5.1.

Table 5.1: Parameters of the kinematic and friction models.

Parameter	**Hip** ($i = 1$)	**Knee** ($i = 2$)
m_i [kg]	2.13	0.84
l_i [m]	0.498	0.428
d_i [m]	0.256	0.256
I_i [kg·m^2]	0.16	0.05
F_s [N·m]	0.9	0.9
F_c [N·m]	0.8	0.8
σ_i [N·m/rad·s^{-1}]	1.2	1.2
K_g [N·m]	160	160

5.3 Transparent Mode (TM)

Even though the actuation mechanism used for the AGoRA exoskeleton can exert torque profiles which are sufficient to assist human lower limbs (as addressed in Section 3.2.2), the assembly motor-gearbox employed in each exoskeleton joint does not allow the unpowered hardware to comply with the user's command. Since such behavior could eventually cause injuries to the patient by restricting their natural gait pattern, the implementation of compliant control strategies appears to be necessary to mitigate these adverse effects.

The above-outlined dynamics requires the free movement of each exoskeleton segment, which can be achieved using a system with force feedback. To this end, admittance controllers have proven to be stable in high stiffness conditions [141]. An admittance controller is a variation of the impedance controller (designed by Hogan in 1984 [142]) whose performance highly depends on the precision of the force sensor and actuator position. The mechanical admittance Y may be expressed as in Eq. 5.13.

$$Y = v/F \tag{5.13}$$

where v is the velocity of the controlled system at the interaction point, and F is the interaction force. Based on this expression, one may infer that a large admittance value corresponds to a rapid velocity caused by external forces. If the mechanical impedance of the exoskeleton could be zero (infinite admittance), its user would not feel any resistance while wearing it. However, this zero-impedance behavior is only ideal, given the actuator's intrinsic inertia and friction, and the controller time delay [143]. Low impedance, nonetheless, can be achieved if the control system takes into account the user's motion intention. This low impedance behavior is widely known as backdrivability [144], and good backdrivability provides numerous benefits in robot-assisted gait training, e.g. the ability to act as a monitoring tool for health professionals [145]. The dynamic behavior of the HRI present in the AGoRA exoskeleton can be modeled as shown in Fig. 5.2.

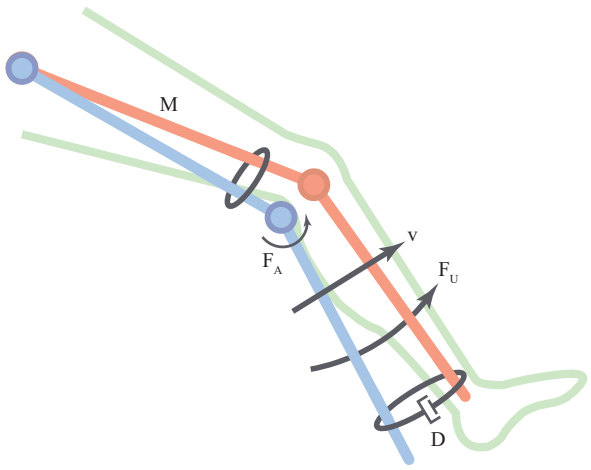

Figure 5.2: Schematic of mass-damping system.

In this model, the exoskeleton is assumed to have a given mass M and a damping constant B, and an actuator should be exerting a force F_a, while the user a force F_u. Thus, the equation that describes the system velocity is given by 5.14.

$$M\dot{v} + Dv = F_a + F_u \tag{5.14}$$

Both F_a and F_u are measured by the strain gauges used as force sensors (see Section 3.2.3), so that an interaction force F_i can be considered as follows: $F_i = F_a + F_u$. In the frequency domain, 5.14 can be expressed as in 5.15.

$$v(s) = F/(Ms + D) \tag{5.15}$$

The output velocity value is passed through the low-level velocity controller (embedded within the motor driver, as depicted in Section 3.3.1.3) as an input. Using equations 5.13 and 5.15, the rendered admittance can be modeled as in 5.16.

$$Y(s) = (Ms + D)^{-1} \tag{5.16}$$

The rationale behind the admittance control is to make the actuation mechanism show low impedance (high admittance) when moved by the patient's extremities (see *Ad-*

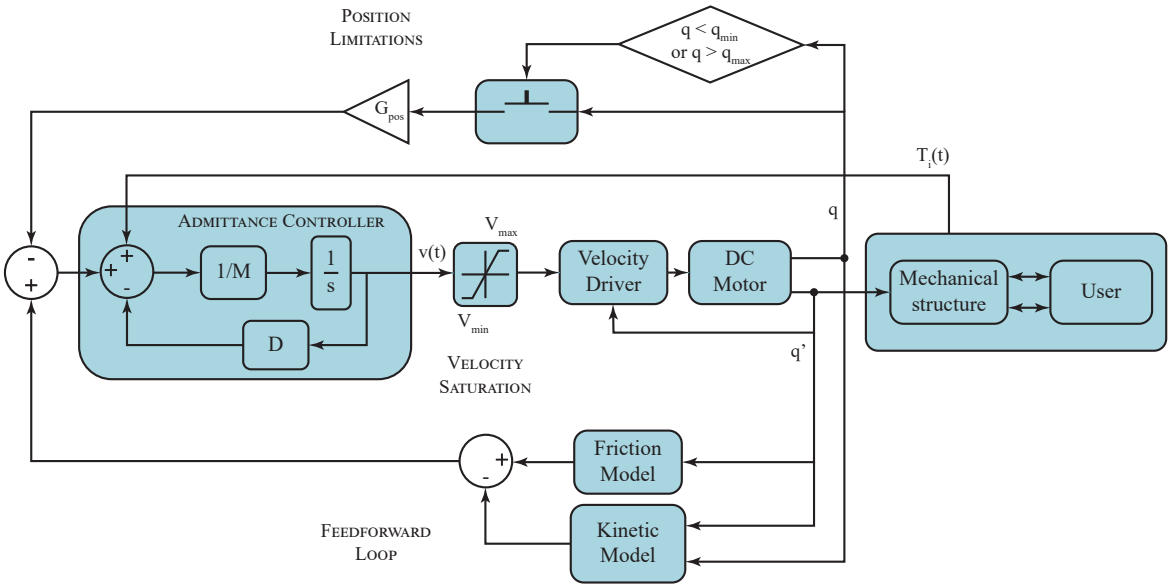

Figure 5.3: *Transparency controller implemented in the AGoRA exoskeleton* to partially compensate the device's intrinsic dynamics. This control approach takes into account the interaction forces between human and machine to render limited velocity profiles accordingly. Additional position limitations are included for the sake of safety.

mittance Controller in Fig. 5.3). The admittance controller normally receives the Human-Robot Interaction (HRI) forces as input and is able to render velocity accordingly as output. The impedance parameters M and D are set to 0.25 kg and 2.5 N/(m/s), respectively, which are obtained empirically from tests undertaken on a test bench. Further, since safety plays a relevant role in the actuation of this type of assistive devices, limits in terms of position are also taken into consideration. This essentially means that, if the user would try to move within ranges of motion which are not anatomical, they should not be allowed to do it. Therefore, in order to avoid exceeding joint limits and subsequently cause damage or instability to the user, TM also includes some position limitations, i.e. the joint speed proportionally decreases if the configured position-based thresholds are surpassed (as depicted as *Position Limitations* in Fig. 5.3). Furthermore, an additional saturation feature also limits the output velocity value (between V_{min} and V_{max}) to prevent possible dangerous high-speed movements (see *Velocity Saturation* in Fig. 5.3).

As the exoskeleton is expected to be very compliant while using the present controller, it is suitable to be used as a passive actuator which captures movements during a preliminary learning phase and reproduces them later during an actual assistance phase. Having realized this functionality, a stationary robot-assisted training session aimed at knee rehabilitation was proposed as a proof of concept of the TM described above (as shown in Fig. 5.4) [146]. During learning mode (LM), the user, being guided by a physical therapist, moves their leg while the exoskeleton acts compliantly and records the joint trajectory (q in Fig. 5.3). The learning process ends once the therapist considers the session to be finished as enough knee flexo-extension repetitions were performed. After the therapy has been saved, the corresponding trajectory can be replayed by means of the low-level position controller (embedded in the motor driver, as depicted in Section 3.3.1.2) coupled together with the FFw loop described in Section 5.2. This control approach is addressed here as Replay Mode (RM).

One healthy subject was involved during this preliminary evaluation, who did not

Figure 5.4: *Stationary therapy of the AGoRA exoskeleton.* This approach was undertaken to prove the effectiveness of the transparent mode in terms of the actuator position and velocity. Scan the QR code to watch a demonstration video of this stationary approach. In case you are unable to scan such code, click here: https://www.youtube.com/watch?v=eseWTEUN3e4.

suffer from any mobility-related impairment on the knee joint. Once the device was donned on the subject by using the fastening system, he was instructed to sit on a chair and press the emergency switch under any unusual situation during therapy. After the volunteer was instructed about safety measures, LM was undertaken as a physical therapist drove the subject's knee throughout three flexo-extension cycles at the speed and within angular ranges that were considered appropriate. RM was subsequently performed while position/velocity profiles of the right knee were supervised to evaluate if the exoskeleton could replicate the recorded trial. Both experimental procedures of one trial are displayed in the video whose QR code is shown in Fig. 5.4.

The stored trajectory (LM) and the trajectory performed by the exoskeleton (RM) are depicted in Fig. 5.5a, along with the maximum found position difference among experimental trials (see Fig. 5.5b). Since the position error was never greater than

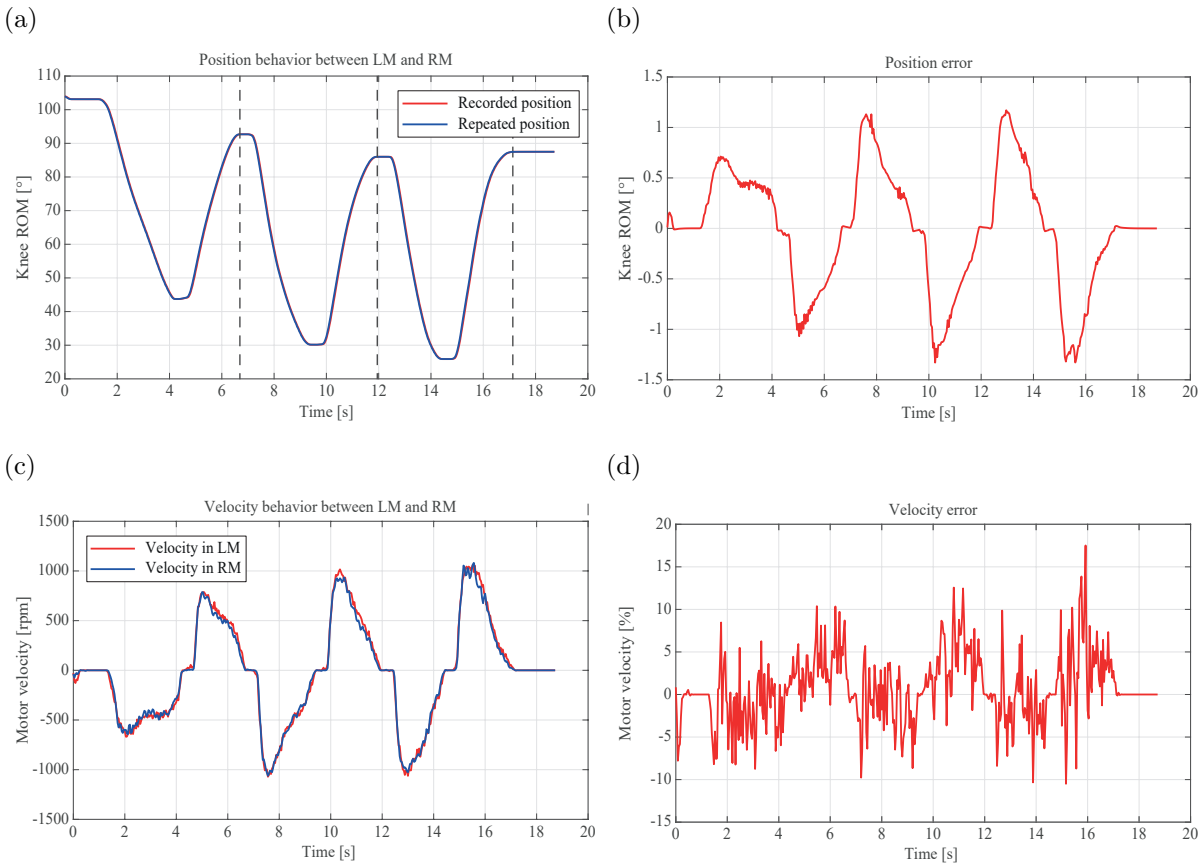

Figure 5.5: *Performance assessment of stationary approach in terms of position and velocity.* (a) Knee ROM, (b) Position error, (c) Motor velocity, and (d) Velocity error compared between LM and RM. Vertical dashed lines denote the end of each knee flexo-extension cycle. RM depicts a smooth repeated trajectory, since the position error does not exceed the ±1.5° and the velocity error is never greater than ±17% of the maximum velocity throughout the whole therapy session.

±1.5°, it can be thus concluded that the device could generate a smooth stationary therapy. The admittance controller seems to make the exoskeleton compliant enough to allow the user to move freely while the applied trajectories are being monitored. Since the RM controller is able to replay this recorded position profile precisely, the actuation mechanism implemented proves to be suitable for this application.

Fig. 5.5c and 5.5d additionally feature velocity profiles between operational modes and its corresponding error. Although the controller implemented in RM is not based

on the motor velocity behavior, the replicated movements exhibit a similar pattern as that corresponding to the recorded therapy, which is borne out by the fact that the velocity error never exceeded ±17% of the maximum recorded velocity (equal to 1062 rpm). This implies that the speed at which the clinician performed the training intervention endures during RM.

The described outcomes are in accordance with those found by studies that also involved robotic knee exoskeletons for therapeutic purposes [19, 26, 147] and present some relevant implications. The performance of the proposed controllers makes the AGoRA exoskeleton a useful tool in the early stage of the rehabilitation, wherein patients normally have weak muscle strength at the knee joint, and continuous and repetitive training is desirable [148].

5.4 Assistance Mode (AM)

While walking, humans change their joint impedance by regulating their posture and muscle contraction levels to maintain stability. Hence, robotic wearable devices must integrate robust methods in pursuit of a suitable impedance modulation throughout gait. An impedance control offers the possibility of regulating the mechanical impedance at joints according to the user's impairment level and their voluntary involvement. This control approach has proven to promote a compliant HRI by providing effective human support in different disability levels [53, 147], thus complying with the AAN premise, which states that an assistive device should only intervene when the patient actually needs some assistance.

Taking into account the above, a stance control strategy was implemented in the AGoRA exoskeleton in order to transition from a stationary therapeutic session to an actual overground assisted gait. A stance controller applies impedance modulation to provide stability and prevent the lower limb joints from collapsing during stance phase, whereas it releases them to allow free movement during swing phase [149].

Studies, which have used this strategy, have reported that it can be used to increase walking speed, reduce energy expenditure and gait asymmetry (for both paretic and non-paretic limbs), thus decreasing muscle stress in patients with muscular weakness [150].

In order to implement a stance controller with the admittance controller described in Section 5.3, an impedance modulation is achieved by directly multiplying a variable gain G by the controller constants M and D (as shown in Eq. 5.17) [147].

$$\begin{aligned} M_i &= M_d \cdot G_i,\ 1 \leq i \leq 4 \\ D_i &= D_d \cdot G_i,\ 1 \leq i \leq 4 \end{aligned} \tag{5.17}$$

where M_d and D_d are the default inertia and damping values, respectively, as stated in Eq. 5.16. G is directly proportional to the system impedance and is updated according to the different gait sub-phases to adapt both joint impedances during gait. The gait cycle is divided here into four gait phases by means of an online variation of the detection algorithm described in Section 4.4 as follows: (i) Heel Strike (HS), (ii) Flat Foot (FF), (iii) Heel-Off (HO), and (iv) Swing Phase (SP), as you may see in Fig. 5.6a.

When varying the controller gain G in terms of this gait partition, typical lower limb angular displacement and moment during gait (as shown in Fig. 5.6b and 5.6c, and Fig. 5.7b and 5.7c, for knee and hip joints respectively) should be displayed. To this end, a different value of G is defined and varies smoothly for each detected gait phase. Fig. 5.6d and 5.7d show an example of G variation within a single gait cycle for the knee and hip joints, respectively. For both cases, $G_i,\ 1 \leq i \leq 4$ require suitable time spans $\Delta t_i,\ 1 \leq i \leq 4$, in which the controller gain linearly decreases/increases until it reaches the desired value for HS, FF, HO and SP, respectively. Such linear change allows the admittance controller to exert smooth velocity profiles in accordance with

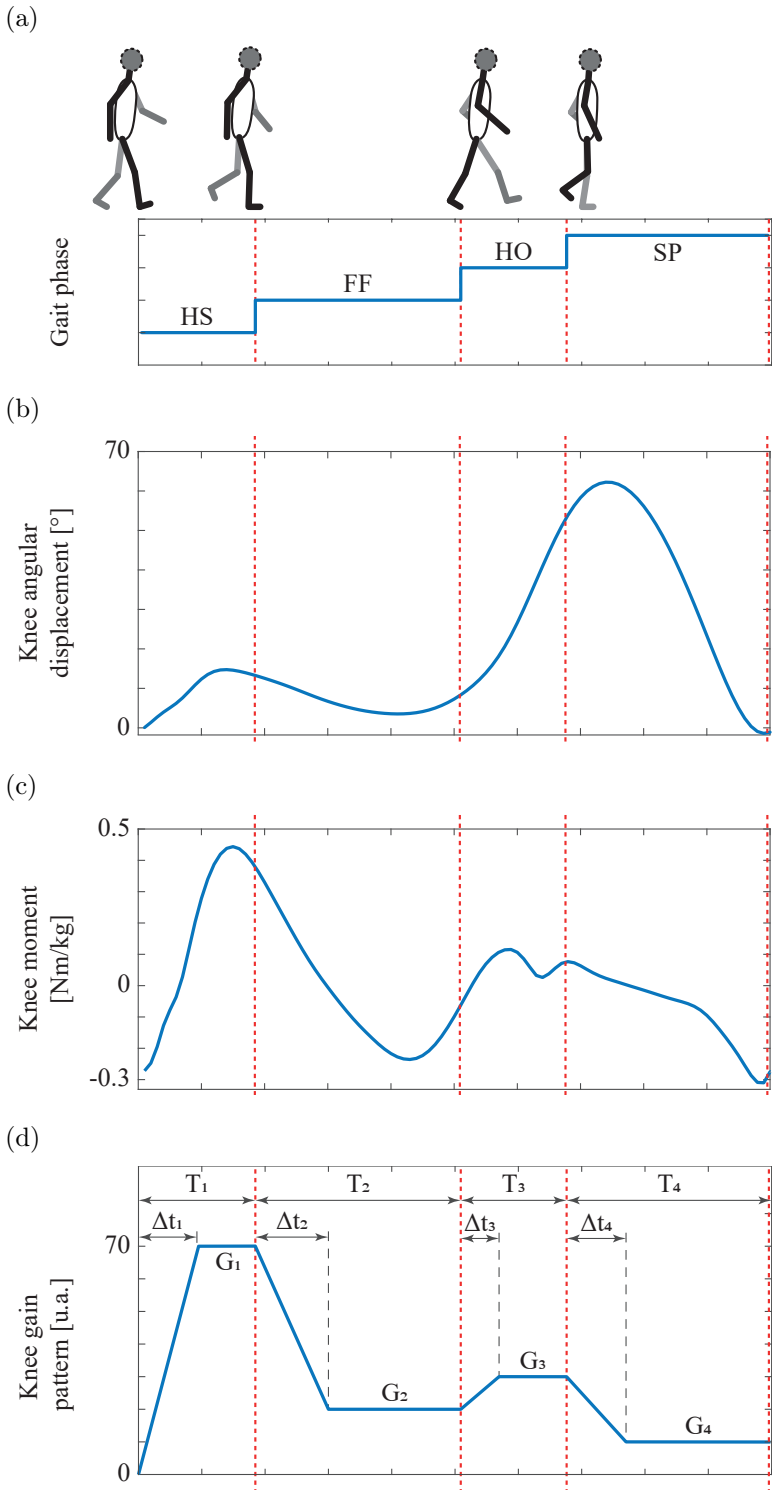

Figure 5.6: *Sagittal knee behaviors related to gait phase detection.* (**a**) Gait phases detected by means of the inertial-based partitioning method. (**b**) Knee angular displacement and (**c**) knee moment throughout the gait cycle in healthy subjects at a comfortable speed [151]. (**d**) Gain pattern based on the knee moment which ensures smooth transitions between gait phases. Adapted from [147].

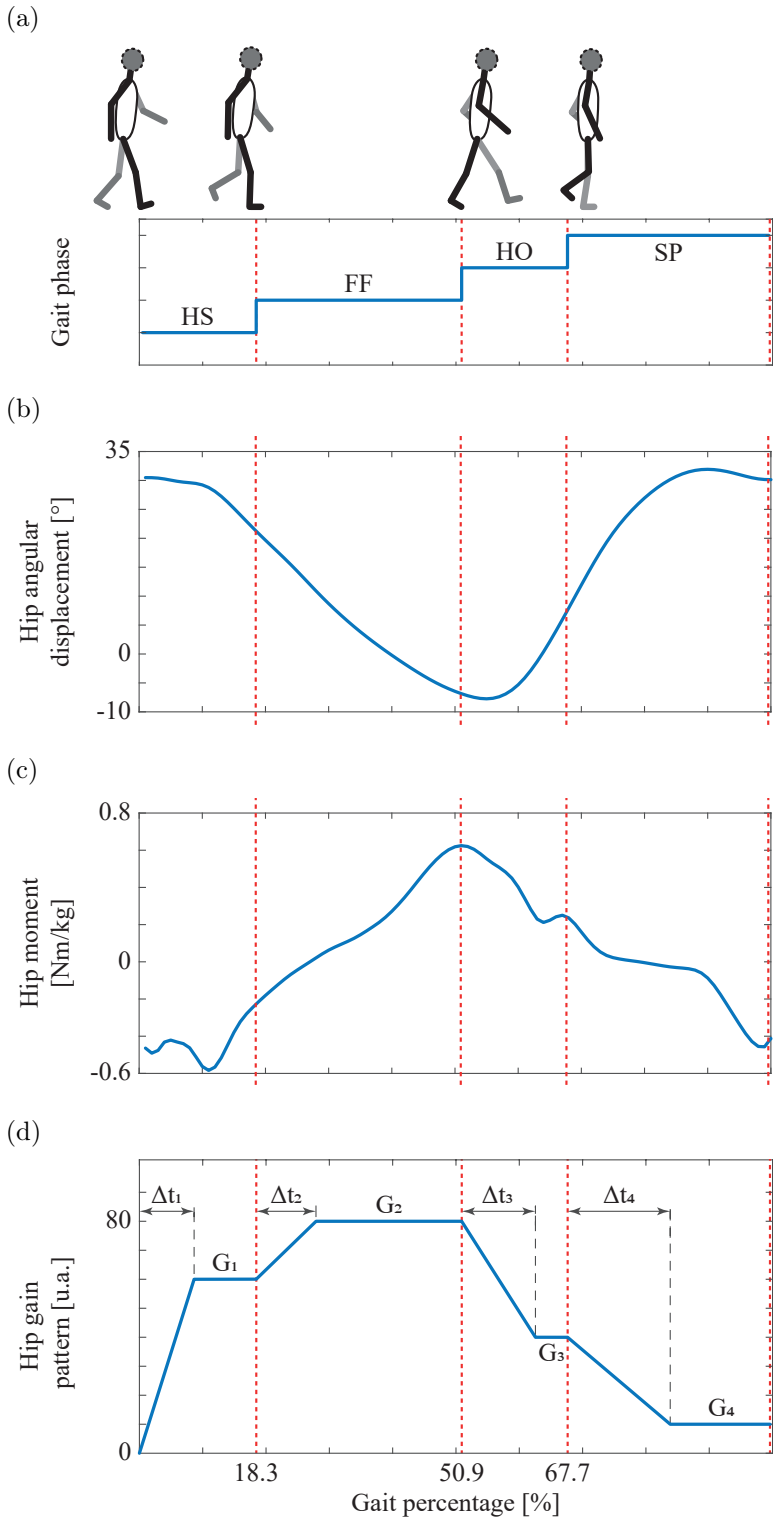

Figure 5.7: *Sagittal hip behaviors related to gait phase detection.* (**a**) Gait phases detected by means of the inertial-based partitioning method. (**b**) Hip angular displacement and (**c**) hip moment throughout the gait cycle in healthy subjects at a comfortable speed [151]. (**d**) Gain pattern based on the hip moment which ensures smooth transitions between gait phases. Adapted from [147].

each subject's gait pattern. Considering that the weight and gait velocity are the anthropometric measures that most affect the knee mechanical behavior [152], these parameters are considered here to define the corresponding G and Δt values [147].

G variations for knee and hip joints (Fig. 5.6d and 5.7d) correspond to patterns based on typical moment variation throughout gait (see Fig. 5.6c and 5.7c, respectively), which are the knee and hip moments reported in a public dataset of overground walking kinematics and kinetics in healthy subjects [151]. And so, for the case of the knee joint, the highest gain value is given during HS when the knee experiences its first flexion, and then it gradually decreases with a slight increase during HO. On the other hand, the impedance modulation for the hip joint keeps the controller gain at high values throughout the stance phase, while there is a significant gain decrease during SP, in pursuit of stability during loading response. For both patterns, the proposed impedance modulation seeks to promote a shock-damping behavior during gait phases associated with weight acceptance (i.e., HS and FF where knee and hip apply a large moment value) [147].

Since time spans Δt_i are fundamental to ensure the smooth variation of G, a relationship between these time periods and known physical properties of the study subject becomes necessary. To this end, the duration of each gait phase T_i may be expressed as in 5.18 [147].

$$T_i = t_{GC} \left(\frac{Q_i}{100} \right) f_s \tag{5.18}$$

where t_{GC} is the duration of the gait cycle, Q_i is the percentage of each gait phase with respect to the entire cycle, and f_s is the sampling frequency. t_{GC} can be estimated through Equation 5.19 [153].

$$t_{GC} = \frac{SL}{v_u} \tag{5.19}$$

where SL is the stride length in meters, and v_u is the user's gait velocity in meters per second. SL can be also estimated from the user's height H by multiplying by the constant 0.826 [153]. Based on this and Equations 5.18 and 5.19, T_i can be expressed as in 5.20.

$$T_i = \frac{0.826(H \cdot Q_i \cdot f_s)}{100 \cdot v_u} \tag{5.20}$$

Experimental trials carried out using the inertial-based detection algorithm (described in Chapter 4) have resulted in the following percentages for each gait phase for healthy subjects: $18.3 \pm 0.02\%$, $32.6 \pm 0.1\%$, $16.8 \pm 0.08\%$ and $32.1 \pm 0.12\%$ for HS, FF, HO and SP, respectively [126]. However, for the sake of simplicity, Q_i is considered to increase by 10% when a new gait phase has been detected ($Q_i = 10 \cdot i$). Assuming that Δt_i represents half of its corresponding T_i, a smooth switching of G is finally obtained by using Eq. 5.21.

$$\Delta t_i = \frac{0.0413 \cdot i \cdot H \cdot f_s}{v_u} \tag{5.21}$$

Algorithm 2 shows the pseudo-code implemented in the Robot Operative System (ROS) for the online gain pattern generation, where Ph_d is the default phase from which the pattern begins to be generated, Ph_c is the current gait phase detected through the inertial-based algorithm, and ΔG is the gain increment added every sample.

Knee moment-based pattern (shown in Fig. 5.6d) is configured to reach the following gain values: $G_1 = 0.7 \cdot W$, $G_2 = 0.2 \cdot W$, $G_3 = 0.3 \cdot W$ and $G_4 = 0.1 \cdot W$, whereas hip moment-based pattern (shown in Fig. 5.7d) is set to follow these gain values: $G_1 = 0.6 \cdot W$, $G_2 = 0.8 \cdot W$, $G_3 = 0.4 \cdot W$ and $G_4 = 0.1 \cdot W$, with W being the user's weight in kg. The performance assessment of both TM and AM during overground robot-assisted gait is described in detail in Chapter 6.

Algorithm 2 Online Gait Pattern Modulation

Require:

procedure INITIALIZATION
    $G_i;\ \Delta t_i \leftarrow (0.0413 \cdot i \cdot H \cdot f_s)/v_u;$
    $Ph \leftarrow Ph_d;\ G \leftarrow G_{Ph_d};$
    $step \leftarrow 1;\ \Delta G \leftarrow 0;$
end procedure

Ensure: G

for each new phase Ph **do**
    if $Ph_c \neq Ph$ **then**
        $\Delta G \leftarrow (G_{Ph_c} - G)/\Delta t_{Ph_c};$
        $step \leftarrow 1;$
        $Ph \leftarrow Ph_c;$
    else
        $G \leftarrow G + \Delta G;$
        $step \leftarrow step + 1;$
        if $step > \Delta t_{Ph}$ **then**
            $\Delta G \leftarrow 0;$
        end if
    end if
end for

5.5 Software Architecture

In recent years, ROS has become the standard framework for software development in the field of robotics [93, 154]. However, ROS (at least in its first version) lacks a real-time communication layer, which represents a fundamental aspect for the control system of wearable robots [53]. In view of this problem, a useful package called `ros_control` has been recently released open-source within this meta-operative system. This package provides the capability to implement and manage robot controllers with a focus on both real-time performance and sharing of controllers in a robot-agnostic way [154]. This means that `ros_control` implements solutions aimed at controller-lifecycle monitoring and hardware resource management by conceiving abstractions (to be further addressed here as hardware interfaces) with minimal assumptions on the hardware and operating system used [154].

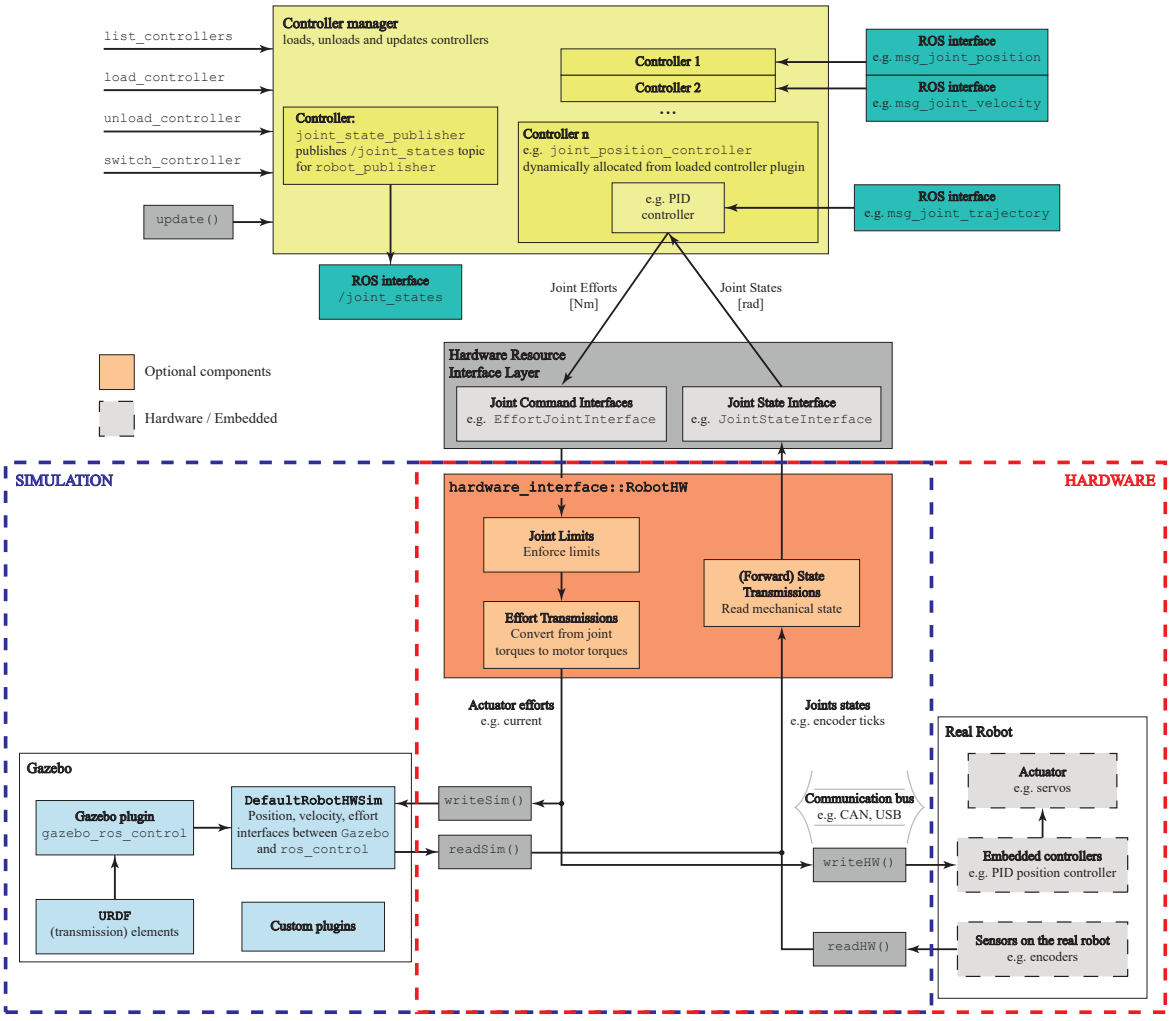

Figure 5.8: High-level software architecture of the AGoRA exoskeleton.

The backbone of the `ros_control` framework is the *Hardware Abstraction Layer* which is provided by the `hardware_interface::RobotHW` class (see Fig. 5.8). This abstraction serves as a bridge to command either real or simulated robots. Many specific robot implementations must inherit from this class since its instances model different hardware resources present in a conventional robot, e.g. electric actuators and low-level sensors such as encoders and force/torque sensors [154]. The rest of the `hardware_interface` package defines read-only or read-write typed joint and actuator interfaces for hardware abstraction, e.g. state, position, velocity and effort interfaces. By means of these typed interfaces, this abstraction enables easy introspec-

tion and increased maintainability [154].

Thanks to the simply-structured software architecture of `ros_control`, only a few configuration files (deployed as `.yaml` files in ROS) had to be modified and an Universal Robot Description Format (URDF) (which is an XML-based robot description [93]) was exported from *Solidworks* to setup a custom hardware interface for the AGoRA exoskeleton. Furthermore, as `ros_control` also provides several libraries to support writing custom controllers, the control modes proposed in Sections 5.3 and 5.4 were implemented relatively easily.

Conversely, the `controller_manager` is responsible for managing the life-cycle of the controllers and hardware resources, and handling resource conflicts between controllers. The controller life-cycles are not necessarily static since they can be queried and modified at runtime through standard `ROS services` provided by the `controller_manager`. Such services (see `list_controllers`, for instance, in Fig. 5.8) allow to monitor, start, stop and setup controllers at runtime [154].

Further, `ros_control` features software libraries addressing transmissions and joint limits. The `transmission_interface` package, for instance, supplies classes implementing different joint- and actuator-space conversions. Particularly, the actuation mechanism of the AGoRA exoskeleton is modeled as a simple reducer to virtually recreate its gear transmission rate (1:160) (see *Effort Transmissions* in Fig. 5.8). A declarative distribution of transmissions is directly supported with the kinematics and dynamics description in the robot's URDF file. Also, the `joint_limits_interface` package contains data structures which represent joint limits and enforce them from the low-level control system (see *Joint Limits* in Fig. 5.8) [154].

Once the transmission interfaces and joint limits have been declared, the simulation of the robot's controllers can be performed in `Gazebo` (the main simulation tool used in ROS) by using `ros_control` and a simple `Gazebo` plugin adapter. An overview between the simulation environment and hardware interface is tagged as *Simulation*

(a)

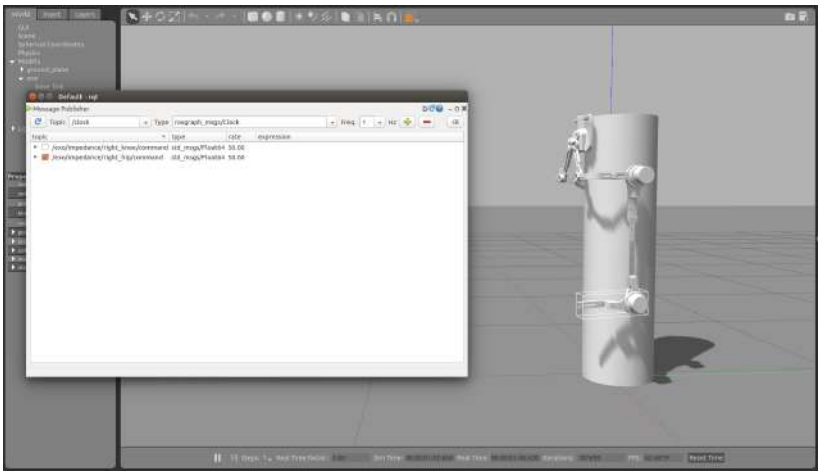

(b)

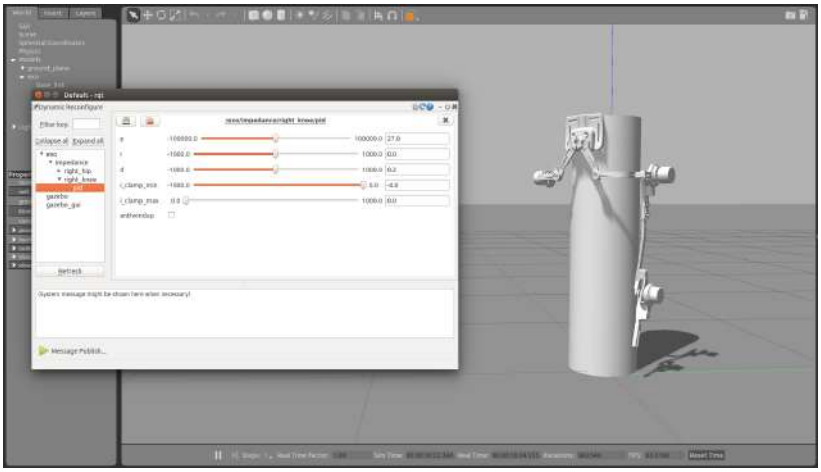

(c)

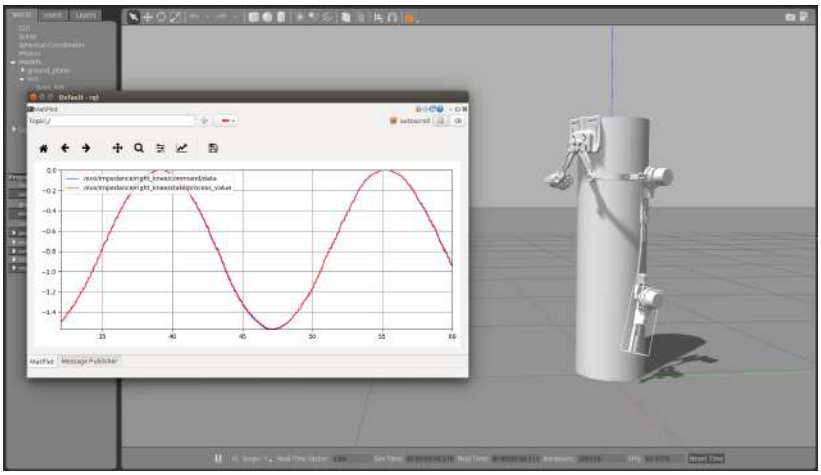

Figure 5.9: `Gazebo` *simulation of the AGoRA exoskeleton.* (**a**) Custom controllers are configured for each joint in pursuit of independent controller handling. (**b**) The controller gains are updated while the simulation runs until (**c**) its performance is optimal.

in Fig. 5.8. In order to load the appropriate hardware interfaces and controller manager into the simulation environment, the `Gazebo` plugin (`gazebo_ros_control` is commonly used) should be added to the robot's URDF. Having the declared controllers already configured on each joint, the visualization tool `rqt_plot` can be then employed to simulate their response upon, e.g., a sine wave, by publishing the signal values to the corresponding controller `topics` (i.e. data buses) at a given transmission rate (as shown in Fig. 5.9a). Moreover, by adding the *Dynamic reconfigure* plugin to `rqt`, the controller gains may be changed at simulation runtime (see Fig. 5.9b), without the need to recompile or modify some configuration file, until the desired performance is reached (see Fig. 5.9c).

By simulating the custom controllers corresponding to TM and AM, one obtains controller gains that are not far away from the optimal values and represent a good start before its actual implementation on the real hardware. Therefore, only a simple empirical variation of the controller gains obtained via simulation is necessary to reach the desired performance in the AGoRA exoskeleton (see *Hardware* in Fig 5.8).

5.6 Conclusions

This chapter features the high-level control architecture of the AGoRA exoskeleton which essentially comprises two control modes: a transparent mode (TM) and an assistance mode (AM). Given the non-backdrivability of the device due to its transmission mechanism, the assessment of the unpowered exoskeleton does not appear to be a feasible option since the proposed hardware is rigid by nature. Therefore, TM deploys a feedforward control loop in series with an admittance controller in order to render velocity profiles based on the user's interaction force with the assistive machine. As a result, the kinematics and dynamics of the exoskeleton are compensated to some extent and its behavior is thus more compliant to the subject's movements. Likewise, AM applies a similar control scheme as the one of TM, but the admittance controller

gain varies according to the detected gait subphases. This gain is computed in terms of the user's weight and height, and its pattern exhibits a moment-based tendency, in order to ensure stability during stance phase. The implementation of these control modes, which take into account the user's motion intention and their gait pattern during overground tasks, represents state-of-the-art control strategies aimed at a proper HRI and complies with the third objective proposed within this thesis.

Chapter 6

Evaluation with Healthy Subjects

6.1 Introduction

Most-commercially available lower-limb assistive devices move the patient's limbs along a predefined, fixed trajectory (i.e., position-controlled approach) [155]. However, it has already been proven that a monotonous repetition of the same gait pattern results in decreased neuromuscular activity, decreased energy consumption, and learned disuse [155, 156]. Whereas passive movements only raise activity in sensory pathways, activate participation induces voluntary neuromuscular recruitment resulting in activation of both efferent motor and afferent sensory pathways [157]. Based on the fact that the patient's active involvement seems to be what primarily promotes mechanisms of neuroplasticity and neural repair during rehabilitation [158, 159], the AGoRA exoskeleton integrates AAN control strategies to be deployed during overground walking in a real environment.

The preceding chapters of this document have provided a detailed description of the theory and technological developments addressed to design and implement the control system of the AGoRA exoskeleton. In order to evaluate such features, this chapter presents the performance assessment of the device and the user's perception towards

its use. The experimental protocol developed for this study comprises a pilot study with healthy subjects walking overground during three experimental conditions: unassisted walking, walking in transparency mode (TM) (see Section 5.3), and walking in assistance mode (AM) (see Section 5.4). The comparison between experimental conditions aims at debugging and optimizing the hardware and software architectures of the AGoRA exoskeleton, and the validation of its control approach before the trials with pathological subjects are conceived.

6.2 Selection Process

The experimental protocol, including all the proposed procedures with healthy subjects, were approved by the local Ethics Committee at the Colombian School of Engineering. All participants recruited for this study signed an informed consent in which they stated to be aware of the possible risks they were facing while undergoing these trials and agree to participate in spite of them. The volunteers of this study were selected based on their health status and physical conditions by taking into account the inclusion and exclusion criteria listed below.

6.2.1 Inclusion Criteria

Male able-bodied adults aged between 18 and 65 y.o. who met the following criteria:

- No history of neurological, neuromuscular or physical disability that may hinder their normal gait pattern.
- Height within the range of 170-185 cm.
- Weight not greater than 100 kg.
- Some specific anthropometric measurements:
  - Femur length: 42-48 cm.

- Distance between trochanters: 32-37 cm.
- Tibia length: 28-31 cm.

These inclusion criteria are established based on the functional range within which the exoskeleton can be adjusted (see Section 3.2.1).

6.2.2 Exclusion Criteria

- Uncontrolled arterial hypertension.
- Some lower-limb abnormality that prevents the participant from wearing the exoskeleton.
- Uncontrolled epilepsy.
- Being under the influence of alcohol, drugs or any kind of narcotic substance during the experimental procedure.
- Any cognitive impairment that prevents the volunteer from reading, understanding or signing the informed consent.

6.3 Experimental Protocol

In order to assess the influence of the proposed control strategies on gait spatiotemporal parameters and lower-limbs kinematics in healthy subjects during exoskeleton-assisted overground gait, a pilot study was conducted at the Institut de Biomécanique Humaine Georges Charpak (Paris, France) involving six neurologically intact subjects (6 males, 25.5±6.07 y.o., height of 1.8±0.027 m, and weight of 71.5±10.9 kg) with no neurological injuries or gait disorders. A unilateral version of the exoskeleton was used for this study in such a way that only right hip and knee joints were actuated, while the left leg was only attached to the mechanical frame (no actuation mechanisms assembled), as may be seen in Fig. 6.1.

At the beginning of the test, the subject's anthropometric features were measured to adjust the exoskeleton segments accordingly and to set up the initial parameters of the admittance controller on the basis of the user's weight and height. Subsequently, the AGoRA exoskeleton was mounted on the volunteer by attaching the Velcro straps to their limbs and donning the backpack containing the battery and the main board. The emergency button was then handed to the subject, as he was instructed to press under any situation that might compromise his safety or comfort. Once the exoskeleton was already worn and powered, ten level-ground 10-m walking trials were performed for each of the two following experimental conditions: TM and AM. Both conditions were randomized for each subject in such a way that he was not aware of which operation mode he was experiencing. After the exoskeleton was removed from the volunteer, ten additional 10-m walking trials were conducted for the assessment of the unassisted

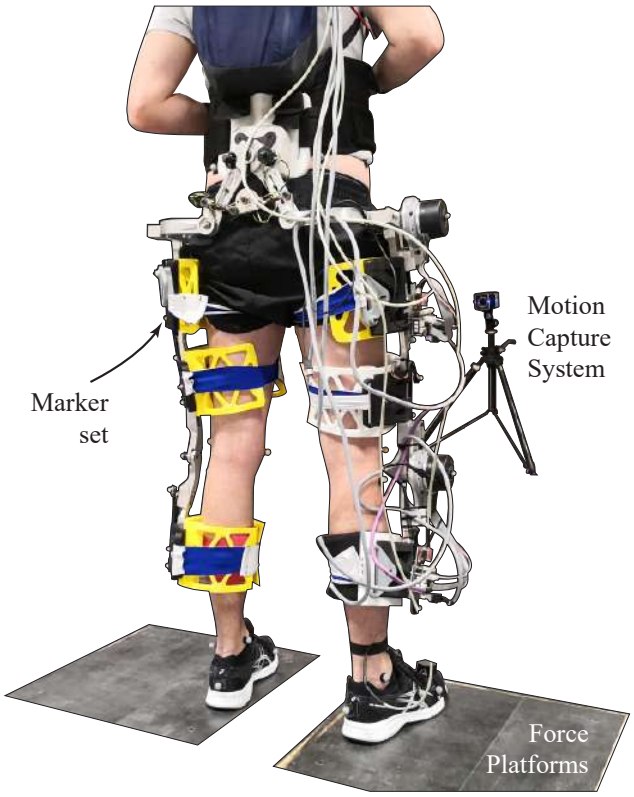

Figure 6.1: Experimental setup for trials with healthy subjects wearing the AGoRA exoskeleton.

mode (baseline level of this study). All subjects were encouraged to walk at their self-selected comfortable speed, while different kinematic and kinetic data were captured as described below.

6.4 Data Acquisition

- **Experimental assistive device:** The first prototype of the AGoRA exoskeleton (described in previous chapters of this document) was not only involved as an assistive tool for overground walking, but also as a means of kinematics and kinetics monitoring. Data acquisition nodes broadcasted the control inputs so that an external computer, which communicated with the main board via Wifi connection, could locally save these parameters for offline analysis.

- **Human joint kinematics:** A 3D-motion analysis system Vicon, equipped with twelve high-speed infrared cameras (Vicon Motion Systems Ltd, Vicon-Oxford, U.K.), was used to monitor human and exoskeleton joint angular displacements at a sampling rate of 200 Hz. The marker set consisted of sixty-five reflective markers, thus allowing a full-body analysis in an indoor analysis laboratory (EPF École d'Ingénieurs, France) (see Fig. 6.1) [160]. The exoskeleton segments were tracked by using custom clusters designed to be taped over the rigid part of the fastening system while they were carrying a set of four markers per-interface (on both assisted and unassisted sides). The subject was instructed to tap the floor once firmly at the beginning of each trial, so that a distinctive peak was recognizable by both measurement systems as a means of data synchronization. Additionally, three force platforms were assembled along a straight pathway to monitor Ground Reaction Forces (GRF) while capturing data at a sampling rate of 1000 Hz [160]. During walking trials, it was ensured that all subjects completely stepped on each force platform at least once. Otherwise, the subjects had to repeat the trial.

6.5 Data Processing

Marker trajectories were first smoothed with an average sliding window (5 values) with two passes in reverse direction to minimize the shifting effect. Any gaps in the raw motion data were filled using a C2-spline interpolation (gaps shorter than 15 frames) within the Vicon's software *Nexus* [161]. Marker trajectories and kinetic data were then imported into OpenSim v.3.3. software and processed through a multibody kinematic optimization technique. To this end, a full-body model was implemented based on Raabe's model [162] to generate a generic full-body model with 25 segments and 54 generalized coordinates. The generic model was then scaled to each participant on the basis of a static acquisition captured before all walking trials. This scaled model was subsequently used to create a second model with a simplified kinematic chain for hip and knee joints. All trials were finally processed using both models and the inverse kinematics tool present in Opensim software in order to obtain gait spatiotemporal parameters and hip-knee kinematics [155, 163].

6.6 Statistical and User's Satisfaction Analysis

Regarding statistical analysis, gait spatiotemporal parameters (e.g. step length, cadence, etc) and hip and knee kinematics from the six involved subjects were loaded into the SPSS software v.23.0 (IBM-SPSS Inc., Armonk, NY, USA), and either one-way repeated-measures ANOVA tests or Friedman tests (non-parametric version of ANOVA test) were conducted to compare among experimental conditions with a statistical significance level of $\rho < 0.05$, depending on whether the data exhibited a normal distribution or not. Bonferroni's tests were carried out as a post-hoc test in case significant differences were found.

Finally, a questionnaire (adapted Quebec User Evaluation of Satisfaction with Assistive Technology, QUEST 2.0) was used to evaluate the subject's perception towards the assistive device [164]. QUEST 2.0 may be also used to assess the user's satisfaction

through questions related to the service provided. However, only the questions related to assistive technology (e.g. weight, safety, durability, simplicity of use, and comfort) were used in this study since the AGoRA exoskeleton is still undergoing validation stages. The score for each question ranges from 1 to 5 (1: not satisfied at all; 2: not very satisfied; 3: more or less satisfied; 4: quite satisfied; and 5: very satisfied), and a final score is obtained from the median value of the valid responses.

6.7 Experimental Results

Spatiotemporal gait parameters among the three experimental conditions, i.e. unassisted, TM, and AM, are presented in Table 6.1. For the six involved participants, these results only demonstrate a significant difference from the unassisted condition for the case of gait velocity while walking in AM ($\rho = 0.048$). Conversely, the other spatiotemporal parameters show no significant difference from the unconstrained baseline (i.e. unassisted condition) which lies close to typical gait parameters found previously for healthy subjects [155].

Table 6.1: *Spatiotemporal gait parameters for all experimental conditions assessed*: Unassisted, Transparent Mode (TM), and Assistance Mode (AM) (mean ± std). Asterisks indicate significant differences from the unassisted condition (Bonferroni, $p < 0.05$).

Parameter	**Unassisted**	**TM**	**AM**
Gait velocity [m/s]	1.12 ± 0.34	0.78 ± 0.35	0.66 ± 0.23 *
Cadence [steps/min]	83.38 ± 21.71	61.95 ± 21.21	58.77 ± 18.33
Stride length [cm]	161.68 ± 9.47	146.88 ± 20.91	135.88 ± 27.77
Step duration (right leg) [s]	0.90 ± 0.46	1.16 ± 0.60	1.15 ± 0.65
Step duration (left leg) [s]	0.70 ± 0.096	1.06 ± 0.51	1.14 ± 0.4
Stride duration [s]	1.59 ± 0.51	2.21 ± 1.02	2.28 ± 0.94
Stance phase (right leg) [%]	53.8 ± 9.52	50.32 ± 11.9	48.28 ± 13.07
Stance phase (left leg) [%]	45.91 ± 9.6	49.32 ± 12.01	51.31 ± 13.09

Likewise, the peak joint angles during unassisted walking and exoskeleton-assisted gait are presented in Table 6.2. Significant differences from the unconstrained condition

were found for the peak knee flexion on the right leg (i.e. the actuated side) during both operation modes: TM ($\rho = 0.001$) and AM ($\rho = 0.000$). Also, the left side, i.e. the inactive side, shows a significant reduction in knee range of motion (RoM) during TM ($\rho = 0.01$). On the other hand, hip kinematics remains untouched while being assisted by the AGoRA exoskeleton since no noteworthy differences were found while the hip RoM lies close to typical values found for healthy subjects during unconstrained overground walking [165].

Table 6.2: *Lower-limb kinematics for all experimental conditions assessed*: Unassisted, Transparent Mode (TM), and Assistance Mode (AM) (mean ± std). Asterisks indicate significant differences from unassisted condition (Bonferroni, $p < 0.05$).

Parameter	**Unassisted**	**TM**	**AM**
Peak knee flexion (right leg) [°]	-66.80 ± 5.59	-47.33 ± 7.10 *	-46.48 ± 5.44 *
Peak knee flexion (left leg) [°]	-64.02 ± 5.65	-52.37 ± 9.46 *	-53.84 ± 11.47
Peak hip flexion (right leg) [°]	26.00 ± 4.62	25.62 ± 7.35	21.97 ± 9.45
Peak hip flexion (left leg) [°]	24.74 ± 4.67	25.04 ± 4.94	26.30 ± 7.71
Peak hip extension (right leg) [°]	-17.22 ± 4.41	-11.58 ± 6.08	-13.86 ± 7.28
Peak hip extension (left leg) [°]	-17.38 ± 4.02	-17.00 ± 3.58	-18.83 ± 5.22

Additionally, the user survey regarding their satisfaction towards the AGoRA exoskeleton controlled by the proposed approaches produced the following median values: weight: 4, dimensions: 3, adjustment (meaning the user's perception towards the system used to attach the exoskeleton to their limbs, i.e. the fastening system and telescopic bars): 3, safety: 5, stability (meaning how close the subject felt as though they were about to fall): 4, durability: 3, ease of use (i.e. how intuitive it is to use): 4, and comfort: 3, within a range between 0 and 5.

Based on the experiences gained during the experimental trials, further use with the designed platform would require a therapist or assistant well aware and capable of adjusting and mounting the exoskeleton on the user. The total time needed for the donning process was found to be around 25-30 min when the orthosis is being used for the first time since more time is required to measure the subject's anthropometric measurements and properly adjust the length of thigh and shank segments.

6.8 Discussion

This work presents the short-term effects on the walking pattern of six healthy subjects while wearing the AGoRA exoskeleton. This lower-limb active orthosis operates using a TM that suppresses the dynamics of a non-backdrivable structure to some extent, and an AM that is meant to provide support to both knee and hip joints during stance phase whereas it allows free movement during swing phase. AM essentially relies on a stance-control approach which varies hip and knee impedances on the basis of two anthropometric measurements: height and weight. Such consideration has been widely taken into consideration in previous designs of stance-controlled orthoses [147, 150].

Regarding spatiotemporal gait parameters, only gait velocity appeared to be significantly affected by the exoskeleton while operating in AM. Even though a slight reduction in gait velocity during AM is not ideal, previous studies have demonstrated that this parameter can reduce up to 0.57 m/s while wearing an orthosis commanded by a stance control approach [150]. Thus, such a variation seems not to be critical, also because further gait parameters did not demonstrate any significant influence by the exoskeleton while they remained close to those which are considered typical among able-bodied individuals. For instance, a study with similar experimental conditions to those imposed in this study found cadence to be around 79.7 ± 3.66 steps/min, whereas the step duration was equal to 0.76 ± 0.04 and 0.75 ± 0.03 seconds for right and left legs respectively, during normal overground walking in a study [155]. Furthermore, a study of gait analysis using an active knee orthosis reports the swing phase to be between 36% and 51% of the gait cycle [166], thus complying with the stance phase percentages found in this work for exoskeleton-aided walking (as may be seen in Table 6.1).

Regarding lower-limb kinematics, at least one significant difference per side was found for the case of the peak knee flexion. Such a reduction in terms of knee angular displacement seems to be attributable to some hardware issue (in particular, to the

fastening system), since the left side, which has no actuation mechanism assembled and thus perceives no electromechanical activation, also shows a significant reduction in knee RoM during TM. An improper attachment to the user's limbs mainly produces joint misalignments which are a well-known problem when dealing with physically coupled systems, e.g. humans wearing exoskeletons [167]. If perfectly-aligned joints are assumed, exoskeleton forces can be modeled as equal. However, the presence of joint misalignment results in the imperfect transmission of torque from the exoskeleton to the user's body [80], thus introducing undesirable forces parallel to the human limb which can cause discomfort or unintended changes in the behavior of the control system. In spite of this, hip kinematics present no considerable change from the baseline condition, which may imply a better attachment to the pelvic region, and thus, better compliance of the exoskeleton's control system on the hip joint.

In relation to user satisfaction, results show that the lowest score (3) was related to the items regarding "dimensions", "adjustment", "durability", and "comfort". It is worth noting that the insight concerning dimensions might be related to the inherent protrusion of the actuation mechanisms which are placed laterally, and whose bulkiness is even more notorious in a unilateral device such as the version proposed for this pilot study. Further, the comfort factor in wearable devices is commonly associated with features such as sensors, straps, and weight [51]. Besides, offering unilateral hip and knee assistance for healthy subjects may be an additional factor that promotes the discomfort experienced by the participants, since some of them expressed to feel some pain at the upper back after wearing the exoskeleton. Physiological theories have been developed to address these limitations [168], but this issue remains to be a major problem for autonomous powered orthoses. On this basis, some hardware modifications are needed to obtain a more robust system and improve the mentioned items, e.g. new materials able to properly adjust the exoskeleton and to suppress relative movement between human and machine.

Finally, it is important to note that this study is limited by the reduced number of

subjects recruited for the pilot study, which compromises to some extent the power of the applied statistical tests. However, since the participants were rather homogeneous in terms of age and anthropometric measures due to the reduced operating spectrum the exoskeleton provided, the outcomes should allow the work team to debug several hardware and software issues discovered during experimental trials for further iterations of the device and prior to the trials with real patients.

6.9 Conclusions

This chapter comprises the performance evaluation of the AGoRA exoskeleton in the short term in healthy subjects. Six neurologically-intact subjects were recruited to perform several overground trials under three experimental conditions: unassisted walking (i.e. no further aids were involved), and exoskeleton-assisted walking while operating in TM and AM (described in previous chapters). Spatiotemporal gait parameters and lower-limb kinematics were processed from measurements captured by the assistive device itself and a motion capture system based on passive optical markers. Additionally, in order to assess the exoskeleton's performance both objectively and subjectively, an user survey was conducted to collect data regarding their satisfaction towards the implemented technology.

Most spatiotemporal parameters did not exhibit any significant change from the unassisted condition for both operation modes, and only knee kinematics was compromised while the user was wearing the exoskeleton. This last issue has been underpinned by an improper attachment to the subject's limbs, as a consequence of a deficient fastening system that did not ensure kinematic compatibility and could have influenced the effect of the torque profiles coming out of the control system. Further iterations of the current device are expected to include a more robust fastening system, in order to improve the impact of the robot-assisted gait training on the knee joint and the user's perception towards the device's adjustment, durability, and comfort. The assessment

of the influence of the AGoRA exoskeleton on the gait pattern of healthy users complies with the final specific objective of this document and represents an advance in the process of actually applying this technology to an impaired patient.

Chapter 7

Conclusions and Future Work

7.1 Conclusions

A robotic lower-limb orthosis, known as the AGoRA exoskeleton, has been designed as a rehabilitation device meant for overground gait training. The long-term goal is to create a tool to help health professionals in the rehabilitation process of stroke and SCI patients. The device mainly consists of a mechanical structure made out of duralumin which is powered along the sagittal plane of both hip and knee joints. A novel passive DoF is included in this design for the hip abduction/adduction motion which is not commonly incorporated in this type of wearable devices. Telescopic bars allow the device to accommodate users from 1.70 to 1.83 m in height. The joint actuators are DC brushless motors coupled with gearboxes: a powerful, energy-efficient, lightweight solution for an ambulatory solution powered via a lithium-ion battery pack. Each actuation mechanism is commanded by an associated motor driver that provides low-level controllers based on position, velocity, and current. This configuration represents a distributed architecture and allows the device to be modular and adapt to the requirements and needs of each user. In order to comply with this modularity, the software architecture also instantiates each connected motor with its characteristic features and

functionalities ready to be used instantly.

Since the gait pattern of neurologically-affected individuals is known to be far removed from the typical walking behavior of healthy subjects, machine-learning-based methods have been lately implemented within the control system of wearable robots to accurately segment the gait cycle. On this basis, the present study proves the optimal performance of an HMM-based detection algorithm trained by means of both intra-subject and inter-subject approaches to partition the gait pattern of healthy and pathological individuals into four gait phases (i.e. HS, FF, HO, and SP), even outperforming the detection via a conventional threshold-based segmentation method. This detection method represents a control middle layer of the AGoRA exoskeleton since the computed gait phase feeds its high-level architecture.

Current control paradigms usually implement normalized kinematics [169], muscle amplification [170] or finite-state controllers [171]. However, relying on pre-defined kinematic trajectories or muscle firing patterns might not be task-specific, thus being inappropriate for rehabilitation purposes [167]. Based on this, the AGoRA exoskeleton operates using a TM that integrates a feedforward control loop and an admittance controller to suppress the dynamics of the non-backdrivable structure to some extent, and an AM that is meant to provide support to both knee and hip joints during stance phase whereas it allows free movement during swing phase. AM virtually amplifies the constants of the impedance controller by a variable gain. This gain varies as a function of the detected gait phase and some user's anthropometric measure (height and weight) and follows a pattern based on the typical walking knee and hip moments. This control strategy intends to behave under the AAN, which dictates that a rehabilitation device should only intervene when the patient needs it.

In order to assess the performance of the control strategies described above, a pilot study involving 6 healthy subjects was conducted within a laboratory setting. An optoelectronic motion capture system collected the trajectories of passive markers placed

at known locations during overground walking trials for three experimental conditions: no exoskeleton attached to the user, the user walking with the device in TM, and the user walking with the exoskeleton operating in AM. These marker trajectories were used to compute spatiotemporal gait parameters and lower-limb kinematics. Since the gait pattern of the involved healthy subjects was significantly compromised during robot-assisted trials, the first prototype of the AGoRA exoskeleton needs further development to reduce this negative influence, and issues such as the fastening system and the resistive nature of the implemented controllers might require reconsideration to this end. Therefore, the findings consigned here should encourage the creation of further versions of the proposed device and should guide subsequent studies regarding the exoskeleton's effectiveness with a larger cohort of participants (potentially pathological).

7.2 Future Work

The research conducted in this study together with the results obtained should serve as preliminary evaluation of the usability of the AGoRA exoskeleton when applied to healthy subjects. However, this work has not intended yet to prove its effectiveness within a gait rehabilitation program. Although the gait pattern of healthy subjects seems to remain unaffected by the actuation of the exoskeleton, further studies should involve actual stroke survivors so that a real comparison with respect to traditional therapy is feasible.

Further modifications should be carried out in the hardware and software architectures prior to trials with pathological patients. Firstly, the fastening system of the device should rely on more resistant and robust materials that prevent relative movement and thus transmit better the torque profiles produced by the control system. Additionally, the author would recommend a different approach for the tuning process of the impedance controller embedded in the proposed strategies, since the current method-

ology is essentially based on empirical tryouts with healthy subjects, and a more robust calibration process might be necessary with pathological individuals. Further, safety-related considerations must be taken into account in subsequent iterations of the current device, e.g. what should happen if a sensor is unintentionally unplugged? what measures should the exoskeleton conduct to avoid eventual malfunction or misoperation? Finally, a graphical user interface should be developed for its use within clinical settings to facilitate the programming and monitoring of the exoskeleton parameters, ranging from inputs such as the patient's info to outcomes such as knee angle and torque.

7.3 Publications

The work presented in this thesis document has been subject of the following scientific publications:

1. **(Conference Proceeding)** Sanchez-Manchola, M., Gomez-Vargas, D., Casas, D., Munera, M., & Cifuentes, C. A. (2018). Development of a Robotic Lower-Limb Exoskeleton for Gait Rehabilitation: AGoRA Exoskeleton. In 2018 IEEE ANDESCON, ANDESCON 2018 - Conference Proceedings. `https://doi.org/10.1109/ANDESCON.2018.8564692`

2. **(Journal Article)** Sánchez Manchola, M. D., Pinto Bernal, M. J., Munera, M., & Cifuentes, C. A. (2019). Gait Phase Detection for Lower-Limb Exoskeletons using Foot Motion Data from a Single Inertial Measurement Unit in Hemiparetic Individuals. Sensors, 19(13), 2988. `https://doi.org/10.3390/s19132988`

3. **(Conference Proceeding)** "Impedance-based Backdrivability Recovery of a Lower-Limb Exoskeleton for Knee Rehabilitation: A Repeatability Pilot Study". 4^{th} IEEE Colombian Conference on Automatic Control (CCAC2019) (*Accepted, waiting for publication*).

Bibliography

1. Lloyd-Jones, D. et al. Heart Disease and Stroke Statistics–2010 Update: A Report From the American Heart Association. *Circulation* **121,** e46–e215. ISSN: 0009-7322 (Feb. 2010).

2. Feigin, V. L. et al. Global and regional burden of stroke during 1990-2010: findings from the Global Burden of Disease Study 2010. *Lancet (London, England)* **383,** 245–54. ISSN: 1474-547X (Jan. 2014).

3. Kwakkel, G., Kollen, B. J. & Wagenaar, R. C. Therapy Impact on Functional Recovery in Stroke Rehabilitation: A critical review of the literature. *Physiotherapy* **85,** 377–391 (July 1999).

4. Simpson, L. A., Eng, J. J., Hsieh, J. T., Wolfe and the Spinal Cord Injury Re, D. L. & Spinal Cord Injury Rehabilitation Evidence Scire Research Team. The Health and Life Priorities of Individuals with Spinal Cord Injury: A Systematic Review. *Journal of Neurotrauma* **29,** 1548–1555 (May 2012).

5. Louie, D. R., Eng, J. J., Lam, T. & Spinal Cord Injury Research Evidence (SCIRE) Research Team. Gait speed using powered robotic exoskeletons after spinal cord injury: a systematic review and correlational study. *Journal of NeuroEngineering and Rehabilitation* **12,** 82 (Dec. 2015).

6. Post, M. & Noreau, L. Quality of life after spinal cord injury. *Journal of neurologic physical therapy : JNPT* **29,** 139–46 (Sept. 2005).

7. *World population ageing* tech. rep. (Department of Economic and Social Affairs (UN), New York, 2017).

8. Chen, B. et al. Recent developments and challenges of lower extremity exoskeletons. *Journal of Orthopaedic Translation* **5,** 26–37 (Apr. 2016).

9. Appelros, P., Nydevik, I. & Viitanen, M. Poor outcome after first-ever stroke: predictors for death, dependency, and recurrent stroke within the first year. *Stroke* **34,** 122–6. ISSN: 1524-4628 (Jan. 2003).

10. Parkes, J., Caravale, B., Marcelli, M., Franco, F. & Colver, A. Parenting stress and children with cerebral palsy: A European cross-sectional survey. *Developmental Medicine and Child Neurology* **53,** 815–821. ISSN: 00121622 (Sept. 2011).

11. Mitra, S. & Sambamoorthi, U. Disability prevalence among adults: estimates for 54 countries and progress toward a global estimate. *Disability and Rehabilitation* **36,** 940–947. ISSN: 0963-8288 (June 2014).

12. *Censo General 2005. 1098 municipios y 20 corregimientos departamentales.* tech. rep. (DANE, 2005).

13. Gaviria Uribe, A., Burgos Bernal, G. & Helfer-Vogel, S. *Línea base del observatorio nacional de discapacidad* 2014.

14. Morone, G. et al. Robot-assisted gait training for stroke patients: current state of the art and perspectives of robotics. *Neuropsychiatric Disease and Treatment* **Volume 13,** 1303–1311. ISSN: 1178-2021 (May 2017).

15. Masiero, S. et al. The value of robotic systems in stroke rehabilitation. *Expert Review of Medical Devices* **11,** 187–198. ISSN: 1743-4440 (Mar. 2014).

16. Belda-Lois, J.-M. et al. Rehabilitation of gait after stroke: a review towards a top-down approach. *Journal of NeuroEngineering and Rehabilitation* **8,** 66 (Dec. 2011).

17. Wolpert, D. M., Diedrichsen, J. & Flanagan, J. R. Principles of sensorimotor learning. *Nature Reviews Neuroscience* **12,** 739–751. ISSN: 1471-003X (Dec. 2011).

18. Cifuentes, C. A. *Human-Robot Interaction Strategies for Walker-Assisted Locomotion* PhD thesis (Federal University of Espirito Santo, 2015), 1–18.

19. Hussain, S., Xie, S. Q. & Jamwal, P. K. Adaptive Impedance Control of a Robotic Orthosis for Gait Rehabilitation. *IEEE Transactions on Cybernetics* **43,** 1025–1034 (June 2013).

20. Young, A. J. & Ferris, D. P. State of the Art and Future Directions for Lower Limb Robotic Exoskeletons. *IEEE Transactions on Neural Systems and Rehabilitation Engineering* **25,** 171–182. ISSN: 1534-4320 (Feb. 2017).

21. Pons, J. L., Ceres, R. & Caldern, L. in *Wearable Robots* 1–16 (John Wiley & Sons, Ltd, Chichester, UK).

22. Tucker, M. R. et al. Control strategies for active lower extremity prosthetics and orthotics: a review. *Journal of NeuroEngineering and Rehabilitation* **12,** 1 (Jan. 2015).

23. Ministerio de Salud y Protección Social. *Plan Decenal de Salud Pública, PDSP, 2012 - 2021* tech. rep. (Bogotá, 2012).

24. Winter, D. A. *Biomechanics and motor control of human movement* 4th ed., 370. ISBN: 9780470398180 (Wiley, 2009).

25. Pasquina, P. F., Emba, C. G. & Corcoran, M. *Lower Limb Disability: Present Military and Civilian Needs* 17–35. ISBN: 978-1-4939-7245-6 (New York, 2017).

26. Bortole, M. *Robotic exoskeleton with an assist-as-needed control strategy for gait rehabilitation after stroke* PhD thesis (Universidad Carlos III de Madrid, 2014).

27. Donnan, G. A., Fisher, M., Macleod, M. & Davis, S. M. Stroke. *The Lancet* **371,** 1612–1623 (May 2008).

28. Knecht, S., Hesse, S. & Oster, P. Rehabilitation After Stroke. *Deutsches Aerzteblatt Online* **108,** 600–6 (Sept. 2011).

29. Carda, S. et al. Efficacy of a Hip Flexion Assist Orthosis in Adults With Hemiparesis After Stroke. *Physical Therapy* **92,** 734–739 (May 2012).

30. Figueiredo, J., Santos, C. & Moreno, J. Assistance and rehabilitation of gait disorders using active lower limb orthoses. *Proceedings - 2015 IEEE 4th Portuguese Meeting on Bioengineering, ENBENG 2015* (2015).

31. Yakimovich, T., Lemaire, E. D. & Kofman, J. Preliminary kinematic evaluation of a new stance-control knee–ankle–foot orthosis. *Clinical Biomechanics* **21,** 1081–1089 (Dec. 2006).

32. Kluding, P. M. et al. Foot Drop Stimulation Versus Ankle Foot Orthosis After Stroke. *Stroke* **44,** 1660–1669 (June 2013).

33. Paolucci, S. et al. Quantification of the Probability of Reaching Mobility Independence at Discharge from a Rehabilitation Hospital in Nonwalking Early Ischemic Stroke Patients: A Multivariate Study. *Cerebrovascular Diseases* **26,** 16–22. ISSN: 1421-9786 (2008).

34. Warlow, C. *Stroke : practical management* 3rd, 995. ISBN: 140512766X (Blackwell Pub, 2008).

35. Dzahir, M. & Yamamoto, S.-i. Recent Trends in Lower-Limb Robotic Rehabilitation Orthosis: Control Scheme and Strategy for Pneumatic Muscle Actuated Gait Trainers. *Robotics* **3,** 120–148 (Apr. 2014).

36. Lin, V. W. & Cardenas, D. D. *Spinal cord medicine : principles and practice* 1043. ISBN: 1888799617 (Demos, 2003).

37. Molinari, M. et al. in *Advanced Technologies for the Rehabilitation of Gait and Balance Disorders* 253–265 (Springer, Cham, 2018).

38. Bax, M. et al. Proposed definition and classification of cerebral palsy, April 2005. *Developmental Medicine & Child Neurology* **47,** 571–576 (2005).

39. Aycardi, L. F. et al. Evaluation of biomechanical gait parameters of patients with Cerebral Palsy at three different levels of gait assistance using the CPWalker. *Journal of NeuroEngineering and Rehabilitation* **16,** 15 (Dec. 2019).

40. *Data and Statistics for Cerebral Palsy* 2018.

41. *Ageing and health* 2018.

42. Lee, W.-S., Cheung, W.-H., Qin, L., Tang, N. & Leung, K.-S. Age-associated Decrease of Type IIA/B Human Skeletal Muscle Fibers. *Clinical Orthopaedics and Related Research* **450,** 231–237 (Sept. 2006).

43. Pollock, A., Baer, G., Pomeroy, V. M. & Langhorne, P. in *Cochrane Database of Systematic Reviews* (ed Pollock, A.) 1, CD001920 (John Wiley & Sons, Ltd, Chichester, UK, Jan. 2007).

44. Paci, M. Physiotherapy based on the Bobath concept for adults with post-stroke hemiplegia: a review of effectiveness studies. *Journal of rehabilitation medicine* **35,** 2–7 (Jan. 2003).

45. Mehrholz, J. et al. Electromechanical-assisted training for walking after stroke. *Cochrane Database of Systematic Reviews* **5,** CD006185 (May 2017).

46. Schwartz, I. & Meiner, Z. Robotic-Assisted Gait Training in Neurological Patients: Who May Benefit? *Annals of Biomedical Engineering* **43,** 1260–1269 (May 2015).

47. Chaparro-Cárdenas, S. L., Lozano-Guzmán, A. A., Ramirez-Bautista, J. A. & Hernández-Zavala, A. A review in gait rehabilitation devices and applied control techniques. *Disability and Rehabilitation: Assistive Technology* **13,** 819–834 (Nov. 2018).

48. Vitiello, N. et al. in *Springer Tracts in Advanced Robotics* 1–40 (Springer Verlag, 2015).

49. Hesse, S. Treadmill training with partial body weight support after stroke: a review. *NeuroRehabilitation* **23,** 55–65 (2008).

50. Sale, P., Franceschini, M., Waldner, A. & Hesse, S. Use of the robot assisted gait therapy in rehabilitation of patients with stroke and spinal cord injury. *European journal of physical and rehabilitation medicine* **48,** 111–21 (Mar. 2012).

51. Huo, W., Mohammed, S., Moreno, J. C. & Amirat, Y. Lower Limb Wearable Robots for Assistance and Rehabilitation: A State of the Art. *IEEE Systems Journal* **10,** 1068–1081 (Sept. 2016).

52. Esquenazi, A. New Bipedal Locomotion Option for Individuals with Thoracic Level Motor Complete Spinal Cord Injury. *Journal of The Spinal Research Foundation* **26** (2013).

53. Cao, J., Xie, S. Q., Das, R. & Zhu, G. L. Control strategies for effective robot assisted gait rehabilitation: The state of art and future prospects. *Medical Engineering & Physics* **36,** 1555–1566 (Dec. 2014).

54. Calabrò, R. S. et al. Robotic gait rehabilitation and substitution devices in neurological disorders: where are we now? *Neurological Sciences* **37,** 503–514 (Apr. 2016).

55. Turchetti, G. et al. Why Effectiveness of Robot-Mediated Neurorehabilitation Does Not Necessarily Influence Its Adoption. *IEEE Reviews in Biomedical Engineering* **7,** 143–153 (2014).

56. Hocoma. *Lokomat* 2019.

57. Jezernik, S., Colombo, G., Keller, T., Frueh, H. & Morari, M. Robotic Orthosis Lokomat: A Rehabilitation and Research Tool. *Neuromodulation: Technology at the Neural Interface* **6,** 108–115 (Apr. 2003).

58. Fleerkotte, B. M. et al. The effect of impedance-controlled robotic gait training on walking ability and quality in individuals with chronic incomplete spinal cord injury: an explorative study. *Journal of NeuroEngineering and Rehabilitation* **11,** 26 (Mar. 2014).

59. Veneman, J. et al. Design and Evaluation of the LOPES Exoskeleton Robot for Interactive Gait Rehabilitation. *IEEE Transactions on Neural Systems and Rehabilitation Engineering* **15,** 379–386 (Sept. 2007).

60. Alias, N. A., Huq, M. S., Ibrahim, B. & Omar, R. The Efficacy of State of the Art Overground Gait Rehabilitation Robotics: A Bird's Eye View. *Procedia Computer Science* **105,** 365–370 (Jan. 2017).

61. Esquenazi, A., Talaty, M., Packel, A. & Saulino, M. The ReWalk Powered Exoskeleton to Restore Ambulatory Function to Individuals with Thoracic-Level Motor-Complete Spinal Cord Injury. *American Journal of Physical Medicine & Rehabilitation* **91,** 911–921 (Nov. 2012).

62. Esquenazi, A., Talaty, M. & Jayaraman, A. Powered Exoskeletons for Walking Assistance in Persons with Central Nervous System Injuries: A Narrative Review. *PM&R* **9,** 46–62 (Jan. 2017).

63. Contreras-Vidal, J. L. et al. Powered exoskeletons for bipedal locomotion after spinal cord injury. *Journal of Neural Engineering* **13,** 031001 (June 2016).

64. Kolakowsky-Hayner, S. A., Crew, J., Moran, S. & Shah, A. Safety and Feasibility of using the EksoTM Bionic Exoskeleton to Aid Ambulation after Spinal Cord Injury. *Journal of Spine* **2,** 1–8 (Sept. 2013).

65. Yan, T., Cempini, M., Oddo, C. M. & Vitiello, N. Review of assistive strategies in powered lower-limb orthoses and exoskeletons. *Robotics and Autonomous Systems* **64,** 120–136 (Feb. 2015).

66. Quintero, H. A., Farris, R. J., Hartigan, C., Clesson, I. & Goldfarb, M. A Powered Lower Limb Orthosis for Providing Legged Mobility in Paraplegic Individuals. *Topics in spinal cord injury rehabilitation* **17,** 25–33 (2011).

67. Federici, S., Meloni, F., Bracalenti, M. & De Filippis, M. L. The effectiveness of powered, active lower limb exoskeletons in neurorehabilitation: A systematic

review. *NeuroRehabilitation* **37** (eds Scherer, M. J. & Federici, S.) 321–340 (Nov. 2015).

68. Zeilig, G. et al. Safety and tolerance of the ReWalk exoskeleton suit for ambulation by people with complete spinal cord injury: A pilot study. *The Journal of Spinal Cord Medicine* **35,** 96–101 (Mar. 2012).

69. Morone, G., Masiero, S., Werner, C. & Paolucci, S. Advances in neuromotor stroke rehabilitation. *BioMed research international* **2014,** 236043 (2014).

70. Kahn, L. E., Lum, P. S., Rymer, W. Z. & Reinkensmeyer, D. J. Robot-assisted movement training for the stroke-impaired arm: Does it matter what the robot does? *Journal of rehabilitation research and development* **43,** 619–30 (2006).

71. Dewar, R., Love, S. & Johnston, L. M. Exercise interventions improve postural control in children with cerebral palsy: a systematic review. *Developmental Medicine & Child Neurology* **57,** 504–520. ISSN: 00121622 (2015).

72. Azorín, J. M., Pons, J. L., Frizera, A., Gil, Á. & Roa, J. in *Exoesqueletos Robóticos para Rehabilitación y Asistencia de Pacientes con Daño Neurológico: Experiencias y Posibilidades en Iberoamérica* 1st ed., 11–35 (2016). ISBN: 978-84-15413-29-5.

73. Geyer, H., Seyfarth, A. & Blickhan, R. Compliant leg behaviour explains basic dynamics of walking and running. *Proceedings. Biological sciences* **273,** 2861–7 (Nov. 2006).

74. Bacek, T. et al. Design and evaluation of a torque-controllable knee joint actuator with adjustable series compliance and parallel elasticity. *Mechanism and Machine Theory* **130,** 71–85 (Dec. 2018).

75. Rietdyk, S., Patla, A. E., Winter, D. A., Ishac, M. G. & Little, C. E. Balance recovery from medio-lateral perturbations of the upper body during standing. *Journal of Biomechanics* **32,** 1149–1158. ISSN: 00219290 (Nov. 1999).

76. Ortlieb, A., Bouri, M., Baud, R. & Bleuler, H. *An assistive lower limb exoskeleton for people with neurological gait disorders* in *2017 International Conference on Rehabilitation Robotics (ICORR)* **2017** (IEEE, July 2017), 441–446. ISBN: 978-1-5386-2296-4.

77. Bohannon, R. W. Comfortable and maximum walking speed of adults aged 20-79 years: reference values and determinants. *Age and ageing* **26,** 15–9. ISSN: 0002-0729 (Jan. 1997).

78. Hughes, A. et al. Feasibility of Iterative Learning Control Mediated by Functional Electrical Stimulation for Reaching After Stroke. *Neurorehabilitation and Neural Repair* **23,** 559–568. ISSN: 1545-9683 (2009).

79. Sánchez-Manchola, M., Gómez-Vargas, D., Casas-Bocanegra, D., Múnera, M. & Cifuentes, C. A. *Development of a Robotic Lower-Limb Exoskeleton for Gait Rehabilitation: AGoRA Exoskeleton* in *IEEE ANDESCON 2018 Proceedings* (IEEE, Cali, 2018).

80. Schiele, A. & van der Helm, F. C. T. Kinematic Design to Improve Ergonomics in Human Machine Interaction. *IEEE Transactions on Neural Systems and Rehabilitation Engineering* **14,** 456–469 (Dec. 2006).

81. Moreno, J. C. et al. in *Wearable Robots* 165–200 (John Wiley & Sons, Ltd, Chichester, UK).

82. Fan, Y. & Yin, Y. Active and Progressive Exoskeleton Rehabilitation Using Multisource Information Fusion From EMG and Force-Position EPP. *IEEE Transactions on Biomedical Engineering* **60,** 3314–3321 (Dec. 2013).

83. Hian Kai Kwa et al. *Development of the IHMC Mobility Assist Exoskeleton* in *2009 IEEE International Conference on Robotics and Automation* (IEEE, May 2009), 2556–2562. ISBN: 978-1-4244-2788-8.

84. Zoss, A. & Kazerooni, H. Design of an electrically actuated lower extremity exoskeleton. *Advanced Robotics* **20,** 967–988 (Jan. 2006).

85. Colombo, G., Joerg, M., Schreier, R. & Dietz, V. Treadmill training of paraplegic patients using a robotic orthosis. *Journal of rehabilitation research and development* **37,** 693–700 (2000).

86. Bayón, C. et al. Development and evaluation of a novel robotic platform for gait rehabilitation in patients with Cerebral Palsy: CPWalker. *Robotics and Autonomous Systems* **91,** 101–114 (May 2017).

87. Gams, A., Petric, T., Debevec, T. & Babic, J. Effects of Robotic Knee Exoskeleton on Human Energy Expenditure. *IEEE Transactions on Biomedical Engineering* **60,** 1636–1644 (June 2013).

88. Anam, K. & Al-Jumaily, A. A. Active Exoskeleton Control Systems: State of the Art. *Procedia Engineering* **41,** 988–994 (Jan. 2012).

89. Maxon Motor AG. *EPOS4 Module/Compact 50/8 Hardware Reference* tech. rep. (Sachseln, 2016), 37–63.

90. Urs, K. *Motion Control for Newbies. Featuring maxon EPOS2 P* tech. rep. (Maxon Motor AG, 2014), 61–72.

91. Maxon Motor AG. *EPOS4 Application Notes* tech. rep. (Sachseln, 2018), 11–103.

92. Maxon Motor AG. *EPOS4 Communication Guide* tech. rep. (Sachseln, 2018), 17–29.

93. Joseph, L. & Cacace, J. in *Mastering ROS for robotics programming : design, build, and simulate complex robots using Robot Operating System* 2nd ed., 27–58 (Packt, Birmingham, 2015). ISBN: 9781788478953.

94. Maxon Motor AG. *EPOS Command Library* tech. rep. (Sachseln, 2016).

95. Maxon Motor AG. *Datasheet. Maxon flat motor EC 60, 68 mm, brushless, 100 Watt* 2017.

96. Harmonic Drive LLC. *Speed Reducers for Precision Motion Control Gear Units CSF-mini Engineering Data* tech. rep. (Boston, 2018).

97. Bortole, M. et al. The H2 robotic exoskeleton for gait rehabilitation after stroke: early findings from a clinical study. *Journal of NeuroEngineering and Rehabilitation* **12,** 54 (Dec. 2015).

98. Rueterbories, J., Spaich, E. G. & Andersen, O. K. Gait event detection for use in FES rehabilitation by radial and tangential foot accelerations. *Medical Engineering & Physics* **36,** 502–508 (Apr. 2014).

99. Wen-Chang Cheng, W.-C. & Ding-Mao Jhan, D.-M. Triaxial Accelerometer Based Fall Detection Method Using a Self-Constructing Cascade-AdaBoost-SVM Classifier. *IEEE Journal of Biomedical and Health Informatics* **17,** 411–419 (Mar. 2013).

100. Mannini, A., Trojaniello, D., Cereatti, A. & Sabatini, A. A Machine Learning Framework for Gait Classification Using Inertial Sensors: Application to Elderly, Post-Stroke and Huntington's Disease Patients. *Sensors* **16,** 134 (Jan. 2016).

101. Figueiredo, J., Ferreira, C., Santos, C. P., Moreno, J. C. & Reis, L. P. *Real-Time Gait Events Detection during Walking of Biped Model and Humanoid Robot through Adaptive Thresholds* in *2016 International Conference on Autonomous Robot Systems and Competitions (ICARSC)* (IEEE, May 2016), 66–71. ISBN: 978-1-5090-2255-7.

102. Vu, H. T. T. et al. ED-FNN: A New Deep Learning Algorithm to Detect Percentage of the Gait Cycle for Powered Prostheses. *Sensors (Basel, Switzerland)* **18** (July 2018).

103. Murray, S. & Goldfarb, M. *Towards the use of a lower limb exoskeleton for locomotion assistance in individuals with neuromuscular locomotor deficits* in *2012 Annual International Conference of the IEEE Engineering in Medicine and Biology Society* **2012** (IEEE, Aug. 2012), 1912–1915. ISBN: 978-1-4577-1787-1.

104. Sánchez Manchola, M. D., Pinto Bernal, M. J., Munera, M. & Cifuentes, C. A. Gait Phase Detection for Lower-Limb Exoskeletons using Foot Motion Data

from a Single Inertial Measurement Unit in Hemiparetic Individuals. *Sensors* **19,** 2988 (July 2019).

105. Taborri, J. et al. *Real-time gait detection based on Hidden Markov Model: Is it possible to avoid training procedure?* in *2015 IEEE International Symposium on Medical Measurements and Applications (MeMeA) Proceedings* (IEEE, May 2015), 141–145. ISBN: 978-1-4799-6477-2.

106. Taborri, J., Palermo, E., Rossi, S. & Cappa, P. Gait Partitioning Methods: A Systematic Review. *Sensors* **16,** 66 (Jan. 2016).

107. Kim, J., Hwang, S., Sohn, R., Lee, Y. & Kim, Y. Development of an Active Ankle Foot Orthosis to Prevent Foot Drop and Toe Drag in Hemiplegic Patients: A Preliminary Study. *Applied Bionics and Biomechanics* **8,** 377–384 (2011).

108. Gu, G. M., Kyeong, S., Park, D.-S. & Kim, J. *SMAFO: Stiffness modulated Ankle Foot Orthosis for a patient with foot drop* in *2015 IEEE International Conference on Rehabilitation Robotics (ICORR)* (IEEE, Aug. 2015), 543–548. ISBN: 978-1-4799-1808-9.

109. Miller, A. Gait event detection using a multilayer neural network. *Gait & Posture* **29,** 542–545 (June 2009).

110. Attal, F., Amirat, Y., Chibani, A. & Mohammed, S. Automatic Recognition of Gait phases Using a Multiple Regression Hidden Markov Model. *IEEE/ASME Transactions on Mechatronics,* 1–1 (2018).

111. Caldas, R., Mundt, M., Potthast, W., Buarque de Lima Neto, F. & Markert, B. A systematic review of gait analysis methods based on inertial sensors and adaptive algorithms. *Gait & Posture* **57,** 204–210 (Sept. 2017).

112. Lim, D.-H., Kim, W.-S., Kim, H.-J. & Han, C.-S. Development of real-time gait phase detection system for a lower extremity exoskeleton robot. *International Journal of Precision Engineering and Manufacturing* **18,** 681–687 (May 2017).

113. Gouwanda, D. & Gopalai, A. A. A robust real-time gait event detection using wireless gyroscope and its application on normal and altered gaits. *Medical Engineering & Physics* **37,** 219–225 (Feb. 2015).

114. Yuwono, M., Su, S. W., Guo, Y., Moulton, B. D. & Nguyen, H. T. Unsupervised nonparametric method for gait analysis using a waist-worn inertial sensor. *Applied Soft Computing* **14,** 72–80 (Jan. 2014).

115. Guenterberg, E. et al. A Method for Extracting Temporal Parameters Based on Hidden Markov Models in Body Sensor Networks With Inertial Sensors. *IEEE Transactions on Information Technology in Biomedicine* **13,** 1019–1030 (Nov. 2009).

116. Catalfamo, P., Ghoussayni, S. & Ewins, D. Gait event detection on level ground and incline walking using a rate gyroscope. *Sensors (Basel, Switzerland)* **10,** 5683–702 (2010).

117. Sabatini, A., Martelloni, C., Scapellato, S. & Cavallo, F. Assessment of Walking Features From Foot Inertial Sensing. *IEEE Transactions on Biomedical Engineering* **52,** 486–494 (Mar. 2005).

118. Chia Bejarano, N. et al. A Novel Adaptive, Real-Time Algorithm to Detect Gait Events From Wearable Sensors. *IEEE Transactions on Neural Systems and Rehabilitation Engineering* **23,** 413–422 (May 2015).

119. Taborri, J., Rossi, S., Palermo, E., Patanè, F. & Cappa, P. A Novel HMM Distributed Classifier for the Detection of Gait Phases by Means of a Wearable Inertial Sensor Network. *Sensors* **14,** 16212–16234 (Sept. 2014).

120. Yu, L., Zheng, J., Wang, Y., Song, Z. & Zhan, E. Adaptive method for real-time gait phase detection based on ground contact forces. *Gait & Posture* **41,** 269–275 (Jan. 2015).

121. Ding, S., Ouyang, X., Li, Z. & Yang, H. Proportion-based fuzzy gait phase detection using the smart insole. *Sensors and Actuators A: Physical* **284,** 96–102 (Dec. 2018).

122. Kotiadis, D., Hermens, H. & Veltink, P. Inertial Gait Phase Detection for control of a drop foot stimulator. *Medical Engineering & Physics* **32,** 287–297 (May 2010).

123. Rabiner, L. A tutorial on hidden Markov models and selected applications in speech recognition. *Proceedings of the IEEE* **77,** 257–286 (1989).

124. Mannini, A. & Sabatini, A. M. Gait phase detection and discrimination between walking–jogging activities using hidden Markov models applied to foot motion data from a gyroscope. *Gait & Posture* **36,** 657–661 (Sept. 2012).

125. Mannini, A. & Sabatini, A. M. *A hidden Markov model-based technique for gait segmentation using a foot-mounted gyroscope* in *2011 Annual International Conference of the IEEE Engineering in Medicine and Biology Society* **2011** (IEEE, Aug. 2011), 4369–4373. ISBN: 978-1-4577-1589-1.

126. González, I., Fontecha, J., Hervás, R. & Bravo, J. An Ambulatory System for Gait Monitoring Based on Wireless Sensorized Insoles. *Sensors* **15,** 16589–16613 (July 2015).

127. Mannini, A., Genovese, V. & Sabatin, A. M. Online Decoding of Hidden Markov Models for Gait Event Detection Using Foot-Mounted Gyroscopes. *IEEE Journal of Biomedical and Health Informatics* **18,** 1122–1130 (July 2014).

128. Abaid, N., Cappa, P., Palermo, E., Petrarca, M. & Porfiri, M. Gait detection in children with and without hemiplegia using single-axis wearable gyroscopes. *PloS one* **8,** e73152 (2013).

129. Taborri, J., Scalona, E., Palermo, E., Rossi, S. & Cappa, P. Validation of Inter-Subject Training for Hidden Markov Models Applied to Gait Phase Detection in Children with Cerebral Palsy. *Sensors* **15,** 24514–24529 (Sept. 2015).

130. González, R. C., López, A. M., Rodriguez-Uría, J., Álvarez, D. & Alvarez, J. C. Real-time gait event detection for normal subjects from lower trunk accelerations. *Gait & Posture* **31,** 322–325 (Mar. 2010).

131. Bloit, J. & Rodet, X. *Short-time Viterbi for online HMM decoding: Evaluation on a real-time phone recognition task* in *2008 IEEE International Conference on Acoustics, Speech and Signal Processing* (IEEE, Mar. 2008), 2121–2124. ISBN: 978-1-4244-1483-3.

132. Mihoub, A., Bailly, G. & Wolf, C. in, 172–183 (Springer, Cham, Oct. 2013).

133. Mannini, A. & Sabatini, A. M. Gait phase detection and discrimination between walking jogging activities using hidden Markov models applied to foot motion data from a gyroscope. *Gait & Posture* **36,** 657–661 (Sept. 2012).

134. Lemke, M. R., Wendorff, T., Mieth, B., Buhl, K. & Linnemann, M. Spatiotemporal gait patterns during over ground locomotion in major depression compared with healthy controls. *Journal of psychiatric research* **34,** 277–83 (2000).

135. Lagoda, C., Moreno, J. C. & Pons, J. L. Human-Robot Interfaces in Exoskeletons for Gait Training after Stroke: State of the Art and Challenges. *Applied Bionics and Biomechanics* **9,** 193–203 (2012).

136. Marchal-Crespo, L. & Reinkensmeyer, D. J. Review of control strategies for robotic movement training after neurologic injury. *Journal of NeuroEngineering and Rehabilitation* **6,** 20 (June 2009).

137. Wu, J. et al. The design and control of a 3DOF lower limb rehabilitation robot. *Mechatronics* **33,** 13–22 (Feb. 2016).

138. Torabi, M., Sharifi, M. & Vossoughi, G. Robust Adaptive Sliding Mode Admittance Control of Exoskeleton Rehabilitation Robots. *Scientia Iranica* **0,** 0–0 (Oct. 2017).

139. Taha, Z. et al. A hybrid active force control of a lower limb exoskeleton for gait rehabilitation. *Biomedical Engineering / Biomedizinische Technik* **63,** 491–500 (July 2018).

140. Craig, J. J. *Introduction to Robotics: Mechanics and Control* 3rd (ed Hall, P. P.) 150–1 (Upper Saddle River, NJ, USA, 2004).

141. Del Ama Espinosa, A. J. *Hybrid Walking Therapy with Fatigue Management for Spinal Cord Injured Individuals* PhD thesis (Universidad Carlos III de Madrid, 2013).

142. Hogan, N. Impedance Control: An Approach to Manipulation. *1984 American Control Conference,* 304–313 (1984).

143. Hoogen, J., Riener, R. & Schmidt, G. Control aspects of a robotic haptic interface for kinesthetic knee joint simulation. *Control Engineering Practice* **10,** 1301–1308. ISSN: 09670661 (Nov. 2002).

144. Krebs, H. I., Volpe, B. T., Aisen, M. L. & Hogan, N. Increasing productivity and quality of care: Robot-aided neuro-rehabilitation. *Journal of Rehabilitation Research and Development* **37,** 639–652. ISSN: 07487711 (2000).

145. Ichinose, W. E. et al. *A robotic device for measuring and controlling pelvic motion during locomotor rehabilitation* in *Annual International Conference of the IEEE Engineering in Medicine and Biology - Proceedings* **2** (2003), 1690–1693.

146. Sanchez Manchola, M. D., Arciniegas Mayag, L. J., Munera, M. & Cifuentes Garcia, C. A. *Impedance-based Backdrivability Recovery of a Lower-limb Exoskeleton for Knee Rehabilitation* in *2019 IEEE 4th Colombian Conference on Automatic Control (CCAC)* (IEEE, Oct. 2019), 1–6. ISBN: 978-1-5386-6962-4.

147. Villa-Parra, A., Delisle-Rodriguez, D., Souza Lima, J., Frizera-Neto, A. & Bastos, T. Knee Impedance Modulation to Control an Active Orthosis Using Insole Sensors. *Sensors* **17,** 2751 (Nov. 2017).

148. Chen, B., Zi, B., Wang, Z., Qin, L. & Liao, W.-H. Knee exoskeletons for gait rehabilitation and human performance augmentation: A state-of-the-art. *Mechanism and Machine Theory* **134,** 499–511 (2019).

149. Ir, M. & Azuan AO, N. Stance-Control-Orthoses with Electromechanical Actuation Mechanism: Usefulness, Design Analysis and Directions to Overcome Challenges. *Journal of Neurology and Neuroscience* **06** (2015).

150. Rafiaei, M. et al. The gait and energy efficiency of stance control knee-ankle-foot orthoses: A literature review. *Prosthetics and orthotics international* **40,** 202–14. ISSN: 1746-1553 (Apr. 2016).

151. Fukuchi, C. A., Fukuchi, R. K. & Duarte, M. A public dataset of overground and treadmill walking kinematics and kinetics in healthy individuals. *PeerJ* **6,** e4640. ISSN: 2167-8359 (2018).

152. Shamaei, K. & Dollar, A. M. *On the mechanics of the knee during the stance phase of the gait.* in *IEEE International Conference on Rehabilitation Robotics* (2011), 5975478.

153. Arnos, P. *Age-Related Changes in Gait: Influence of Upper-Body Posture* PhD thesis (University of Toledo, 2007).

154. Chitta, S. et al. ros_control: A generic and simple control framework for ROS. *The Journal of Open Source Software* **2,** 456. ISSN: 2475-9066 (Dec. 2017).

155. Knaepen, K. et al. Human-robot interaction: Kinematics and muscle activity inside a powered compliant knee exoskeleton. *IEEE Transactions on Neural Systems and Rehabilitation Engineering* **22,** 1128–1137. ISSN: 15344320 (Nov. 2014).

156. Taub, E., Uswatte, G., Mark, V. W. & Morris, D. M. *The learned nonuse phenomenon: Implications for rehabilitation* Sept. 2006.

157. Sawicki, G. S. & Ferris, D. P. Mechanics and energetics of level walking with powered ankle exoskeletons. *Journal of Experimental Biology* **211,** 1402–1413. ISSN: 0022-0949 (May 2008).

158. Lotze, M., Braun, C., Birbaumer, N., Anders, S. & Cohen, L. G. Motor learning elicited by voluntary drive. *Brain* **126,** 866–872. ISSN: 00068950 (Apr. 2003).

159. Kaelin-Lane, A., Sawaki, L. & Cohen, L. G. Role of voluntary drive in encoding an elementary motor memory. *Journal of Neurophysiology* **93,** 1099–1103. ISSN: 00223077 (Feb. 2005).

160. Bourgain, M. et al. Effect of shoulder model complexity in upper-body kinematics analysis of the golf swing. *Journal of Biomechanics* **75,** 154–158. ISSN: 18732380 (June 2018).

161. Hybois, S. et al. Comparison of shoulder kinematic chain models and their influence on kinematics and kinetics in the study of manual wheelchair propulsion. *Medical Engineering and Physics* **69,** 153–160. ISSN: 18734030 (July 2019).

162. Raabe, M. E. & Chaudhari, A. M. An investigation of jogging biomechanics using the full-body lumbar spine model: Model development and validation. *Journal of Biomechanics* **49,** 1238–1243. ISSN: 18732380 (May 2016).

163. Zacharias, B. & Kannenberg, A. Clinical Benefits of Stance Control Orthosis Systems: An Analysis of the Scientific Literature. *JPO: Journal of Prosthetics and Orthotics* **24,** 2–7 (2012).

164. Demers, L., Monette, M., Lapierre, Y., Arnold, D. L. & Wolfson, C. Reliability, validity, and applicability of the Quebec User Evaluation of Satisfaction with assistive Technology (QUEST 2.0) for adults with multiple sclerosis. *Disability and Rehabilitation* **24,** 21–30. ISSN: 09638288 (Jan. 2002).

165. Ward, S., Wiedemann, L., Stinear, C., Stinear, J. & McDaid, A. *The influence of the Re-Link Trainer on gait symmetry in healthy adults* in *IEEE International*

Conference on Rehabilitation Robotics (IEEE Computer Society, Aug. 2017), 276–282. ISBN: 9781538622964.

166. Arazpour, M. et al. The influence of a powered knee-ankle-foot orthosis on walking in poliomyelitis subjects: A pilot study. *Prosthetics and Orthotics International* **40,** 377–383. ISSN: 17461553 (2016).

167. Gordon, D. F. N., Henderson, G. & Vijayakumar, S. Effectively Quantifying the Performance of Lower-Limb Exoskeletons Over a Range of Walking Conditions. *Frontiers in Robotics and AI* **5.** ISSN: 2296-9144 (June 2018).

168. Li, N. et al. *Review on Lower Extremity Exoskeleton Robot* tech. rep. (2015), 441–453.

169. Riener, R., Lünenburger, L., Maier, I. C., Colombo, G. & Dietz, V. Locomotor training in subjects with sensori-motor deficits: An overview of the robotic gait orthosis Lokomat. *Journal of Healthcare Engineering* **1,** 197–216. ISSN: 20402309 (2010).

170. Ferris, D. P. & Lewis, C. L. *Robotic lower limb exoskeletons using proportional myoelectric control* in *Proceedings of the 31st Annual International Conference of the IEEE Engineering in Medicine and Biology Society: Engineering the Future of Biomedicine, EMBC 2009* (IEEE Computer Society, 2009), 2119–2124. ISBN: 9781424432967.

171. Blaya, J. & Herr, H. Adaptive Control of a Variable-Impedance Ankle-Foot Orthosis to Assist Drop-Foot Gait. *IEEE Transactions on Neural Systems and Rehabilitation Engineering* **12,** 24–31. ISSN: 1534-4320 (2004).